

NAVAL POSTGRADUATE SCHOOL

Monterey, California



19980414 092

THESIS

**DESIGN OF AN ATTITUDE DYNAMICS AND CONTROL
SUBSYSTEM FOR A MEDIUM EARTH ORBIT
SATELLITE**

by

Danny K. Busch

December, 1997

Thesis Advisor:
Co-Advisor:

Brij Agrawal
Gangbing Song

Approved for public release; distribution is unlimited.

DTIC QUALITY INSPECTED 3

REPORT DOCUMENTATION PAGE

Form Approved
OMB No. 0704-0188

Public reporting burden for this collection of information is estimated to average 1 hour per response, including the time for reviewing instruction, searching existing data sources, gathering and maintaining the data needed, and completing and reviewing the collection of information. Send comments regarding this burden estimate or any other aspect of this collection of information, including suggestions for reducing this burden, to Washington headquarters Services, Directorate for Information Operations and Reports, 1215 Jefferson Davis Highway, Suite 1204, Arlington, VA 22202-4302, and to the Office of Management and Budget, Paperwork Reduction Project (0704-0188) Washington DC 20503.

1. AGENCY USE ONLY (Leave blank)

2. REPORT DATE
December 1997

3. REPORT TYPE AND DATES COVERED
Master's Thesis

4. TITLE AND SUBTITLE
DESIGN OF AN ATTITUDE DYNAMICS AND CONTROL SUBSYSTEM FOR A
MEDIUM EARTH ORBIT SATELLITE

5. FUNDING NUMBERS

6. AUTHOR(S)
Busch, Danny K.

7. PERFORMING ORGANIZATION NAME(S) AND ADDRESS(ES)
Naval Postgraduate School
Monterey, CA 93943-5000

8. PERFORMING
ORGANIZATION REPORT
NUMBER

9. SPONSORING / MONITORING AGENCY NAME(S) AND ADDRESS(ES)

10. SPONSORING /
MONITORING
AGENCY REPORT NUMBER

11. SUPPLEMENTARY NOTES

The views expressed in this thesis are those of the author and do not reflect the official policy or position of the Department of Defense or the U.S. Government.

12a. DISTRIBUTION / AVAILABILITY STATEMENT

Approved for public release; distribution is unlimited.

12b. DISTRIBUTION CODE

13. ABSTRACT (maximum 200 words)

The Department of Defense has a continuing need for satellite communications to satisfy the demand for information exchange for strategic, operational, and tactical warfighters. There is currently a transition planning effort to develop a satellite communications architecture for the 2007-2010 time frame. During this time all three current communication satellite systems; UFO, DSCS, and MILSTAR, are expected to degrade rapidly. As part of the transition planning effort, the U.S. Navy was tasked to form a Mobile Users Study to establish a framework for completing the detailed requirements and engineering work needed to develop the UHF/Mobile User transition plan. Then, as part of the Navy effort, the Naval Postgraduate School's Astronautical Engineering class SE-61 under Professor Brij Agrawal's guidance designed a proposed medium Earth orbit communications satellite. This thesis is a design of the Attitude Dynamics and Control Subsystem for the subject medium Earth MUS communications satellite. The thesis describes and explores the five major steps in designing an Attitude, Dynamics and Control Subsystem and focuses on key ADCS related areas that are peculiar to a MEO satellite as compared to a GEO satellite.

14. SUBJECT TERMS

Attitude Dynamics and Control Subsystem, ADCS, Medium Earth Orbit, MEO, Satellite Design, Spacecraft Design, Communications Satellite.

15. NUMBER OF
PAGES
198

16. PRICE CODE

17. SECURITY CLASSIFICATION OF
REPORT
Unclassified

18. SECURITY CLASSIFICATION OF
THIS PAGE
Unclassified

19. SECURITY CLASSIFI- CATION
OF ABSTRACT
Unclassified

20. LIMITATION
OF ABSTRACT
UL

NSN 7540-01-280-5500

Standard Form 298 (Rev. 2-89)
Prescribed by ANSI Std. Z39-18

DTIC QUALITY INSPECTED 3

This Page Intentionally Left Blank

Approved for public release; distribution is unlimited.

**DESIGN OF AN ATTITUDE DYNAMICS AND CONTROL SUBSYSTEM FOR A
MEDIUM EARTH ORBIT SATELLITE**

Danny K. Busch
Lieutenant, United States Navy
B.S., Belmont University, 1989

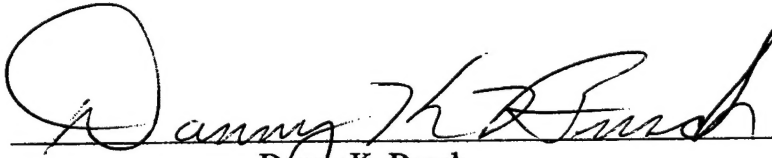
Submitted in partial fulfillment of the
requirements for the degree of

MASTER OF SCIENCE IN ASTRONAUTICAL ENGINEERING

from the

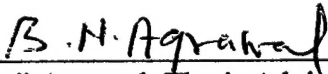
**NAVAL POSTGRADUATE SCHOOL
December 1997**

Author:




Danny K. Busch

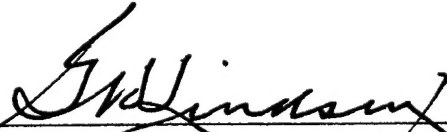
Approved by:



Brij Agrawal, Thesis Advisor



Gangbing Song, Co-Advisor



Gerald H. Lindsey, Chair, Department of Aeronautics
and Astronautics

This Page Intentionally Left Blank

ABSTRACT

The Department of Defense has a continuing need for satellite communications to satisfy the demand for information exchange for strategic, operational, and tactical warfighters. There is currently a Deputy Undersecretary of Defense for Space (DUSD (Space)) transition planning effort to develop a satellite communications architecture for the 2007-2010 time frame. During this time all three current satellite systems; UFO, DSCS, and MILSTAR, are expected to degrade rapidly. As part of the DUSD - Space effort the U.S. Navy was tasked to form a Mobile Users Study to establish a framework for completing the detailed requirements and engineering work needed to develop the UHF/Mobile User transition plan. Then, as part of the Navy effort the Naval Postgraduate School's Astronautical Engineering class SE-61 under Professor Brij Agrawal's guidance designed a proposed medium Earth orbit communications satellite. This thesis is a design of the Attitude Dynamics and Control Subsystem for the subject medium Earth orbit MUS communications satellite. The thesis describes and explores the five major steps in designing an Attitude, Dynamics and Control Subsystem and focuses on key ADCS related areas that are peculiar to a MEO satellite as compared to a GEO satellite.

This Page Intentionally Left Blank

TABLE OF CONTENTS

I. INTRODUCTION.....	1
A. BACKGROUND.....	1
1. Mission Overview and Requirements.....	1
2. Management Responsibilities.....	4
3. Concept of Operations.....	7
4. Spacecraft Description.....	9
B. ATTITUDE DYNAMICS AND CONTROL SUBSYSTEM - CONCEPTS AND DESIGN PROCESS.....	16
II. DEFINE CONTROL MODES AND SYSTEM LEVEL REQUIREMENTS.....	23
A. DEFINE CONTROL MODES.....	23
1. Orbit Insertion Mode.....	23
2. Acquisition Mode.....	23
3. Sun Acquisition Mode / Sun Hold Mode.....	23
4. Earth Acquisition Mode.....	23
5. Normal, On-Station Mode.....	24
6. Slew Mode.....	24
7. Contingency / Safe Mode.....	24
8. Orbit Maintenance / Orbit Transition Mode.....	24
B. SYSTEM LEVEL REQUIREMENTS.....	24
III. FUNCTIONAL DESCRIPTION AND TYPE OF SPACECRAFT CONTROL BY ATTITUDE CONTROL MODE.....	27
A. ADCS FUNCTIONAL DESCRIPTION AND COMPONENT OVERVIEW.....	27
1. TT&C.....	29
2. Reaction Wheels.....	29

3. Magnetic Torque Rods.....	29
4. Star Sensor	29
5. Global Positioning System.....	30
6. Inertial Reference Unit.....	30
7. Three Axis Magnetometer.....	30
8. Central Processor.....	31
9. Sun Sensor	31
10. Earth Sensor.....	31
B. TYPE OF SPACECRAFT CONTROL BY	
ATTITUDE CONTROL MODE.....	31
1. Orbit Insertion Mode.....	31
2. Acquisition Mode.....	32
3. Sun Acquisition Mode / Sun Hold Mode.....	32
4. Earth Acquisition Mode.....	32
5. Normal, On-Station Mode.....	33
6. Slew Mode.....	33
7. Contingency / Safe Mode.....	33
8. Orbit Maintenance / Orbit Transition Mode.....	33
C. THE MOTION OF THE SATELLITE AND THE	
SOLAR ARRAYS.....	36
IV. QUANTIFY DISTURBANCE ENVIRONMENT.....	43
A. EXTERNAL DISTURBANCE TORQUES.....	43
1. Solar Pressure Torques.....	44
2. Gravity Gradient Torques.....	45
3. Aerodynamic Torques.....	46
4. Disturbance Torques Due to the	
Geomagnetic Field.....	47
B. MATLAB SIMULATION OF EXTERNAL	
DISTURBANCE TORQUES.....	50

1. Solar Pressure Torques.....	50
2. Gravity Gradient Torques.....	54
3. Aerodynamic Pressure Torques.....	56
4. Combined External Disturbance Torques.....	60
C. INTERNAL DISTURBANCE TORQUES.....	63

V. ATTITUDE DYNAMICS AND CONTROL SUBSYSTEM

HARDWARE SELECTION AND DESCRIPTION.....	65
A. SIZING THE ADCS REACTION WHEELS.....	65
1. Torque and Angular Momentum Requirements	
Due to Yaw Steering.....	65
2. Torque and Angular Momentum Requirements	
Due to External Disturbances.....	69
B. SIZING THE MAGNETIC TORQUERS.....	69
C. OTHER SENSOR SELECTION ISSUES.....	70
D. HARDWARE SELECTION.....	70
1. Spacecraft Control Processor.....	70
2. Magnetic Acquisition and De-spin System.....	73
3. Earth Sensor / Sun Sensor Assembly.....	74
a. Overview.....	74
b. Theory of Operation.....	74
4. The Reaction Wheel Assembly.....	76
a. Application.....	76
b. Design Description.....	77
5. The Satellite Inertial Reference System.....	79
a. Heritage.....	79
b. Miniature Inertial Measurement Unit.....	79
6. HD-1003 Star Tracker.....	83
7. Global Positioning System.....	87
8. Sun Sensor.....	89

a. Overview.....	89
b. Theory of Operation.....	89
VI. YAW CONTROLLING.....	93
A. YAW DISTURBANCES.....	93
B. SUN AND NADIR POINTING GEOMETRY.....	93
C. SUN AND NADIR YAW POINTING STRATEGY.....	94
D. SUN AND NADIR ARRAY CONTROL STRATEGY.....	96
E. NORMAL, ON-STATION CONTROL FUNCTIONAL BLOCK DIAGRAM.....	97
F. ATTITUDE DETERMINATION SOFTWARE FUNCTIONAL OVERVIEW.....	98
G. SUN ANGLE ESTIMATION (β AND δ).....	100
H. YAW DATA PROCESSING.....	101
VII. SIMULATION OF THE ATTITUDE DYNAMICS AND CONTROL SUBSYSTEM.....	103
A. PROBLEM STATEMENT.....	103
B. THREE-AXIS STABILIZATION.....	104
1. Small Angle Approximation.....	104
2. Large Angle Requirements.....	106
C. THREE-AXIS REACTION WHEEL SYSTEM.....	109
1. Small Angle Approximation.....	110
2. Yaw Steering Requirements.....	121
D. ADCS CONTROL AND PERFORMANCE ANALYSIS - YAW STEERING.....	126
VIII. CONCLUSION.....	137
A. SUMMARY OF DESIGN PROCESS.....	137
B. SUMMARY OF SPACECRAFT ADCS DESIGN.....	139

APPENDIX A - ACRONYMS.....	143
APPENDIX B - GLOSSARY.....	145
APPENDIX C - MATLAB CODE FOR YAW STEERING.....	149
APPENDIX D - MATLAB CODE TO COMPUTE DCM.....	155
APPENDIX E - SIMULATION OF THE TOTAL EXTERNAL DISTURBANCES.....	157
APPENDIX F - SMALL ANGLE SIMULATION.....	169
APPENDIX G - LARGE ANGLE SIMULATION.....	175
LIST OF REFERENCES.....	181
INITIAL DISTRIBUTION LIST.....	185

This Page Intentionally Left Blank

I. INTRODUCTION

A. BACKGROUND

The MEO UHF Satellite Constellation for Robust Assured Telecommunications (MUSCRAT) communications system design described in this chapter was created as a project for AA4871, Spacecraft Design II at the Naval Postgraduate School. The project provided experience in the design of a complex satellite at both the system and subsystem levels. Each student in the project team was assigned responsibility for a major subsystem or design support function. Design and analysis of each subsystem was performed over a period of eleven weeks using facilities available at the Naval Postgraduate School. Additional support was obtained from government and commercial sources as documented in this report. [Ref. 40]

The MUSCRAT project was sponsored by the Naval Space Command. The goal of this project was to design a spacecraft bus and payload to meet the essential requirements for a Medium Earth Orbit (MEO) satellite communications system which will replace the aging UHF Follow-on (UFO) Constellation. Supporting trade studies, analyses, and options for increasing spacecraft capability are presented along with associated impacts on spacecraft mass, power, cost and schedule. [Ref. 40]

1. Mission Overview and Requirements

Advances in information technology place us at the point of a revolution in military operations – one in which the ability to collect, process, and disseminate information causes new thinking in doctrine, strategy, tactics, and procedures. Information and the dominant battlespace knowledge that it imparts allows a smaller, mobile joint force structure to be increasingly lethal and survivable in the battlespace. Success in modern warfare depends heavily upon achieving information dominance and that dominance depends upon the connectivity provided by communications systems. [Ref. 40]

There is a compelling need for space-based communications assets to help meet the growing information needs of the advanced warfighting and supporting systems the

Department of Defense (DoD) is investing in for today and the future. Although land, sea, and air-based communications systems are vital to the warfighter, they cannot meet all of the warfighters' information needs. Space based communication assets, due to their instant accessibility, survivability, coverage, flexibility, and ability to support mobile subscribers, are in some cases the only practical means to support mobile warfighter platforms, such as ships, submarines, aircraft, and land combat vehicles. As a result, the demands on space-based communications are growing. Recent DoD studies and industry assessments project *at least* a three to five-fold growth in warfighter information requirements that must be satisfied by SATCOM systems in the next decade. [Ref. 40]

Under the direction of the Deputy Under Secretary of Defense for Space (DUSD(Space)), a Mobile Users Study (MUS) was commissioned on 19 February 1997 to define the requirements, architecture, and cost for a replacement to UFO. The Naval Space Command was tasked as the lead for the Navy-directed MUS Requirements Working Integrated Product Team (WIPT). This product team, consisting of 52 members from all military staffs, the Joint Chiefs of Staff (JCS-J65), the National Reconnaissance Office (NRO), and the Defense Information Systems Agency (DISA), reviewed over 100 general requirements for low data rate netted communications and narrowed them into a basic set of 8 high level needs:

a. Assured Access

Assured access to SATCOM services is the most fundamental SATCOM need of the warfighter. The SATCOM study process confirmed that deployed and mobile warfighters are largely dependent on SATCOM to satisfy their most critical beyond-line-of-sight information transfer needs. Unified Combatant Commanders have repeatedly requested the ability to access SATCOM on demand and to control the resources apportioned to them by the Joint Chiefs of Staff (JCS). A warfighter's access to SATCOM support must therefore, be available on-demand when and where needed for the duration of the mission. [Ref. 40]

b. Netted Communications

A communications topology should be provided that allows multiple users to transmit (one at a time) and receive (all users less the one transmitting) with others on a common data stream. Netted communications on demand exists when flexible and reconfigurable nets enable the net control to bring on new members to the net without difficulty. [Ref. 40]

c. Communications on the Move

This capability shall provide the ability of the warfighter to move, and talk, at the same time. This capability enables the user to have voice and data communications in any natural environment to include a double canopy / jungle, in rain at rain rate mode "H", and in a sea environment. [Ref. 40]

d. Jointly Interoperable Communications

Current and emerging warfighting doctrine require joint operations to include inter-service compatibility and operating with allies. Joint service and allied operations require jointly interoperable communications. [Ref. 40]

e. Worldwide Coverage

Worldwide coverage is defined as 24 hours a day communications service from 65 degrees N to 65 degrees S latitude without gaps in geographical coverage. [Ref. 40]

f. Point to Point Communications

The system shall provide a communications topology that allows a single terminal to connect to another single terminal. Examples are communications link between a commander and a single subordinate element, a control platform or a remote device, or even a normal telephone connection. [Ref. 40]

g. Broadcast Communications

The system shall provide a communications topology that allows a single user to transmit while multiple users receive. A “one to many” broadcast capability is particularly valuable for the transmission of intelligence products or any information that needs to be distributed from a single source to multiple users. [Ref. 40]

h. Polar Coverage

Polar coverage is defined as 24 hours a day communications service for the area of the Earth's surface that is above 65° N and below 65° S latitude. Communications service coverage primarily directed at the northern polar regions is important for reasons of national security. [Ref. 40]

2. Management Responsibilities

Management functions and responsibilities for MUSCRAT will mirror those assigned to current Military Satellite Communications (MILSATCOM) systems as set forth in CJCS MOP-37. Figure 1-1 illustrates the organizational structure for MUSCRAT. Table 1-1 outlines the responsibilities of each of the organizations involved. [Ref. 40]

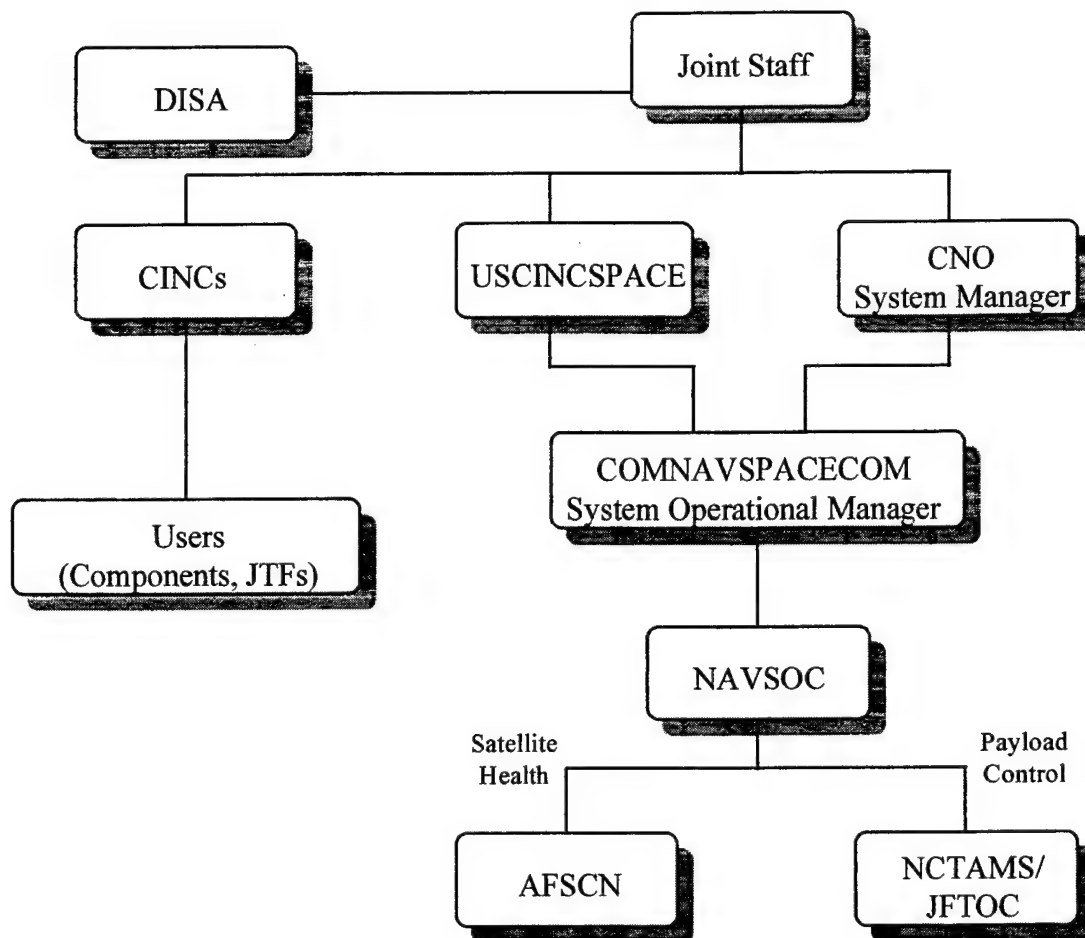


Figure 1-1: Organization Structure for MUSCRAT

Organization	Responsibilities
Joint Staff	<ol style="list-style-type: none"> 1. Approve requirements as part of the Integrated Communications Data Base (ICDB) process 2. Apportion satellite resources to CINCs 3. Adjudicate resource apportionment conflicts not resolved at lower levels 4. Approve the Operational Requirements Document (ORD)
Defense Information Systems Agency (DISA)	<ol style="list-style-type: none"> 1. Administer the ICDB
Unified Commanders-in-Chief (CINCs)	<ol style="list-style-type: none"> 1. Review, validate, and forward requirements to the Joint Staff 2. Collect, validate, and prioritize satellite access requests from their components 3. Manage satellite resources apportioned to them by the Joint Staff
Commander-in-Chief, United States Space Command (USCINCSpace)	<ol style="list-style-type: none"> 4. Provide management oversight of communications payload control at the direction of the Joint Staff and in coordination with the System Manager
Chief of Naval Operations (CNO N63)	<ol style="list-style-type: none"> 1. Carry out the Department of the Navy's responsibilities as the System Manager for MUSCRAT
Commander, Naval Space Command (COMNAVSPACECOM)	<ol style="list-style-type: none"> 1. COMNAVSPACECOM is MUSCRAT's system operational manager 2. Develop and coordinate procedures for payload control 3. Manage communications payload configuration to support CINC requirements 4. Review requirements and perform analyses to determine feasibility of satisfaction via the MUSCRAT system 5. Recommend apportionments to the Joint Staff 6. Provide system use and status information to the Joint Staff, DISA, and USCINCSpace
Naval Satellite Operations Center (NAVSOC)	<ol style="list-style-type: none"> 1. Coordinate MUSCRAT payload health and welfare with the AFSCN ground stations and perform payload control functions 2. Perform anomaly detection and resolution in conjunction with the AFSCN ground stations 3. Act as controlling authority for the transmission security (TRANSEC) crypto key system, and direct uploading of the new key segment variables to the onboard TRANSEC device as required
Air Force Satellite Control Network (AFSCN)	<ol style="list-style-type: none"> 1. Coordinate with NAVSOC concerning satellite health/welfare and anomaly detection/resolution
Naval Computer and Telecommunications Area Master Stations (NCTAMS) and Joint Fleet Telecommunication Operations Centers (JFTOCs)	<ol style="list-style-type: none"> 1. Coordinate with NAVSOC concerning satellite payload control 2. Provide connectivity to the Defense Switching Network (DSN) and Public Switching Telephone Network (PSTN)
Users	<ol style="list-style-type: none"> 1. Obtain approval of their requirements through the ICDB process 2. Adhere to the network/terminal configurations and precedences assigned by the CINC communications manager 3. Ensure that payload resources are used as assigned

Table 1-1: Responsibilities of Organizations Involved with MUSCRAT

3. Concept of Operations

MUSCRAT will be launched out of Cape Canaveral, Florida onboard either a Delta III or one of the Atlas family of launch vehicles (IIAS, IIAR, IIARS). Operational checkout is expected to last for approximately one month, after which time, the satellite will be placed in a non-operational mode until the entire constellation has been placed in orbit. The MUSCRAT system will then be activated.

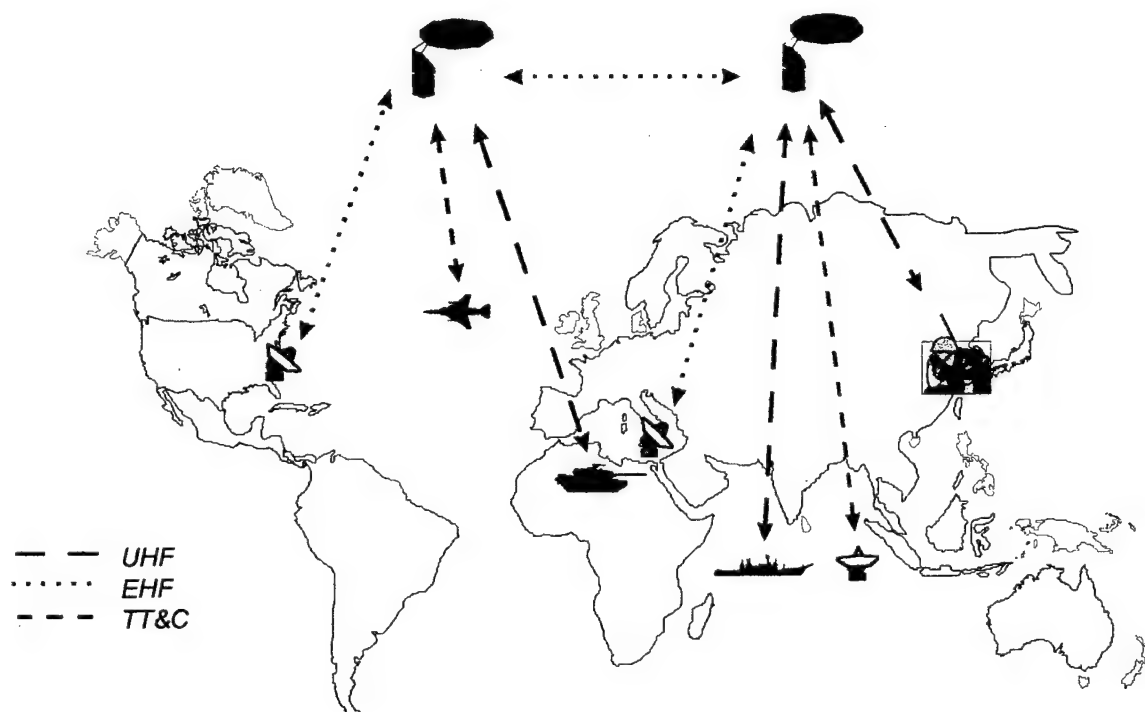


Figure 1-2: MUSCRAT Concept of Operations

Figure 1-2 illustrates MUSCRAT's concept of operations. The system uses current Air Force Satellite Control Network (AFSCN) stations for controlling satellite bus operations, as well as for monitoring standard satellite telemetry parameters. Control of payload operations will be accomplished through the current Naval Computer and Telecommunications Area Master Stations (NCTAMS) and Joint Fleet Telecommunications Operations Centers (JFTOCs) via an S/EHF link. The MUSCRAT

design allows for connectivity of payload control commands when a satellite is not within line of sight of a NCTAMS/JFTOC via EHF satellite crosslinks (60/61 GHz).

MUSCRAT provides direct UHF connectivity between users (uplink: 290-320 MHz, downlink: 243-270 MHz). If one of the users are non-mobile and is using the Defense Switching Network (DSN) or the Public Switching Telephone Network (PSTN), gateways located at the NCTAMS/JFTOCs will be used. This greatly increases MUSCRAT's capacity and flexibility. The gateways connect to the satellite via an S/EHF link (downlink: 20 GHz, uplink: 44 GHz). The EHF satellite crosslinks will also be used for payload communications connectivity. Examples of these different modes are shown in the figure.

4. Spacecraft Description

MUSCRAT will provide an assured, netted, global (including the North and South Poles) UHF communications link between both mobile and fixed-site users. The MUSCRAT constellation consists of ten operational satellites divided into two orbital planes separated by 180° in longitude of ascending node. Their circular orbits have an altitude of 11,000 km and an inclination of 48 degrees. MUSCRAT can be launched on Atlas IIAR, Atlas IIAS, and Delta III launch vehicles. The constellation guarantees global coverage with at least one satellite within view of a user with a ten degree elevation angle. [Ref. 40]

Figures 1-3 through 1-5 depict MUSCRAT's deployed and stowed configurations. MUSCRAT is basically rectangular in shape, with a bus height of six meters and a base measuring two meters square. The panels for the main "box" are constructed of aluminum honeycomb and are supported with aluminum shear webs. MUSCRAT also uses an aluminum central cylinder for load support. [Ref. 40]

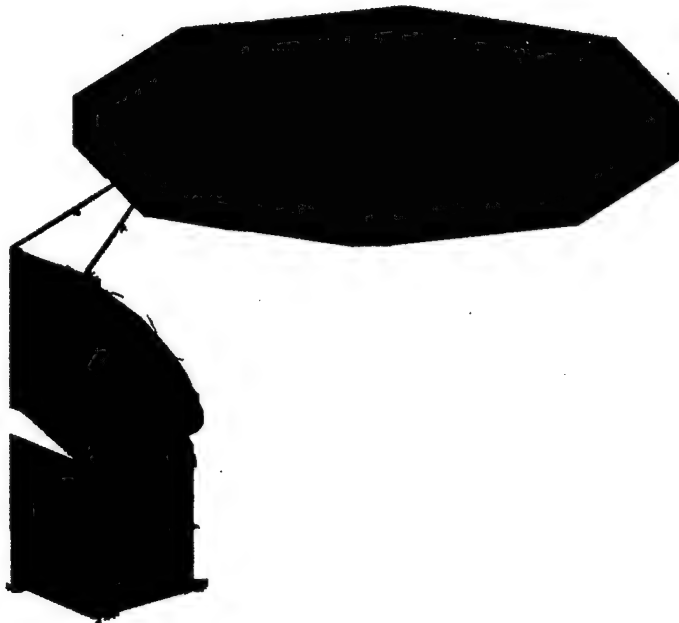


Figure 1-3: MUSCRAT Deployed Configuration

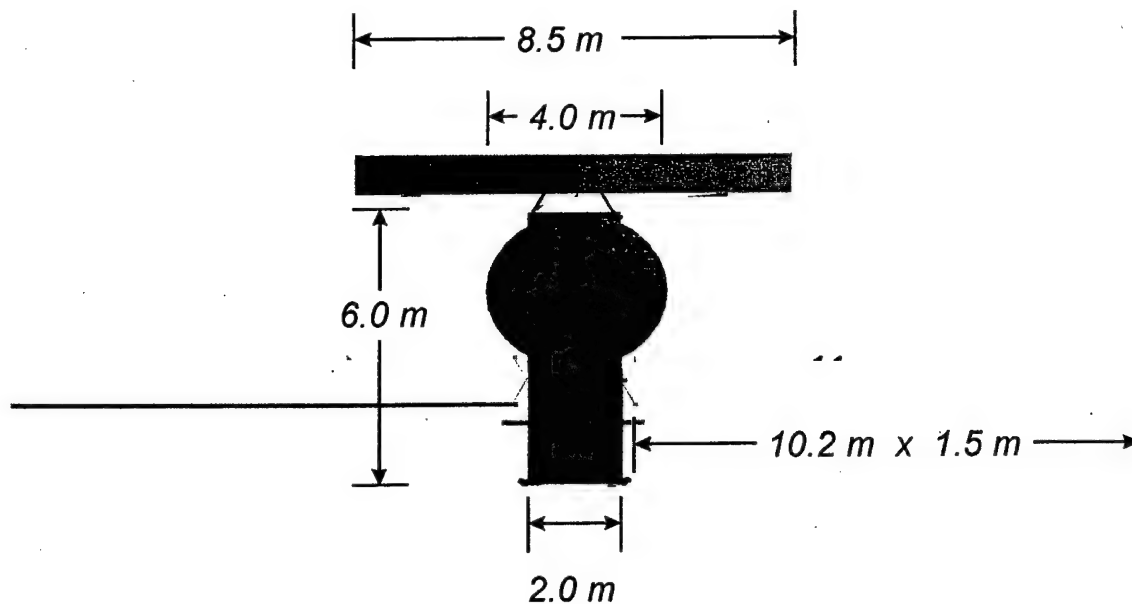


Figure 1-4: MUSCRAT Deployed Configuration

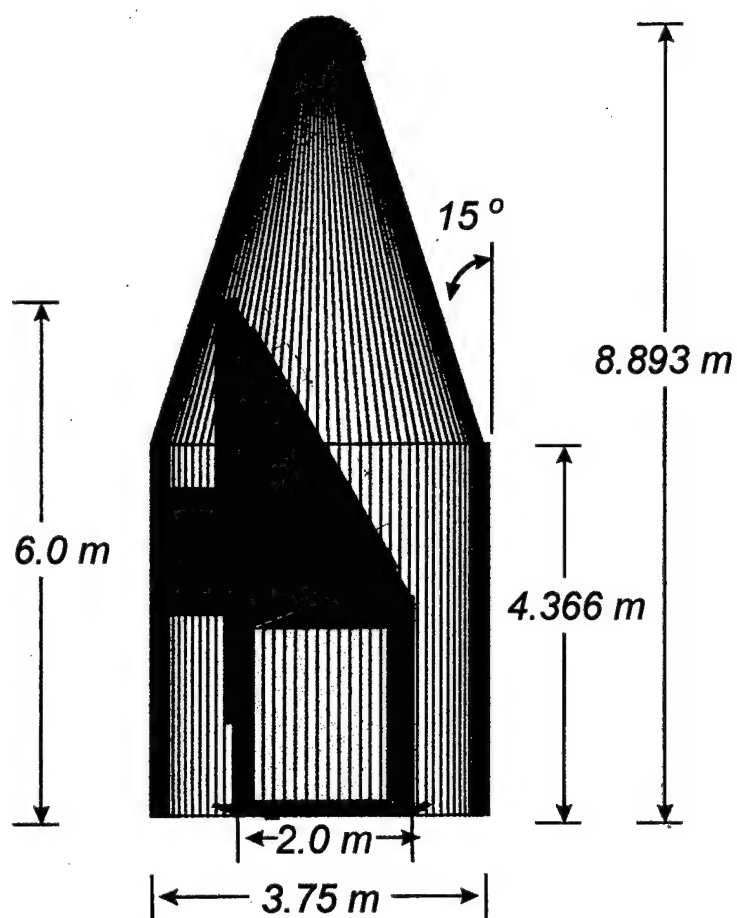
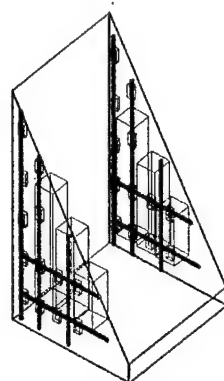


Figure 1-5: MUSCRAT Stowed Configuration Inside Delta Fairing

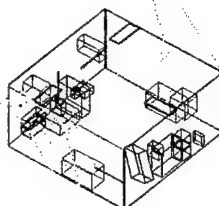
The bus has a modular design (Figure 1-6). The upper module contains the UHF components. The middle module houses the EHF downlink components, solar arrays, attitude control equipment, and control electronics. The lower module includes the EHF satellite crosslink components and batteries. The aluminum central cylinder runs the length of the bus, and encloses one pressurant and two propellant tanks (Figure 1-7).

[Ref. 40]



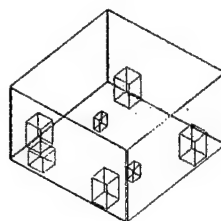
UPPER MODULE:

*UHF Payload Components
Heat Pipes*



MIDDLE MODULE:

*Central Computer
EHF Gateway Components
ADCS Components
EPS Solar Arrays and
Control Electronics*



LOWER MODULE:

*EHF Satellite Crosslink Components
EPS Batteries*

Figure 1-6: MUSCRAT's Modular Bus Design

The most prominent feature of MUSCRAT is its 8.5 meter diameter reflector. It deploys on a graphite truss structure 5.3 meters above the bus. The ground plane, with a diameter of four meters, contains 19 crossed dipole antennas. Twenty-six high heat dissipating solid state power amplifiers (SSPA's) are mounted on the north and south panels of the spacecraft. Seven of these are for redundancy. The remaining UHF components, except the data processing units, are located throughout the upper module.

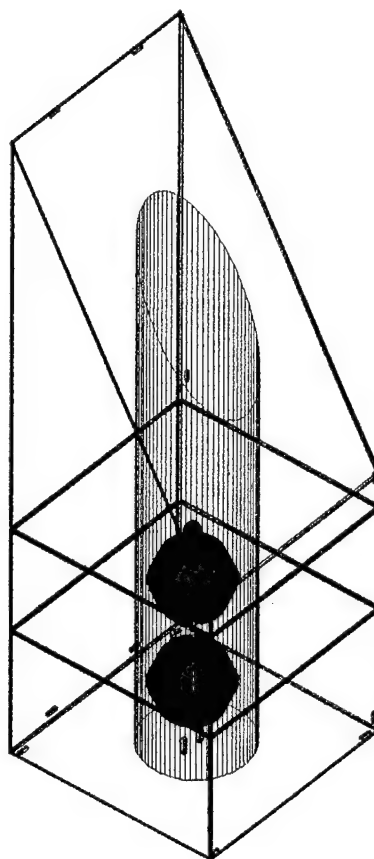


Figure 1-7: MUSCRAT's Central Cylinder

MUSCRAT uses an EHF link to connect to gateway ground stations. These stations are used to link communications to the Defense Switching Network (DSN) and the Public Switching Telephone Network (PSTN). Two EHF antennas (plus one for redundancy) accomplish this connection. MUSCRAT also uses EHF satellite crosslinks to ensure timely netted communications. Four EHF 0.45 meter dish antennas are located on the lower corners of the bus.

Control of spacecraft operations, with the exception of attitude determination and control, is accomplished using a central data processor. It contains eight Motorola Power PC 603e microprocessors mounted on modified Radstone PCP2 conduction cooled integrated circuit cards.

MUSCRAT is three-axis stabilized and yaw steered. Pointing requirements of 0.1° are met using three reaction wheels, with a fourth reaction wheel for redundancy. Positional and three axis attitude data are acquired using GPS and star trackers. The reaction wheels are desaturated using magnetic torque rods and 0.5 lb thrusters as primary and secondary systems respectively. The attitude determination and control subsystem (ADCS) is controlled by its own redundant processor. Other supporting ADCS components include a magnetometer, two inertial reference units (IRU's), sun trackers located on the solar arrays, and two earth/sun sensor assemblies used to initially orient the spacecraft once it gets to orbit.

The telemetry, tracking, and control (TT&C) subsystem provides for both autonomous operations and direct ground control of MUSCRAT. The satellite has two patch TT&C omni-directional antennas for assured telemetry download and command reception. Onboard TT&C operations will be controlled by redundant spacecraft control electronics. TT&C ground functions will take place at Air Force Satellite Control Network (AFSCN) Space-Ground Link System (SGLS) stations.

The electric power subsystem (EPS) is a dual bus, with a fully regulated bus voltage of 51 volts. MUSCRAT requires 8083 W of power in non-eclipse periods. Two GaAs solar arrays with a combined area of 30 m^2 provide this power, and it is stored in four NiH_2 batteries, each having 27 cells. Shunt regulators are located on the solar array yokes.

The propulsion subsystem is comprised of two monopropellant (hydrazine) tanks and a nitrogen pressurant tank housed inside MUSCRAT's central cylinder. Propellant will be used for satellite re-phasing, orbital insertion corrections, as a backup for reaction wheel desaturation, and for satellite deorbit at the end of mission life. Twelve 0.5 lb thrusters are used for reaction wheel desaturation, and two 5.0 lb thrusters are used for gross orbit maneuvers. All thruster valves have dual series seat valves for redundancy.

MUSCRAT's thermal subsystem provides the required temperature control throughout the satellite's lifetime. The primarily passive system design uses heat pipes in the north and south panels to cool concentrated heat sources (i.e. SSPA's) and minimize panel temperature gradients. These panels are radiators, and are covered with OSR.

Multi-layer insulation (MLI) blankets are also used to maintain proper temperatures. Heaters are used to maintain the batteries and hydrazine system within required temperature limits.

Table 1-2 is a summary of MUSCRAT's mass budget. The total launch mass of 2380.5 kg is broken down by subsystem, and includes a 15% mass margin, propellant, and the spacecraft adapter.

Subsystem	Mass (kg)	% Dry Mass
Structure	214.6	12.1 %
Payload/TT&C	871.9	49.4 %
EPS	336.6	19.0 %
Thermal	50	2.8 %
ADCS	90.7	5.1 %
Propulsion	45.2	2.6 %
Integration	110.1	6.2 %
Mechanisms	50	2.8 %
Dry Mass	1769.1	---
15% Margin	265.3	---
Propellant	246.1	---
Spacecraft Adapter	100	---
Launch Mass	2380.5	---

Table 1-2: MUSCRAT Mass Summary

Table 1-3 summarizes MUSCRAT's power budget during eclipse and non-eclipse periods. It includes a 5% growth margin in sun, a 10% growth margin in eclipse, and an additional 10% solar array design margin.

Subsystem	Non-Eclipse Requirements (W)	Eclipse Requirements (W)
Payload	5661	5661
EPS	1102	105
ADCS	205.7	205.7
Thermal	30	30
Propulsion *	108	108
Margin	1084.7	600.2
Total	8083.4	6601.9
* Not included in total power requirements due to extremely low average power requirements		

Table 1-3: MUSCRAT's Power Budget

Table 1-4 lists MUSCRAT's propellant budget. The total propellant mass of 246.1 kg includes a 10% margin.

Propellant Use	Mass (kg)
Orbit Injection Correction	12.69
Orbit Rephasing	72.54
Reaction Wheel Desaturation	17.28
Deorbit	118.98
10% Margin	24.61
Total Propellant Mass	246.1

Table 1-4: MUSCRAT's Propellant Budget

B. ATTITUDE DYNAMICS AND CONTROL SUBSYSTEM - CONCEPTS AND DESIGN PROCESS

The attitude determination and control subsystem (ADCS) stabilizes the vehicle and orients it in desired directions during the mission despite the external disturbance torques acting on it. This requires that the vehicle determine its attitude, using sensors, and control it, using actuators. The ADCS is often tightly coupled to other subsystems on board, especially the propulsion and navigation functions. [Ref. 6: p. 340]

This paper begins by discussing several useful concepts and definitions, including mass properties, disturbance torques, angular momentum, and reference vectors. The mass properties of a spacecraft are key in determining the size of control and disturbance torques. And, a knowledge of the location of the center of mass or gravity (cg) as well as the elements of the inertia matrix is a requirement. As well as the moments and products of inertia about chosen reference axes. The direction of the principal axes, those axes for which the inertia matrix is diagonal and the products of inertia are zero, are also of interest. Finally, we need to know how these properties change with time, as fuel or other consumables are used, or as appendages are moved or deployed. [Ref. 6: p. 340]

A body in space is subject to small but persistent disturbance torques (i.e., 10^{-4} Nm) from a variety of sources. These torques are categorized as cyclic, varying in a sinusoidal manner during an orbit, or secular, accumulating with time, and not averaging out over an orbit. These torques would quickly reorient the vehicle unless resisted in some way. An ADCS system resists these torques either passively, by exploiting inherent inertia or magnetic properties to make the "disturbances" stabilizing and their effects tolerable, or actively, by sensing the resulting motion and applying corrective torques. [Ref. 6: p. 340]

Angular momentum plays an important role in space, where torques typically are small and spacecraft are unconstrained. For a body initially at rest, an external torque will cause the body to angularly accelerate proportionally to the torque - resulting in an increasing angular velocity. Conversely, if the body is initially spinning about an axis perpendicular to the applied torque, then the body spin axis will precess, moving with a

constant angular velocity proportional to the torque. Thus, spinning bodies act like gyroscopes, inherently resisting disturbance torques in two axes by responding with constant, rather than increasing, angular velocity. This property of spinning bodies, called gyroscopic stiffness, can be used to reduce the effect of small, cyclic disturbance torques. This is true whether the entire body spins or just a portion of it, such as a momentum wheel or spinning rotor. [Ref. 6: p. 340]

Conservation of vehicle angular momentum requires that external torques change the system angular momentum. Thus, external disturbances must be corrected by external control torques (i.e., thrusters or magnetic torquers) or the resulting momentum buildup must be stored internally (i.e., by reaction wheels) without reorienting the vehicle beyond its allowable limits. The momentum build up due to secular disturbances ultimately must be reduced by applying compensating external control torques. [Ref. 6: p. 340]

Often, in addition to rejecting disturbances, the ADCS must reorient the vehicle (in slew maneuvers) to re-point the payload, solar arrays, or antennas. These periodic re-pointing requirements may drive the design to larger actuators than would be required for disturbance rejection alone. [Ref. 6: p. 341]

To orient the vehicle correctly, external references must be used to determine the vehicle's absolute attitude. These references include the Sun, the Earth's IR horizon, the local magnetic field direction, and the stars. In addition, inertial sensors (gyroscopes) also can be carried to provide a short-term attitude reference between external updates. External references (i.e., Sun angles) are usually measured as body-centered angular distances to a vector. Such measurements provide only two of the three independent parameters needed to specify the orientation of the spacecraft. This results in the need for multiple sensor types on board most spacecraft. [Ref. 6: p. 341]

The Attitude Dynamics and Control Subsystem design process is summarized very nicely with Table 1-5. Much of the input information for this table comes from other subsystems and the overall concept of operations for the satellite. This can be seen in Figure 1-8. [Ref. 6: p. 344]

Step #	Description	Inputs	Outputs
1a) 1b)	- Define control modes. - Define or derive system level requirements.	- Mission requirements, mission profile, type of insertion for launch vehicle	- List of different control modes during mission (table 7-2). - Requirements and constraints (table 7-3).
2	- Select type of spacecraft control by attitude control mode and subsystem functional description	- Payload, thermal & power needs - Orbit, pointing direction - Disturbance Environment	- Method for stabilizing and control: three axis, spinning, or gravity gradient
3	- Quantify disturbance environment	- Spacecraft geometry, orbit, solar/magnetic models, mission profile	- Values for forces from gravity gradient, magnetic aerodynamics, solar pressure, internal disturbances, and powered flight effects on control (cg off-sets, slosh)
4	- Select & size ADCS hardware	- Spacecraft geometry, pointing accuracy, orbit conditions, mission requirements, lifetime, orbit, pointing direction, slew rates	- Sensor suite: Earth, Sun, inertial, or other sensing devices - Control actuators, i.e., reaction wheels, thrusters, or magnetic torquers - Data processing electronics, if any, or processing requirements for other subsystems or ground computer
5	- Define determination and control algorithms	- All of above	- Algorithms, parameters, and logic for each determination and control mode
6	- All of above	- Refined requirements and design - Subsystem specifications	

Table 1-5: Attitude Dynamics Control Sub-System Design Process

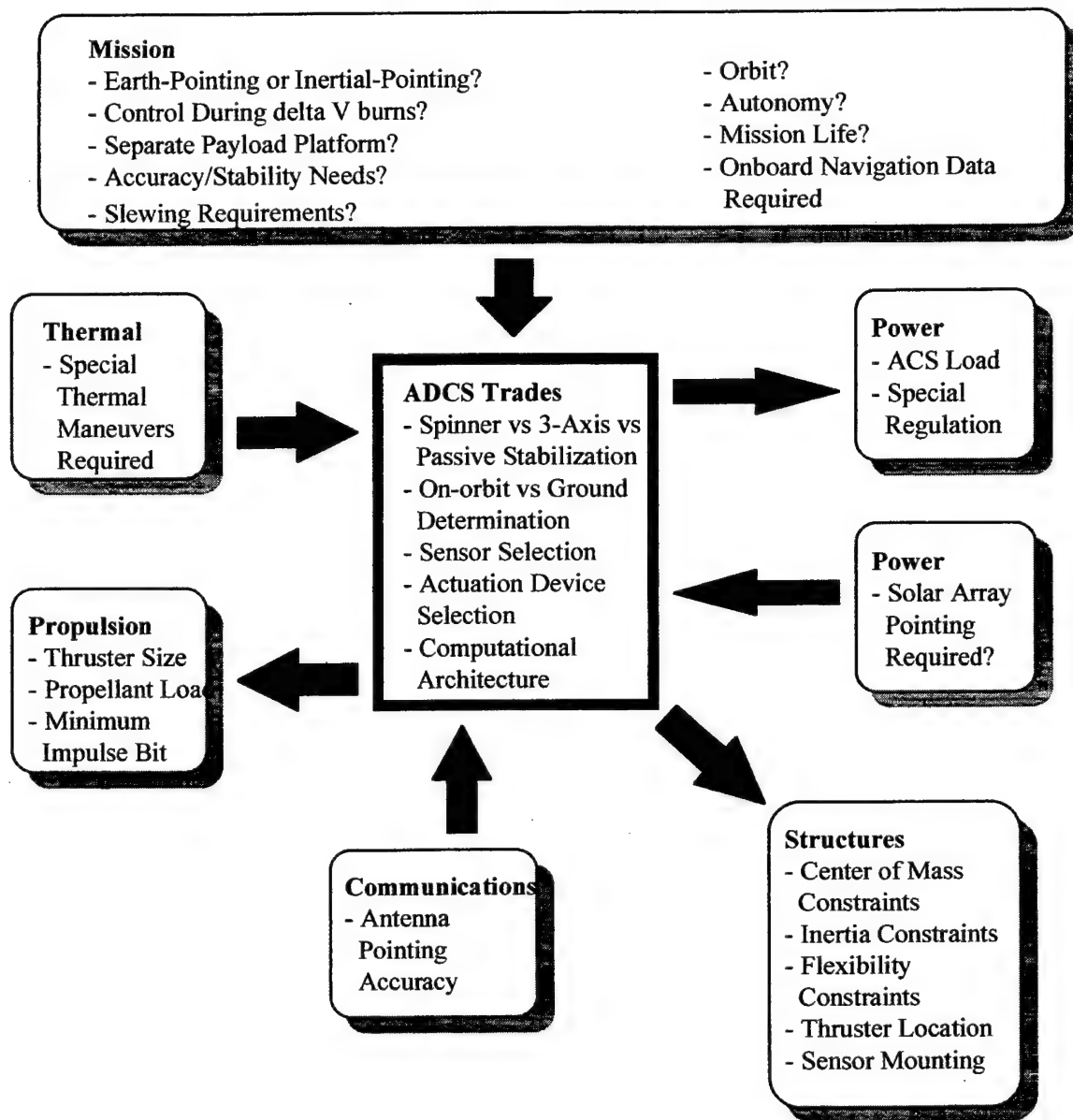


Figure 1-8: The Impact of Mission Requirements and Other Subsystems on the ADCS Subsystem. Direction of arrows show requirements flow from one subsystem to another.

The first step in designing the Attitude Dynamics and Control Subsystem is to define the control modes. Each control mode is related to the different phases of the spacecraft life. The ADCS for this satellite will have eight control modes which are described in chapter 2. The sensor and actuator requirements for each control mode may vary drastically. As a result, the designer of the ADCS must ensure the requirements of each control mode are satisfied while at the same time producing as simple and reliable a subsystem as possible.

Next, a thorough understanding of the system level requirements is required. These requirements usually originate from the other spacecraft subsystems and flow down to the ADCS designer. For example, the payload designer in this design specified the UHF antenna must maintain a pointing accuracy of 0.1° . Then, the systems engineer and structures designer determined the UHF antenna would be fixed to the spacecraft. This can then be translated into a spacecraft attitude control accuracy of 0.1° along the roll and pitch axes.

Then, based on mission requirements and inputs from other subsystems, a decision has to be made on the type of spacecraft control to be used. For example, a spin stabilized spacecraft may be most suitable for some missions while a three-axis control momentum wheel system may be best for others. When the type of spacecraft control is determined an understanding of the type of sensors and actuators should be developed. This is not actually selecting the components, but instead performing trade studies for determining which types of sensor and actuator are best suited for the spacecraft mission. An example might be determining whether to use a star sensor or earth sensor. Chapter three discusses these issues and presents a functional description of the attitude dynamics and control subsystem.

The next step in the design process is to quantify the disturbance environment. There are generally four external disturbances to consider: Gravity Gradient, Solar Pressure, Aerodynamic Pressure and Geomagnetic field disturbances. These disturbances should be estimated so that appropriate actuators and sensors can be selected to counteract their effects. Chapter four presents a thorough explanation on quantifying the external disturbance torques.

With information from the analysis discussed above a selection of ADCS components was performed. The components of the ADCS include sensors, actuators, and control processors. Chapter 5 presents this selection process and provides a detailed description of each component selected.

The final portion of the design process is the definition of determination and control algorithms. This also includes simulation and modeling of the ADCS. This begins in chapter six which focuses exclusively on yaw controlling and control algorithms. Chapter 7 then focuses on simulating the motion of the spacecraft and presents a thorough explanation of the differences between a non yaw steering satellite and a yaw steering one. The thesis concludes with several spacecraft attitude control simulations.

This Page Intentionally Left Blank

II. DEFINE CONTROL MODES AND SYSTEM LEVEL REQUIREMENTS

Attitude control modes are related to the different phases of the spacecraft life. Basically, the ADCS must be designed to meet the requirements of each mode. These ADCS requirements are tightly coupled to other spacecraft subsystems and the overall mission needs. Since the requirements change drastically with each mission phase, the ADCS designer may be challenged to build one system that meets all requirements.

A. DEFINE CONTROL MODES

1. Orbit Insertion Mode

The orbit insertion is the period during and after boost while the spacecraft is brought to final orbit. Options in this control mode include no spacecraft control, simple spin stabilization of solid rocket motor, and full spacecraft control using liquid propulsion system.

2. Acquisition Mode

This is normally where the initial determination of attitude and stabilization of the vehicle occurs. But, attitude determination and stabilization may also need to occur due to recovery from power upsets and / or emergencies.

3. Sun Acquisition Mode / Sun Hold Mode

After attitude determination and stabilization is complete Sun acquisition takes place in order to ensure an adequate power supply.

4. Earth Acquisition Mode

A critical aspect of this mode is acquiring a nadir pointing payload orientation while simultaneously keeping the solar arrays tracking the sun. Information from the sun sensors and additional navigational aids allow the spacecraft to re-orient such that

simultaneous Nadir payload pointing and solar array sun tracking is attained. Much more will be discussed on this topic later.

5. Normal, On-Station Mode

The Normal, On-Station mode is used for the vast majority of the mission. As a result, the requirements for this mode will drive the system design. And, the majority of discussion will focus on this mode of operation.

6. Slew Mode

This mode occurs when a reorientation of the vehicle is required (i.e. the spacecraft executes a slew maneuver).

7. Contingency / Safe Mode

This mode of operation is used in emergencies for when the regular mode fails or is disabled. Also, this mode may be selected to meet unexpected requirements like power or thermal constraints; at the expense of normal operations.

8. Orbit Maintenance / Orbit Transition Mode

This mode occurs when the spacecraft needs to be repositioned in the orbit. This either could be due to an accumulation of error over several years; or due to a satellite failure which requires selected satellites to be repositioned in the orbit.

B. SYSTEM LEVEL REQUIREMENTS

Following are the system level requirements for the Attitude Dynamics and Control Subsystem of the MUS communications satellite.

1. The ADCS must be fully operational without the aid of ground base control.
2. The operational lifetime of the ADCS must meet or exceed ten years.
3. The ADCS must maintain a UHF antenna beam pointing accuracy of less than or equal to 0.1° .

4. The ADCS must have the capability to provide continuous yaw steering and solar array tracking such that the solar array pointing accuracy is better than or equal to 5° .

5. The spacecraft must be fully operational during eclipse.

6. The spacecraft must be stabilized and under control during all phases of the mission.

7. The ADCS system should have system redundancy such that there are no single point failures.

8. The ADCS should have a ground override capability.

9. The spacecraft must have a cross-link antenna pointing accuracy of 0.07° which requires a spacecraft attitude knowledge requirement of 0.02° in roll, pitch, and yaw.

10. The Attitude Dynamics and Control Subsystem must have a positional knowledge requirement of 350 meters.

This Page Intentionally Left Blank

III. FUNCTIONAL DESCRIPTION AND TYPE OF SPACECRAFT CONTROL BY ATTITUDE CONTROL MODE

A. ADCS FUNCTIONAL DESCRIPTION AND COMPONENT OVERVIEW

A Zero Momentum three axis system was selected which can provide any combination of slew maneuvers in the pitch, roll and yaw directions. The Attitude Dynamics and Control Subsystem will maintain Nadir pointing accuracies to within 0.1° . At the same time it will continuously rotate in the yaw direction while the solar arrays are simultaneously rotating in order to keep a perpendicular orientation towards the sun. This will greatly decrease the complexity of the solar array control mechanisms. In a zero-momentum system, reaction wheels respond to disturbances on the vehicle. For example, a vehicle-pointing error creates a signal which speeds up the wheel, initially at zero. This torque corrects the vehicle and leaves the wheel spinning at low speed, until another pointing error speeds the wheel further or slows it down again. If the disturbance is cyclic during each orbit, the wheel may not approach saturation speed for several orbits. Secular disturbances, however, cause the wheel to drift toward saturation. We then must apply an external torque with a thruster, a magnetic torquer or both, to force the wheel speed back to zero. This process is called desaturation, momentum unloading, or momentum dumping and can be done automatically or by command from the ground. [Ref. 6: p. 348]

The Zero Momentum Three Axis Control system chosen was one of three options seriously considered. The other two were Dual Spin Stabilization and a Zero Momentum Control Momentum Gyro. The Dual Spin Stabilization was dismissed because the antenna configuration did not fit well on the despun platform and the power requirements were greater than a Dual Spin Stabilization could provide. The Control Moment Gyro (CMG) would work for this system, but it was dismissed because it is heavier and would not be conducive to yaw steering. Yaw steering enables a decrease in mass and complexity of the solar array drive assembly. In addition the Zero Momentum Three Axis Stabilization system would be lighter. Also, the Control Moment Gyro is best suited for high torque

demands and fast slewing requirements. Neither of which we have. It should be pointed out however, that the three axis stabilization has more moving parts and could therefore be considered more complex. So, a legitimate argument could be made for either system. Figure 3-1 is a general block diagram of the Zero Momentum Attitude Dynamics and Control Subsystem. [Ref. 6: p. 348, Ref. 21: p. 46]

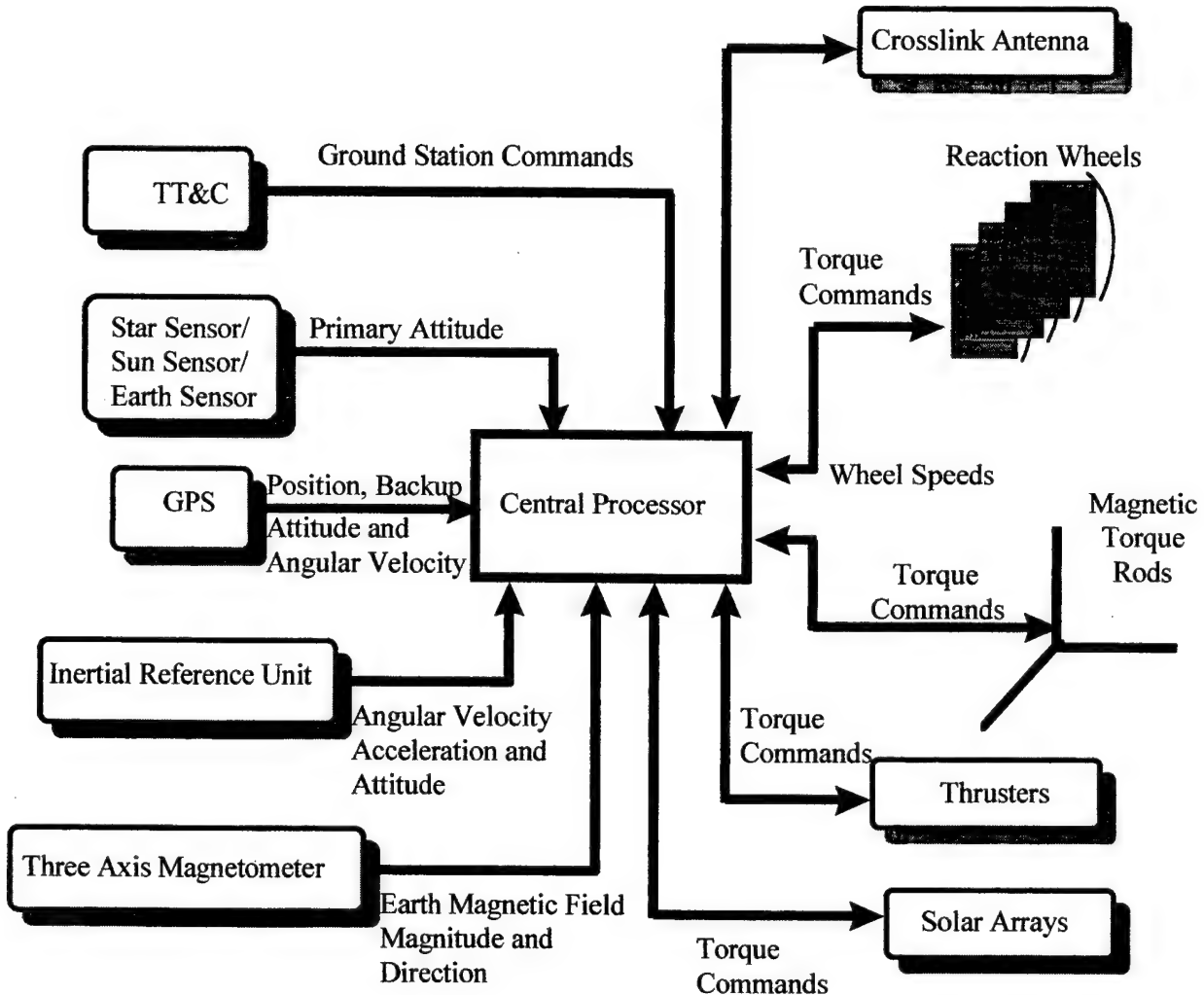


Figure 3-1: Block Diagram of Attitude Determination and Control Subsystem

1. TT&C

Telemetry, Tracking and Control will take place at the seven Air Force Satellite Control Network ground stations with one of the stations exercising overall control. Signals will be sent to the spacecraft as required where they will be processed in the Spacecraft's main computer. Those commands relating to Attitude Dynamics and Control will be sent to the ADCS central processor and then executed. In addition, data will be sent from the ADCS system to the ground stations in order to monitor the health, welfare and position of both the satellite and the ADCS. The TT&C subsystem will consist of dedicated antennas, a receiver, a transmitter, and a command and data handling system. [Ref. 15: p.13]

2. Reaction Wheels

The Zero Momentum reaction wheel system will counteract disturbance torque and provide the momentum to perform slew maneuvers as required. Reaction wheels are characterized by being light weight and capable of producing a continuous range of torque. This will work well for our satellite since we will continuously need to track the sun in order to attain maximum capacity with our solar arrays. [Ref. 21: p. 47]

3. Magnetic Torque Rods

Magnetic Torque Rods will be used to efficiently dump angular momentum in the reaction wheels produced by secular disturbance torques. By providing electric current through the torque rod coil a magnetic dipole moment results. This moment causes a torque that tries to align the torque rod with the earth's magnetic field. When this torque is produced an equal and opposite torque will be produced by the Reaction Wheels; thus allowing a means to dump momentum. [Ref. 21: p.55]

4. Star Sensor

Based on the crosslink antenna pointing requirements of 0.02° some type of star sensing system will have to be used. In order to provide a continuous star sensing three

star sensors will be required. In the worst case scenario two of the three sensors may be obstructed by the sun and moon. If this occurs the Inertial Reference Unit will be able to provide the required data for the short period of time required.

5. Global Positioning System

A Global Positioning System (GPS) is required on the spacecraft in order to allow for an ability to accurately determine orbit position without the aid of a ground station. And, the GPS will be a back-up for attitude determination. [Ref. 21: p. 53]

6. Inertial Reference Unit

The Inertial Reference Unit will provide continuous angular velocity information. Then, with the knowledge of angular velocity, angular acceleration can be obtained using a pseudorate modulator. In the event of star tracker failure or temporary un-availability, the Inertial Reference Unit will also provide continuous attitude information for a limited period of time. [Ref. 21: p. 52]

7. Three Axis Magnetometer

Magnetometers are simple, reliable, lightweight sensors that measure both the direction and size of the Earth's magnetic field. When compared to the Earth's known field, their output helps establish the spacecraft's attitude. But their accuracy is not as good as that of star, sun or horizon references. The Earth's field can shift with time and cannot be calculated precisely in the first place. To improve accuracy, data is often combined with the data from Sun or horizon sensors. When the vehicle is using the magnetic torquers and passes through magnetic field reversals during each orbit, the magnetometer will be used to control the polarity of the torquer output. And, the torquers will have to be turned off while the magnetometer is sampled to avoid corrupting the measurement. [Ref. 6: p. 361]

8. Central Processor

The Attitude Dynamics and Control Subsystem Central Processor will be a commercial off the shelf product produced by Honeywell. The Central Processor is the brain of the ADCS. As can be seen from Figure 3-1, input data is fed into the central processor from the TT&C, Star Sensors, GPS, IRU, Three Axis Magnetometer and Reaction Wheels. Based on this input data the central processor will calculate the spacecraft's position, velocity, orientation, angular velocity and angular acceleration. Then, the central processor will calculate the required spacecraft orientation, angular velocity and angular acceleration profile to maintain Nadir earth pointing, an adequate sun pointing profile, momentum limits and orbit repositioning/transfers. Finally, appropriate commands will be sent to the reaction wheels, torque rods, thrusters and solar array drive mechanisms.

9. Sun Sensor

A sun sensor is a visible light detector which can measure one or two angles between their mounting base and incident sunlight. One sun sensor assembly will be mounted on or near each solar array assembly and will be used to track the sun's rays.

10. Earth Sensor

An Earth Sensor is an infrared device that detects the contrast between the cold of deep space and the heat of the Earth's atmosphere. These sensors provide Earth relative information directly for earth pointing spacecraft, which simplifies on board processing.

B. TYPE OF SPACECRAFT CONTROL BY ATTITUDE CONTROL MODE

1. Orbit Insertion Mode

The launch vehicles we have selected will allow for direct orbit insertion with no need for an apogee kick motor or a perigee kick motor. As a result, under normal

condition there will be no spacecraft control until after the spacecraft is in or very near its final orbit and has separated from the launch vehicle.

2. Acquisition Mode

When the spacecraft is separated from the launch vehicle the acquisition mode of operation will begin. At this time the spacecraft will normally have a spin about the z axis. Each of the two sun sensor assemblies have two perpendicular fan shaped fields of view, α_1 and α_2 . Each sensor generates an output pulse as the sun passes through the field of view of the light sensitive element. Then, the time of arrival of the pulse is detected in the ADCS central processor. In addition, the earth sensor provides a pulse which is also detected by the central processor. The central processor is then able to take these measurements and compute the attitude of the spacecraft with respect to the sun and earth.

3. Sun Acquisition Mode / Sun Hold Mode

Using angular position, angular rate and data from the pitch sun sensor, the spacecraft is able to lock into and hold the sun in pitch. At this time the yaw and roll axes are under gyro reference control. Then, a slow yaw rotation occurs in order to acquire the sun with the yaw sun sensor. When both sensors have locked onto the sun, the sun hold mode automatically begins. Then, with the sun's position firmly established, the solar arrays are deployed and the remaining ADCS components are brought on line and thoroughly tested.

4. Earth Acquisition Mode

The earth acquisition mode occurs at either 0600 or 1800 local time. At this time the earth line and sun line relative to the spacecraft are perpendicular. With the yaw and pitch axis locked onto the sun a gentle roll maneuver takes place until the earth is acquired by the earth sensors. When an adequate Nadir pointing accuracy is attained by the earth sensors, both roll and pitch control transfer from the Gyros over to the earth sensors.

5. Normal, On-Station Mode

The Normal/On-Station operating mode is by far the most significant of the Attitude Control Modes. The vast majority of the spacecraft's time will be spent under normal operation. As a result, the design of the spacecraft's Attitude Dynamics and Control Subsystem was driven by this mode. And, that is why a vast majority of the discussion will be on the Normal, On-Station operating mode. The other mode operations will largely feed from how the Normal/On-Station operations are conducted. [Ref. 6: p. 340]

6. Slew Mode

We will utilize the Zero Momentum Three Axis Control System to simplify the solar array design. The spacecraft will continually slew about the unconstrained yaw axis in order to keep the solar array axis perpendicular to the solar radiation. Thus, the reduced array size possible with two degrees of freedom can be achieved with one array axis drive and continual spacecraft rotation about the yaw axis. It is important to ensure the reaction wheel selected can deliver the required torque. Slewing about the roll and pitch axis will not normally occur. If however, commanded to do so, the process and dynamics of slewing about the roll and pitch axis will be the same as that about the yaw axis. [Ref. 6: p. 351]

7. Contingency / Safe Mode

This mode is enabled in emergencies or when a certain level of uncertainty exists concerning the operational status of the spacecraft. In the Contingency/Safe Mode all non-essential equipment and actuators are turned off. Then, when given approval, the spacecraft will enter the Sun Acquisition Mode followed by extensive testing as the various components and actuators are brought back on line.

8. Orbit Maintenance / Orbit Transition Mode

If the spacecraft needs to be repositioned due to accumulated orbital error or a newly assigned orbit position it will enter the Orbit Maintenance/Orbit Transition Mode.

The first step in this mode is to shut down non-essential operations. Then, the spacecraft will orient itself such that the yaw axis of rotation points in the desired direction of movement. Then a spin up will take place followed by the firing of appropriate control thrusters. When the spacecraft has reached its new position satisfactorily, it will enter into the acquisition mode.

Table 3-1 summarizes the type of spacecraft control and the sensors utilized by each attitude control mode.

MODE	SENSORS	ACTUATORS	FUNCTION
Orbit Insertion	- None	- None	Insert spacecraft into final orbit
Acquisition Mode	- Sun Sensors (Pri) - Earth Sensor (Pri) - Sun Sensors (Sec) - Earth Sensor (Sec)	- Torque Rods (Pri) - Thrusters (Sec)	Determine Spacecraft attitude and stabilize spacecraft
Sun Acquisition / Sun Hold Mode	- Sun Sensor #1 (Pri) - Sun Sensor #2 (Sec)	- Reaction Wheels (Pri) - Torque Rods (Sec) - Thrusters (Sec)	Acquire and or hold a sun pointing orientation
Earth Acquisition Mode	- Earth Sun Sensor Assembly #1 (Pri) - Sun Sensor #1 (Pri) - Earth Sun Sensor Assembly #2 (Sec) - Sun Sensor #2 (Sec)	- Reaction Wheels (Pri) - Torque Rods (Sec) - Thrusters (Sec)	Acquire and maintain Nadir Earth pointing
Normal, On-Station	- Sun Sensor #1 (Pri) - Earth Sun Sensor #1 (Pri) - Star Tracker (Pri) - Earth Sun Sensor #2 (Sec) - GPS (Sec) - Sun Sensor #2 (Sec)	- Reaction Wheel (Pri) - Torque Rods (Sec) - Thrusters (Sec)	Maintain Nadir Earth pointing, Solar Array tracking and attitude / position accuracy requirements
Slew	- Star Trackers (Pri) - IRU (Sec)	- Reaction Wheels (Pri) - Torque Rods (Sec) - Thrusters (Sec)	- Reorient Spacecraft as required
Contingency / Safe	- Sun Sensor #1 (Pri) - Earth/Sun Sensor #1 (Pri) - Sun Sensor #2 (Sec) - Earth/Sun Sensor #2 (Sec)	- Reaction Wheels (Pri) - Torque Rods (Sec) - Thrusters (Sec)	Ensures spacecraft remains within limited operating constraints
Orbit Maintenance / Orbit Transition Mode	- GPS (Pri) - IRU (Sec)	- Thrusters (Pri) - Thrusters (Sec)	spacecraft reposition / change in orbital parameters

Table 3-1: Type of Spacecraft Control by Attitude Control Mode

C. THE MOTION OF THE SATELLITE AND THE SOLAR ARRAYS

As a spacecraft decreases in altitude the time spent in eclipse becomes a considerable part of the total lifetime of the satellite. For instance, at 11,000 km the maximum eclipse will occur when the Sun is in the orbital plane and the eclipse time will be 12% of the orbital period. [Ref. 37: pp. 75-78]

To take maximum advantage of the solar radiation, the solar arrays must be sun pointed. At the same time, the payload requires a constant nadir pointing configuration. At every position in the orbit these two demands must be satisfied. This will be accomplished with a combination of yaw steering and solar array pointing. Assuming the satellite has an arbitrary earth-pointing attitude, it must first rotate about the Z_s -axis (axis parallel to the antenna; yaw-axis) with an angle ψ , so that the axis about which the solar arrays rotate (BAPTA-axis) is in the plane perpendicular to the direction of the solar radiation. The second part of the motion consists of a rotation of the solar arrays about the BAPTA-axis with an angle η , so that the arrays point to the Sun. These two motions will now be looked at in much greater detail. [Ref. 37: pp. 75-78]

The angles η and ψ are functions of time. They also depend on the position of the satellite in the orbital plane and the position of the Sun with respect to the orbital plane. To aid in our analysis the following definitions are made: First, β is defined as the angle in the orbital plane between the point with minimum distance (sub-solar point) to the Sun and the satellite, and δ as the angle between the orbital plane and the direction of the Sun. This is illustrated in Figure 3-2. Because of the direct relation between β and time, ψ and η will be expressed as functions of β and δ . [Ref. 37: pp. 75-78]

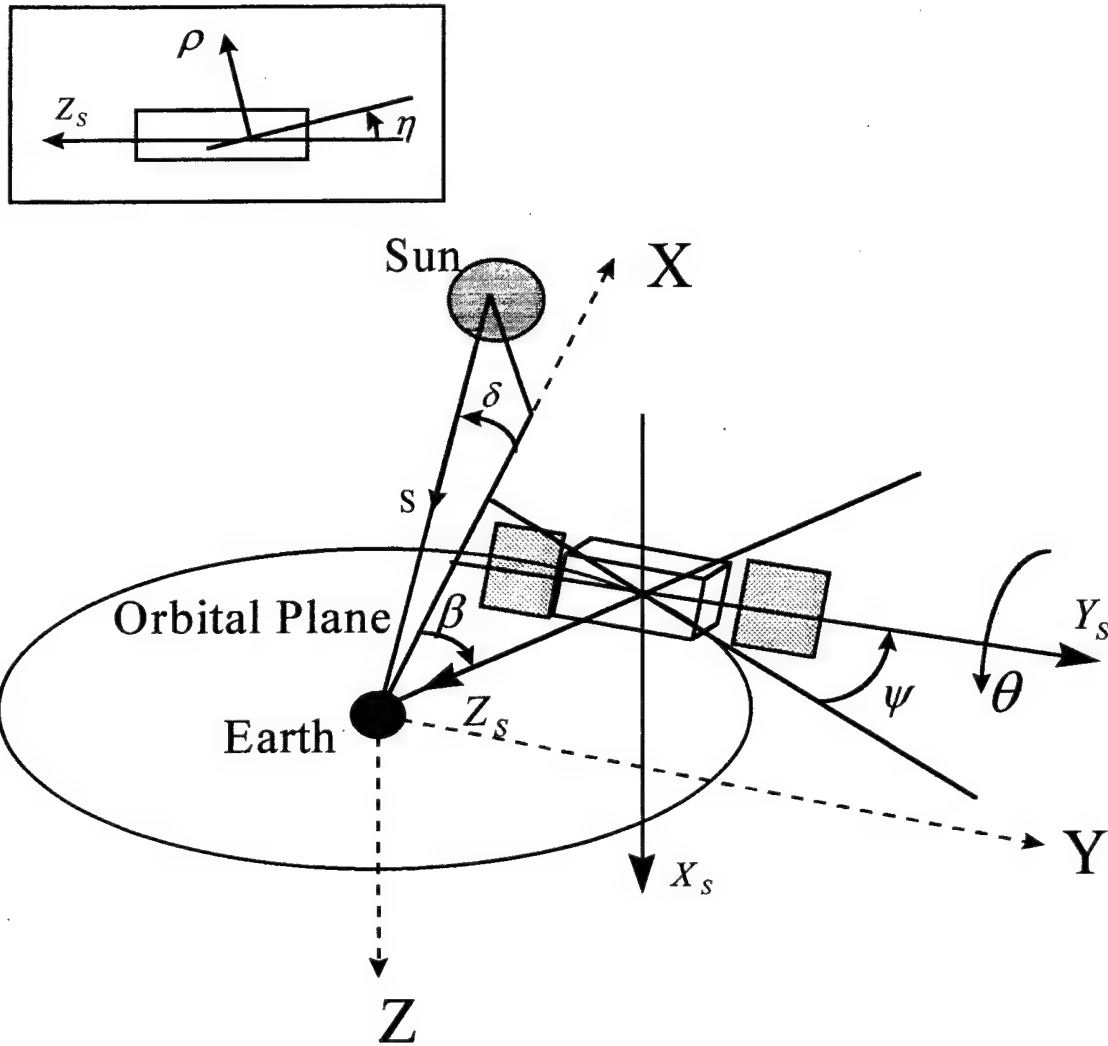


Figure 3-2: Definition of the angles ψ , η , β and δ .

The derivation of these functions $\psi(\beta, \delta)$ and $\eta(\beta, \delta)$ will be done below by means of vector algebra. [Ref. 37: pp. 75-78]

The direction of satellite axes X_s , Y_s , Z_s and of the sunlight s in the inertial XYZ coordinate system are:

$$\bar{X}_s = \begin{bmatrix} -\sin(\beta)*\sin(\psi) \\ \cos(\beta)*\sin(\psi) \\ \cos(\psi) \end{bmatrix}; \quad \bar{Y}_s = \begin{bmatrix} \sin(\beta)*\cos(\psi) \\ \cos(\beta)*\cos(\psi) \\ -\sin(\psi) \end{bmatrix}; \quad \bar{Z}_s = \begin{bmatrix} -\cos(\beta) \\ -\sin(\beta) \\ 0 \end{bmatrix};$$

$$\bar{s} = \begin{bmatrix} -\cos(\delta) \\ 0 \\ \sin(\delta) \end{bmatrix}$$

While the vector of the sunlight s stands perpendicular to the BAPTA-axis, and because the BAPTA-axis and the Y_s -axis are parallel, Y_s is also perpendicular to s . Now $\psi(\beta, \delta)$ can be determined:

$$\bar{Y}_s \cdot \bar{s} = -\sin(\beta) \cos(\psi) \cos(\delta) - \sin(\psi) \sin(\delta) = 0$$

$$\Rightarrow \quad \tan(\psi) = \left(\frac{-\sin(\beta)}{\tan(\delta)} \right); \quad \text{and} \quad \psi = \tan^{-1} \left(\frac{-\sin(\beta)}{\tan(\delta)} \right)$$

The direction of the solar panels in the X_s, Y_s, Z_s satellite coordinate system

$$\text{(see figure III.2) is: } \bar{p}_s = \begin{pmatrix} -\cos(\eta) \\ 0 \\ \sin(\eta) \end{pmatrix}$$

The direction of the solar panels in the XYZ system is obtained by performing the matrix multiplication $\bar{p} = [\bar{X}_s \bar{Y}_s \bar{Z}_s] * [\bar{p}_s]$:

$$\Rightarrow \quad \bar{p} = \begin{bmatrix} \sin(\beta)*\sin(\psi)*\cos(\eta) - \cos(\beta)*\sin(\eta) \\ -\cos(\beta)*\sin(\psi)*\cos(\eta) - \sin(\beta)*\sin(\eta) \\ -\cos(\psi)*\cos(\eta) \end{bmatrix}$$

Since \bar{p} and \bar{s} have to point exactly in opposite direction, also $\eta(\beta, \delta)$ can be determined:

$$\bar{p} \times \bar{s} = \det \begin{bmatrix} \bar{e}_x & \bar{e}_y & \bar{e}_z \\ p_1 & p_2 & p_3 \\ s_1 & s_2 & s_3 \end{bmatrix} =$$

$$\begin{bmatrix} (-\cos(\beta) \sin(\psi) \cos(\eta) - \sin(\beta) \sin(\eta)) \sin(\delta) \\ (-\sin(\beta) \sin(\psi) \cos(\eta) - \cos(\beta) \sin(\eta)) \sin(\delta) + \cos(\psi) \cos(\eta) \cos(\delta) \\ -(\cos(\beta) \sin(\psi) \cos(\eta) + \sin(\beta) \sin(\eta)) \cos(\delta) \end{bmatrix} = \bar{0}$$

$$\tan(\eta) = -\frac{\sin(\psi)}{\tan(\beta)} ; \Rightarrow \eta = \tan^{-1} \left(-\frac{\sin(\psi)}{\tan(\beta)} \right)$$

$\psi(\beta)$ and $\eta(\beta)$ are plotted in Figures 3-3 and 3-4. From these figures it is clear that when $\delta \rightarrow 0^\circ$ (when the Sun is almost in the orbital plane) the satellite has to make radical short-time movements. Especially the motion of the satellite about the yaw axis nearby $\beta = 0^\circ$ and $\beta = 180^\circ$ is critical because of the relatively large moment of inertia about this axis (I_z) and the high rotation speed (see Appendix C). [Ref. 37: pp. 75-78]

For this reason a limit value δ_L was chosen. If the satellite is in an orbit with $\delta > |\delta_L|$ then an alternative motion will be executed. The yaw-axis will keep a constant attitude: $\psi = 90^\circ$, so that the BAPTA-axis is perpendicular to the orbital plane. In this case the solar arrays would rotate $360^\circ/\text{orbit}$ in one direction. The power lines would therefore turn around the BAPTA-axis and after a while make the rotation of the arrays impossible. The only way to anticipate this is rotating them in the opposite direction during the eclipse. This alternative motion is plotted in Figure 3-5. [Ref. 37: pp. 75-78]

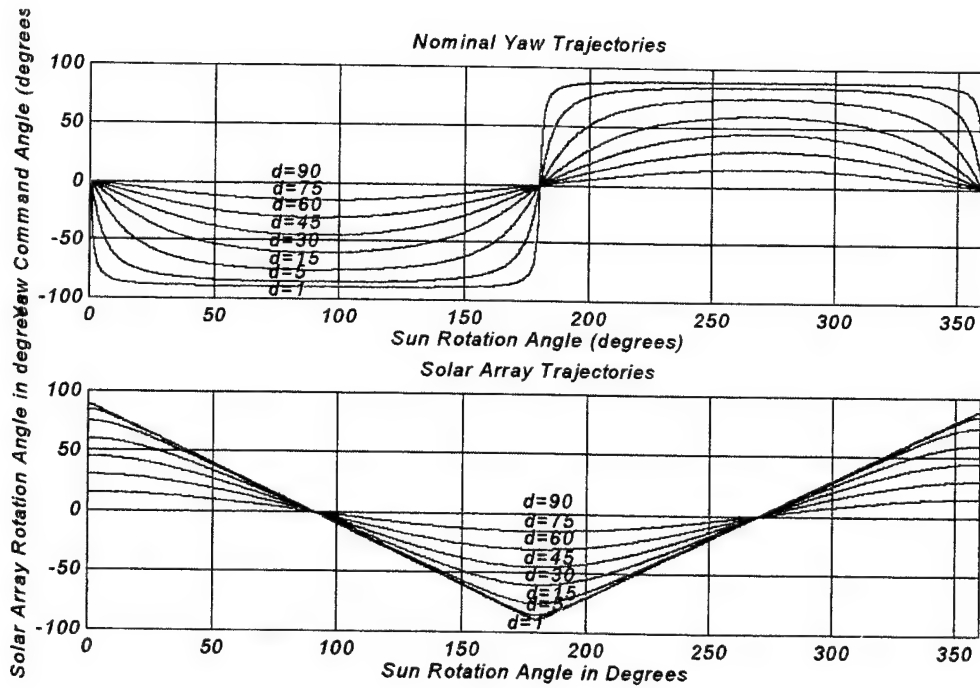


Figure 3-3: Motion of Yaw-axis (ψ) and solar array (η) during one orbit, starting at the sub-solar point (i.e., Noon) in terms of the sun rotation angle.

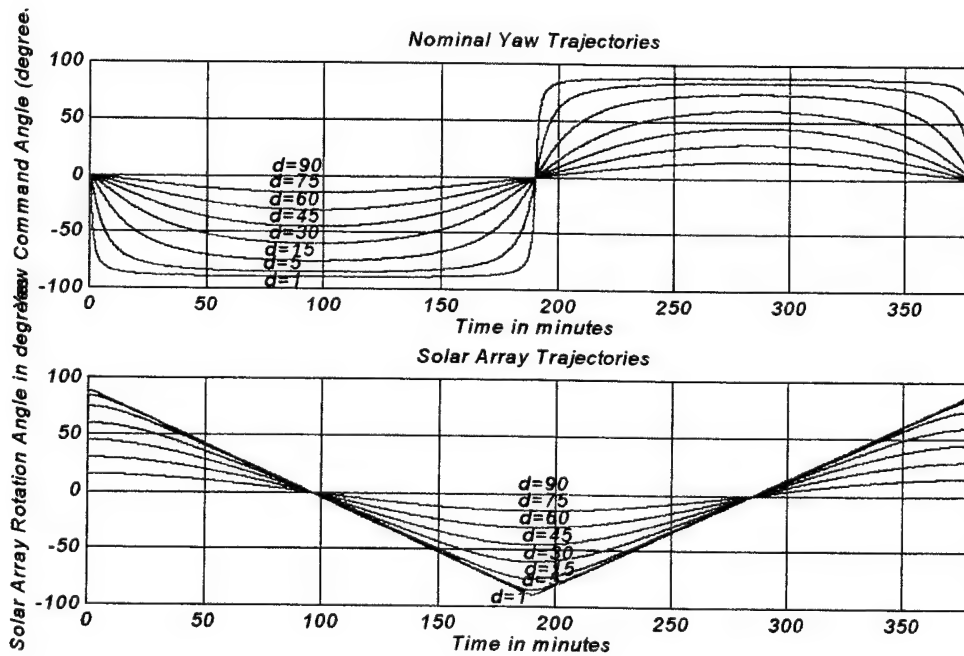


Figure 3-4: Motion of Yaw-axis (ψ) and solar arrays (η) during one orbit, starting at the sub-solar point in terms of the time in minutes.

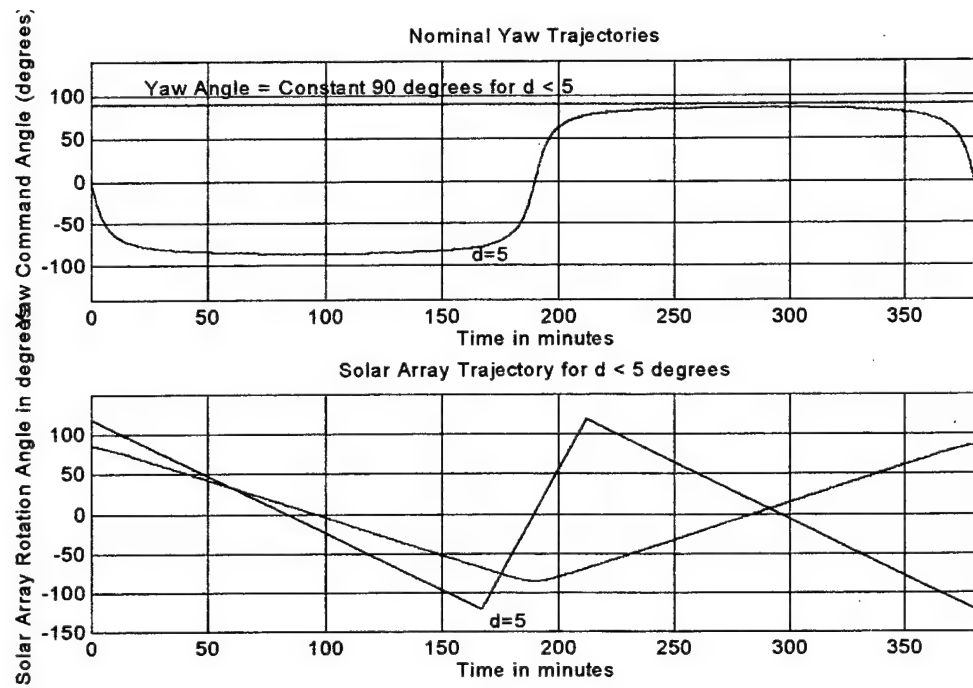


Figure 3-5: Alternative motion of yaw-axis (ψ) and solar arrays (η) during one orbit, starting at the sub-solar point, for $|\delta| > 5^\circ$.

This Page Intentionally Left Blank

IV. QUANTIFY DISTURBANCE ENVIRONMENT

In this part of the design we must understand what disturbances are acting on the spacecraft and then try to quantify them. Disturbance torques can be either external or internal. External disturbance torques consist of gravity gradient effects, magnetic field torques acting on the vehicle, the effects of solar radiation, and aerodynamic effects. These external disturbance torques are most likely the largest source of disturbance to the spacecraft and may be easier to quantify. Internal disturbance torques come from within the spacecraft. As a result, we have a great amount of control over these. [Ref. 6: p. 352]

In this section an investigation of both external and internal disturbance torques will be performed. And, a knowledge of both magnitude and direction of disturbance torques and angular momentum will be attained. This information will be very useful in selecting and sizing the ADCS hardware. [Ref. 6: p. 352]

A. EXTERNAL DISTURBANCE TORQUES

From the standpoint of stability and control, the principal external torques come from four environmental effects: solar radiation pressure, gravity gradients, aerodynamics and magnetics. Solar radiation pressure is generally a significant source of attitude and trajectory errors for high altitude (> 1000 km). Gravity gradients, which result from the extended dimensions of the spacecraft, may either cause disturbing or perturbing torques or provide restoring torques when the effect is used for attitude control. Gravity gradients, as well as the magnetic torques caused by the interaction of the spacecraft's magnetic materials with the planetary magnetic field are most significant at low altitudes (< 1000 km). Similarly, aerodynamic effects are significant only below 500 km altitude and are generally negligible above 1000 km. Finally, aerodynamic torques acting on the spacecraft are functions of spacecraft geometry, attitude and altitude. Figure 4-1 illustrates the change in external disturbance as a function of altitude. [Ref. 22: pp. 77-78]

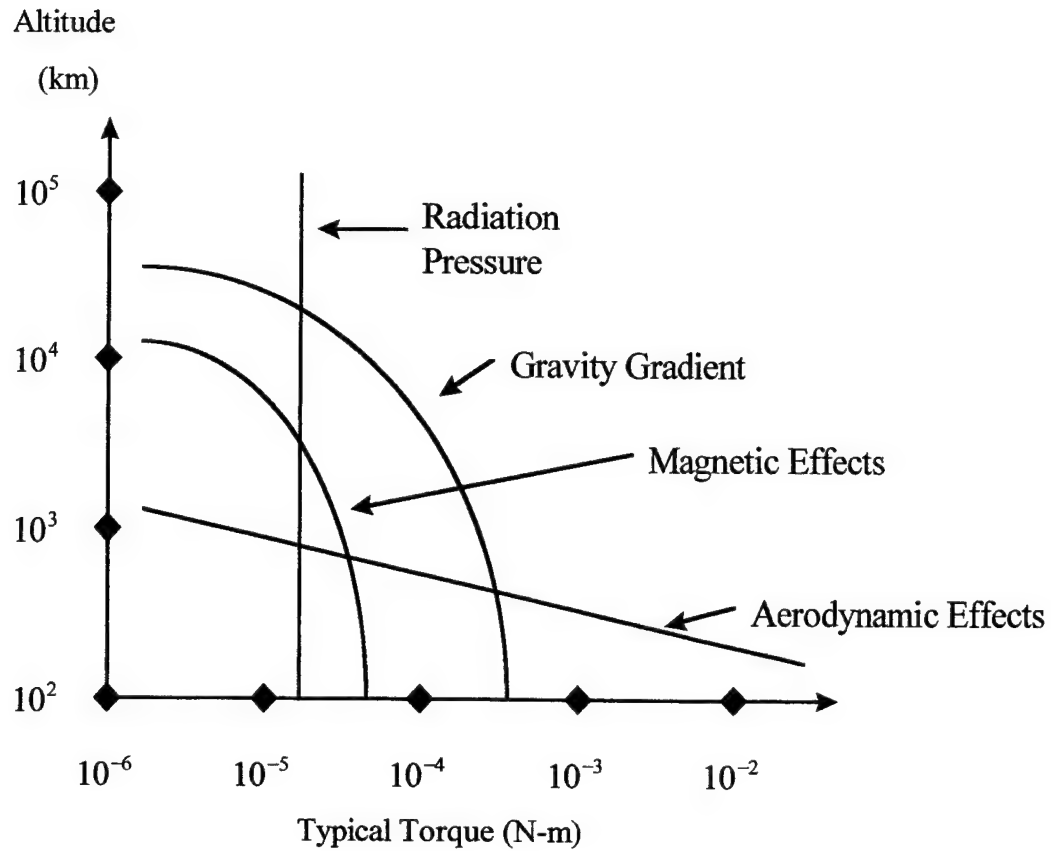


Figure 4-1: Typical torques on a satellite as a function of altitude

1. Solar Pressure Torques

The solar pressure torque is the major long-term disturbance torque for a spacecraft at higher altitudes. The solar radiation forces are due to photons impinging on the spacecraft surfaces. In general a fraction, ρ_s , of the impinging photons will be specularly reflected, a fraction, ρ_d , will be diffusely reflected, and a fraction, ρ_a , will be absorbed by the surface (see Figure 4-2). The solar pressure moment \bar{M}_s is given by equation 4-1. [Ref. 25: pp. 133-134]

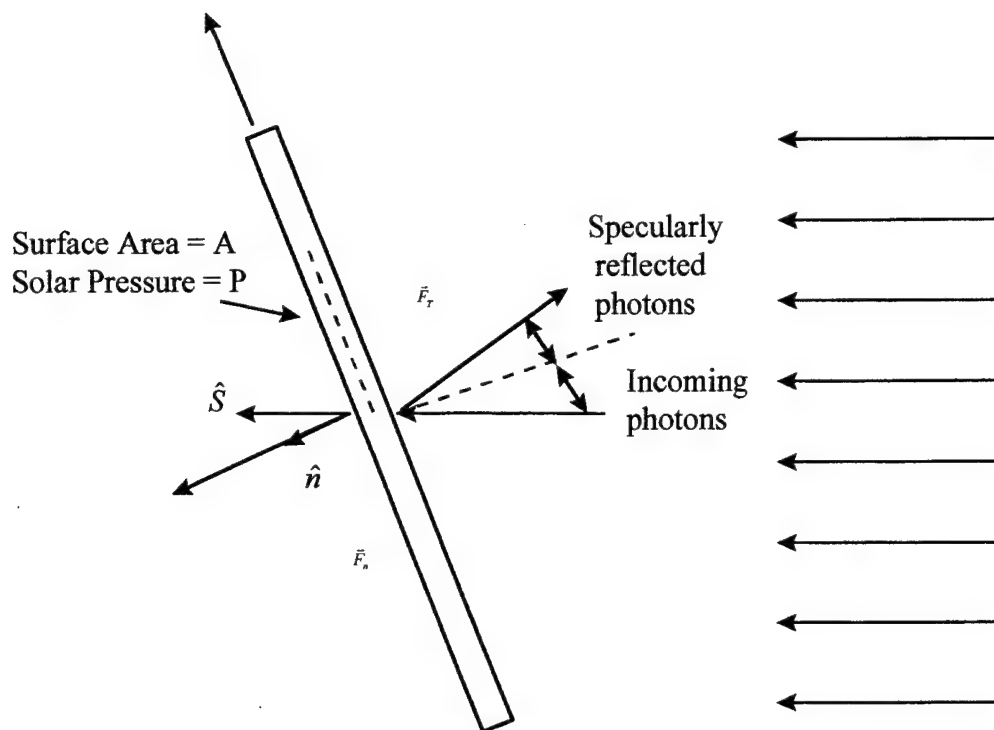


Figure 4-2: Solar Radiation Force on a Spacecraft Surface

$$\vec{M}_s = PA(\hat{n} \cdot \hat{S})\vec{r} \times \left[(1 - \rho_s)\hat{S} + 2\left(\rho_s + \frac{1}{3}\rho_d\right)\hat{n} \right] \quad (4-1)$$

where \vec{r} is the vector from the center of mass of the spacecraft to the center of pressure of a given area, A . The solar radiation pressure, P , is generally assumed to be constant and to have the value $4.644 \times 10^{-6} \text{ N/m}^2$. [Ref. 25: pp. 133-134]

2. Gravity Gradient Torques

A spacecraft body experiences a gravity-gradient torque due to the variation of distances between the spacecraft mass points and the center of the mass of the earth. The gravity gradient has been used on early low earth-orbit satellites to maintain the earth pointing of antennas or other instruments. The gravitational torques about the principal body axes e_1 , e_2 , and e_3 are given in equation 4-2. [Ref. 25: p. 131]

$$\begin{aligned}
T_1^{(g)} &= -K(I_{33} - I_{22})\cos(\theta_2)\sin(\theta_3)\sin(\theta_2) = 0 \quad \text{for } \theta_2 = \theta_3 = 0 \\
T_2^{(g)} &= K(I_{11} - I_{33})\cos(\theta_3)\cos(\theta_2)\sin(\theta_2) \\
T_3^{(g)} &= -K(I_{22} - I_{11})\cos(\theta_3)[\cos(\theta_2)]^2\sin(\theta_3).
\end{aligned} \tag{4-2}$$

3. Aerodynamic Torques

The satellite will, in general, pass through an atmosphere of density ρ , with a velocity \vec{v} . The magnitude of the aerodynamic force $F^{(a)}$ is then given as

$$F^{(a)} = \frac{1}{2}\rho\vec{v} \cdot \vec{v}AC_d \tag{4-3}$$

where A is the reference area of the satellite (such as the cross section along \vec{v}) and C_d is the total drag coefficient. Torque is given by

$$T^{(a)} = \frac{1}{2}\rho v^2 l SC_d \tag{4-4}$$

or

$$\vec{T}^{(a)} = \frac{1}{2}\rho C_d A v^2 (\hat{u} \times \vec{l}_p) \tag{4-5}$$

where l is the length of the perpendicular from the mass center to the force line of action and \hat{u} is the unit vector in the velocity direction. [Ref. 22: p. 90]

Difficulties arise in determining ρ , l , and C_d . At satellite altitudes, ρ is highly dependent on the time of day and the level of solar activity. For example, at 600 km the solar daytime maximum density and the nighttime minimum density may differ by a factor of 100. Table 4-1 gives typical values of the daytime maximum air density as a function of orbital height. It is important to note that as altitude increase the aerodynamic pressure effects decrease. As a result, our satellite orbit of 11,000 km will have negligible aerodynamic pressure effects. [Ref. 22: p. 90]

HEIGHT (km)	Density (kg / m^3)
200	4×10^{-10}
300	5×10^{-11}
400	1.5×10^{-11}
500	5×10^{-12}
600	2×10^{-12}
700	8×10^{-13}

Table 4-1: Density as a function of height above the earth's surface

For a satellite having a spherical shape, an average value of $C_d = 2.2$ can be taken which is computed assuming "free molecular flow" (i.e., the molecular mean free path is assumed to be large compared to the size of the satellite and, therefore, inter-particle collisions are ignored). For a cylinder C_d may be taken as 3. [Ref. 22: p. 90]

4. Disturbance Torques Due to the Geomagnetic Field

a. Geomagnetic Field

The geomagnetic field can be represented to a first order approximation as a magnetic dipole with the axis inclined to the Earth's spin axis by approximately 11.5° . Observations have shown that the sources of the geomagnetic field are in the core and at the surface of the Earth as well as in the upper atmosphere. The primary source is presumed to be a system of electric currents in the Earth's molten interior. The changes in these currents account for the migration of the geomagnetic poles on the Earth's surface. [Ref. 22: p. 84]

The geomagnetic field, \vec{B} , is a function of altitude, longitude, and latitude. And, can be expressed in units of gauss, gamma (γ), or tesla (webers per square meter). A one gauss magnetic field intensity acting on a unit magnetic pole produces a force on one dyne. The magnitude of the field is given by equation 4-6. [Ref. 22: p. 84]

$$|\vec{B}_o| = \frac{\mu_E}{r^3} (1 + 3 \sin \theta_m)^{1/2} \quad (4-6)$$

where θ_m is the magnetic latitude measured from the geomagnetic equator. At the earth's surface along the geomagnetic equator, $\theta_m = 0$, and $B_o = 0.311$ gauss. At the magnetic pole, $B_o = 0.622$ gauss or twice the equatorial value. [Ref. 22: p. 84]

A plot of the Earth's equatorial magnetic field intensity B_{eq} in tesla units as a function of altitude is shown in Figure 4-3. The effect of latitude is given in Figure 4-4, where for any latitude $B_o = \alpha B_{eq}$. [Ref. 22: pp. 87-88]

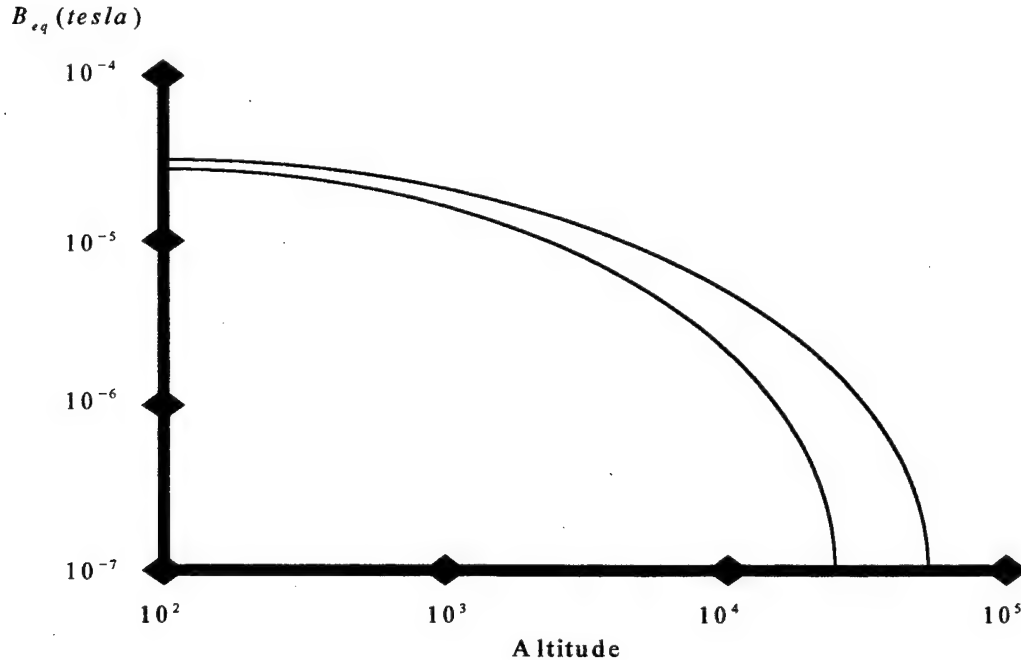


Figure 4-3: Earth's Magnetic field intensity vs altitude above the magnetic equator.

Factor, α

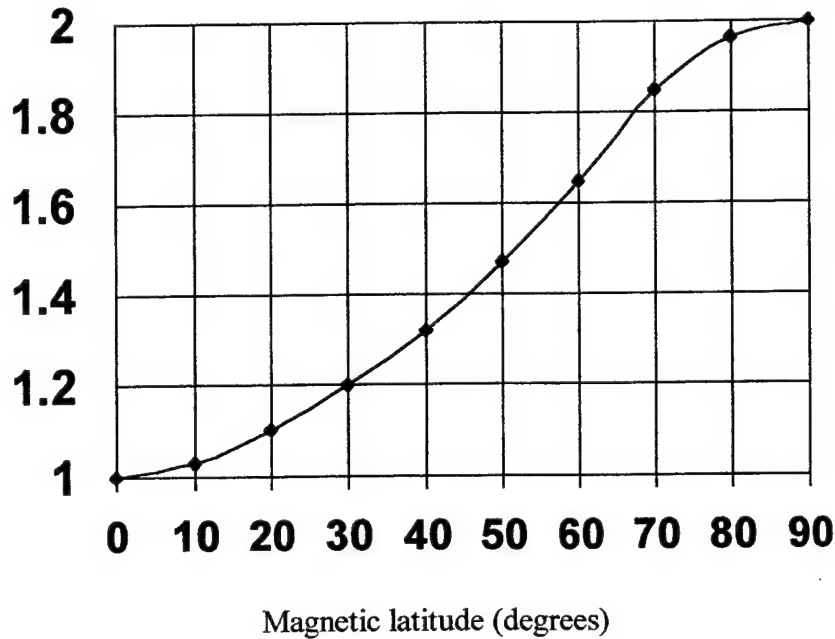


Figure 4-4: Multiplication factor α for magnetic field intensity as a function of magnetic latitude. For any latitude $B_o = \alpha B_{equatorial}$.

b. Magnetic Torques

Magnetic torques acting on a spacecraft can result from the interaction of the spacecraft's residual magnetic field and the geomagnetic field. Thus, if \vec{M} is the sum of all magnetic moments in the spacecraft the torque acting on the spacecraft is

$$\vec{T}^{(m)} = \vec{M} \times \vec{B} \quad (4-7)$$

where \vec{B} = the geomagnetic field vector. In general, \vec{M} can be caused by permanent and induced magnetism or by spacecraft-generated current loops. This is how Magnetic torque rods operate and can be used for momentum dumping. The units of M may be gauss-cm³, ampere-m², or pole-cm. For example, if M is in ampere-m², then $T^{(m)}$ is in Newton-meters. [Ref. 22: p. 89]

The concept of Magnetic Torquers is simple, but there is a difficulty in quantifying external disturbance torques due to the geomagnetic field. \vec{M} is the magnetic field produced by the spacecraft and is generally unknown until the spacecraft is built and tested. Once tested, an estimate for the magnetic disturbance torque can be made. [Ref. 22: p. 89]

B. MATLAB SIMULATION OF EXTERNAL DISTURBANCE TORQUES

To attain an accurate quantifiable value for external disturbance torques a matlab simulation was developed for each of the external disturbances. A brief explanation of each scenario follows:

1. Solar Pressure Torques

1. Developed the Simulink model appropriate for the Solar Pressure Simulation (see Appendix E).
2. Established the initial conditions for the velocity and position vector of the spacecraft relative to the earth centered inertial system (see Appendix E).
3. Defined various constants and solved for v and δ as a function of time. v is the earth centered true anomaly and δ is the sun orbital element analogous to v (see Appendix E).
4. Established numerous direction cosine matrices. This part of the process was very tedious. The details are excluded because it is assumed the reader is familiar with the various orbit frames of reference (see Appendix E).
5. Computed the unit vector from the spacecraft to the sun (see Appendix E).
6. Defined unit vectors that are perpendicular to each exterior piece of the spacecraft (see Appendix E).
7. Defined dr vectors from the center of mass to each external piece's center of pressure (see Appendix E).
8. Performed various vector operations (see Appendix E).

9. Calculated the moment due to solar pressure as given by equation 4-1 [Ref. 25: p. 133]:

$$\vec{M}_s = PA(\hat{n} \cdot \vec{S})\vec{r} \times \left[(1 + p_s)\vec{S} + 2\left(p_s + \left(\frac{1}{3}\right)p_d\hat{n}\right) \right]$$

where,

$\vec{M}_s \equiv$ The solar radiation pressure moment.

$\vec{r} \equiv$ The vector from the center of mass of the spacecraft to the center of pressure of a given area, A.

$P \equiv$ The solar radiation pressure.

$A \equiv$ Area

$p_s \equiv$ Fraction of photons impinging on the spacecraft's surface that are specularly reflected.

$p_d \equiv$ Fraction of photons impinging on the spacecraft's surface that are diffusely reflected.

10. Computed the M_1 , M_2 , and M_3 for solar pressure torques for each instant in time (see Appendix A-10 to A-17).

11. Solved for angular velocities iteratively (see Appendix E).

12. Utilized Poisson's equations to solve for the dcm components from the body frame to the orbit frame iteratively (see Appendix E).

13. Solved for r and v iteratively utilizing state space variables (see Appendix E).

Figures 4-5 through 4-7 are the result of the calculations described above. A brief explanation of each figure follows:

a. Figure 4-5

Figure 4-5 is a graph of the three components of torque, (i.e., T_x , T_y , and T_z) acting on the spacecraft due only to solar pressure disturbances, when the spacecraft is not being controlled by the Attitude Dynamics and Control Subsystem. Also, the torque components are with respect to the spacecraft's body fixed frame.

b. Figure 4-6

Figure 4-6 is a graph of the three components of the spacecraft's angular velocity due only to solar pressure disturbances when the spacecraft is not being controlled by the Attitude Dynamics and Control Subsystem. Also, the angular velocity components are expressed with respect to the spacecraft's body fixed frame.

c. Figure 4-7

Figure 4-7 is a graph of the three components of torque, (i.e., T_x , T_y , and T_z) acting on the spacecraft due only to solar pressure disturbances, when the spacecraft is being controlled by the Attitude Dynamics and Control Subsystem and is maintaining a nadir pointing configuration. Also, the torque components are with respect to the spacecraft body fixed frame.

It should be noted that the solar radiation torque component along the pitch axis is periodic and secular, with a period equal to the orbit period. Hence the net effect of this torque is a build up of Angular Momentum. On the other hand, the components along the other axes have cyclic components, resulting in no net change in the spacecraft angular momentum over a full orbit.

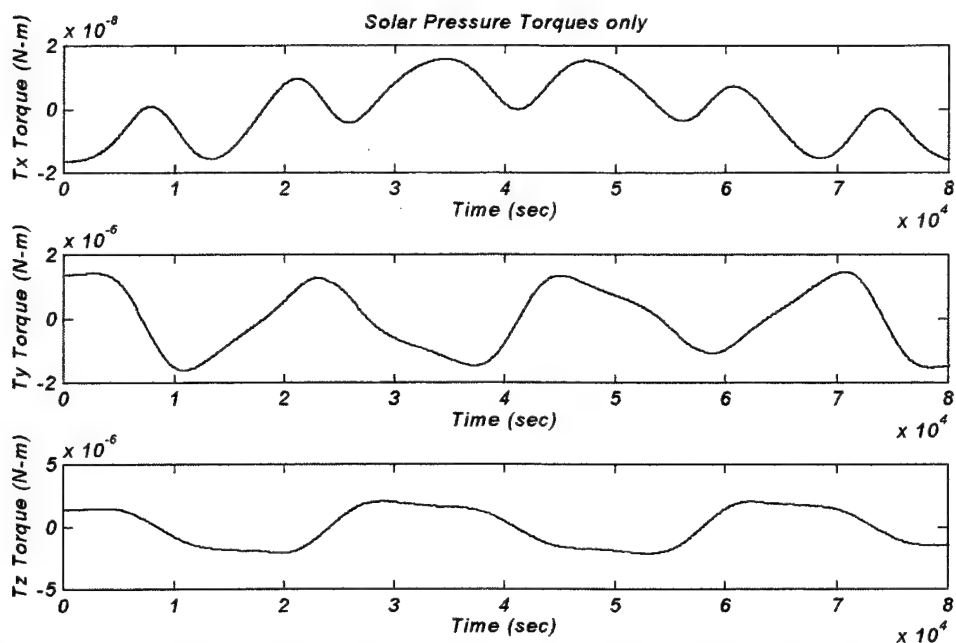


Figure 4-5: The three components of torque due to solar pressure as a function of time, with no control.

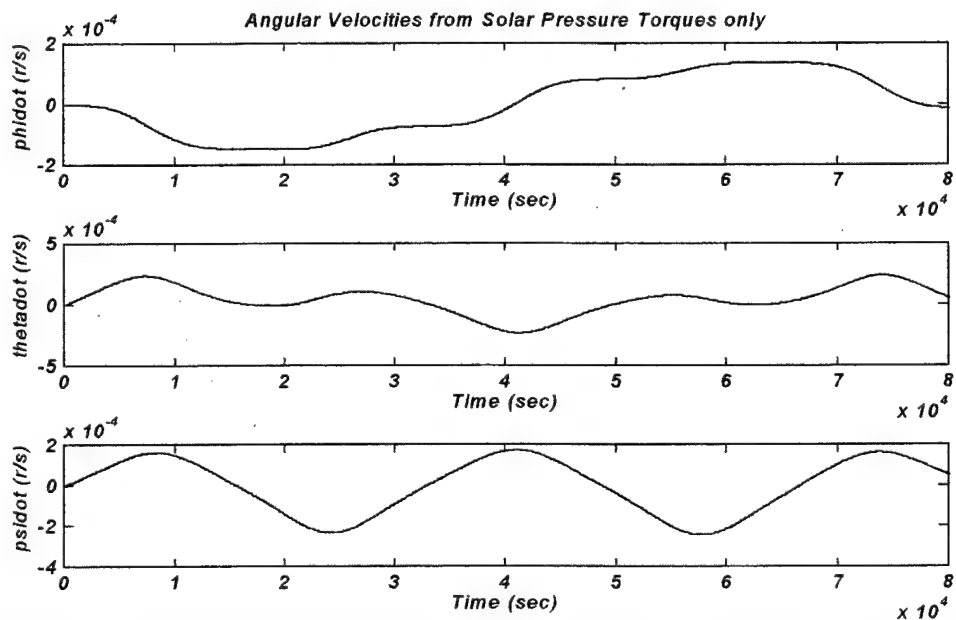


Figure 4-6: The three body components of angular velocity due to solar pressure as a function of time, with no control.

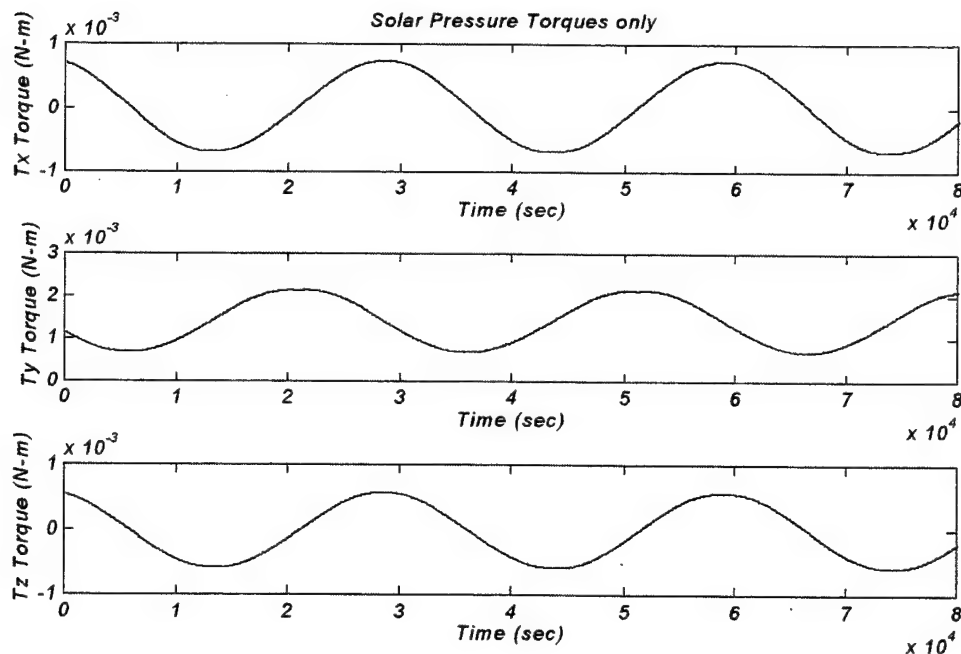


Figure 4-7: The three components of torque due to solar pressure as a function of time, with active control.

2. Gravity Gradient Torques

1. Developed the simulink diagram (see Appendix E).
2. Defined constants and user friendly conversions (see Appendix E).
3. Determined initial conditions for r , v , and the dcm between orbit frame and principal inertia frame (see Appendix E).
4. Solved for angular velocities iteratively (see Appendix E).
5. Utilized Poisson's equations to solve for the dcm components from the body frame to the orbit frame iteratively (see Appendix E).
6. Solved for r and v iteratively utilizing state space variables (see Appendix E).
7. Calculated the moment due to Gravity Gradient as given by equation 4-11.

$$T_1^{(g)} = K(I_{33} - I_{22})a_{21}a_{31}$$

$$T_2^{(g)} = K(I_{11} - I_{33})a_{11}a_{31}$$

$$T_3^{(g)} = K(I_{22} - I_{11})a_{11}a_{21}$$

Figures 4-8 and 4-9 are the result of the calculations described above. A brief explanation of each figure follows:

a. Figure 4-8

Figure 4-8 is a graph of the three components of torque, (i.e. T_x , T_y , and T_z) acting on the spacecraft due only to gravity gradient disturbances, when the spacecraft is not being controlled by the Attitude Dynamics and Control Subsystem. Also, the torque components are with respect to the spacecraft's body fixed frame and increase over time such that they cause the spacecraft to become unstable.

b. Figure 4-9

Figure 4-9 is a graph of the three components of the spacecraft's angular velocity due only to gravity gradient disturbances when the spacecraft is not being controlled by the Attitude Dynamics and Control Subsystem. Also, the angular velocity components are expressed with respect to the spacecraft's body fixed frame.

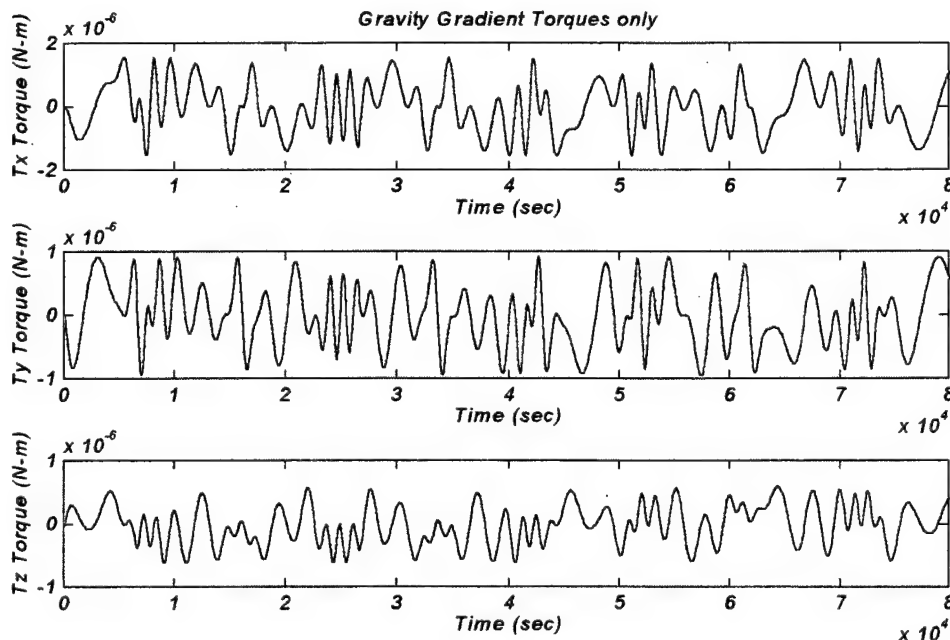


Figure 4-8: The three components of torque due to gravity gradients as a function of time, with no control.

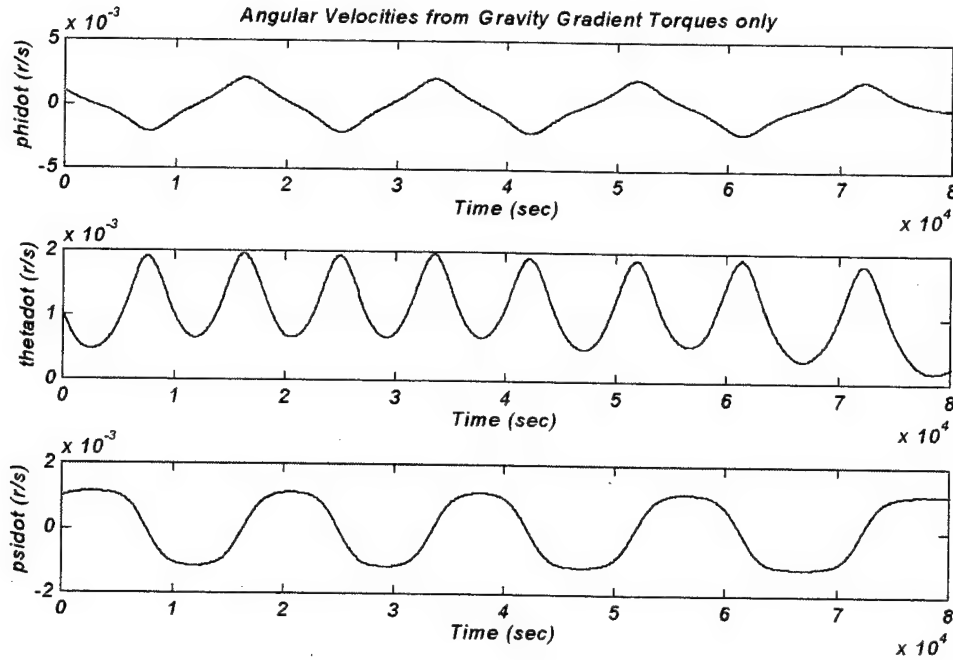


Figure 4-9: The three body components of angular velocity due to gravity gradients as a function of time, with no control.

3. Aerodynamic Pressure Torques

1. Calculating the Aerodynamic Pressure Torques was very similar to calculating solar pressure torques. Nearly the same technique was used except for the following (see Appendix E).

2. The fundamental equation used to compute is given by equation 4-5 [Ref. 6: p. 309]:

$$\vec{M} = \left(\frac{1}{2}\right) \rho C_d A v^2 (\hat{u}_v \times \vec{I}_{cp})$$

where,

- $\vec{M} \equiv$ Torque due to Aerodynamic Pressure
- $\rho \equiv$ Atmospheric density
- $C_d \equiv$ Coefficient of drag
- $A \equiv$ Area perpendicular to \hat{u}_v

$\hat{u}_v \equiv$ Unit vector in velocity direction

$\vec{I}_{cp} \equiv$ Vector distance from center of mass to center-of-

pressure

3. Computed the density (ρ) as a function of height above the earth (see Appendix E).
4. Computed the cross sectional areas of the spacecraft in the three body frame coordinate axis directions (see Appendix E).
5. Used the same Euler rates and Poisson's equations to solve iteratively (see Appendix E).
6. Utilized state space variables to solve for r and v iteratively (see Appendix E).

Figures 4-10 through 4-12 are the result of the calculations described above. A brief explanation of each figure follows:

a. Figure 4-10

Figure 4-10 is a graph of the three components of torque, (i.e., T_x , T_y , and T_z) acting on the spacecraft due only to aerodynamic pressure disturbances, when the spacecraft is not being controlled by the Attitude Dynamics and Control Subsystem. The torque components are with respect to the spacecraft's body fixed frame. Also, these torque magnitudes are orders of magnitude less than gravity gradient and solar pressure disturbances. And, catastrophic cancellation (i.e., computer noise) most likely occurred when calculating T_y . This was probably due to the fact that the torque values were so small. As a result, the torques due to aerodynamic pressure are inconsequential.

b. Figure 4-11

Figure 4-11 is a graph of the three components of the spacecraft's angular velocity due only to aerodynamic pressure disturbances when the spacecraft is not being controlled by the Attitude Dynamics and Control Subsystem. The angular velocity components are expressed with respect to the spacecraft's body fixed frame. Also, the

aerodynamic torques are orders of magnitude less than gravity gradient and solar pressure disturbances. Therefore, the effects are inconsequential.

c. Figure 4-12

Figures 4-12 is a graph of the three components of torque, (i.e., T_x , T_y , and T_z) acting on the spacecraft due only to aerodynamic pressure disturbances, when the spacecraft is being controlled by the Attitude Dynamics and Control Subsystem and maintaining a nadir pointing configuration. The torque components are with respect to the spacecraft body fixed frame. Also, the effects of aerodynamic pressure disturbances are orders of magnitude less than gravity gradient and solar pressure disturbances. Also, catastrophic cancellation (i.e., computer noise) may have occurred. As a result, the torques due to aerodynamic pressure are inconsequential.

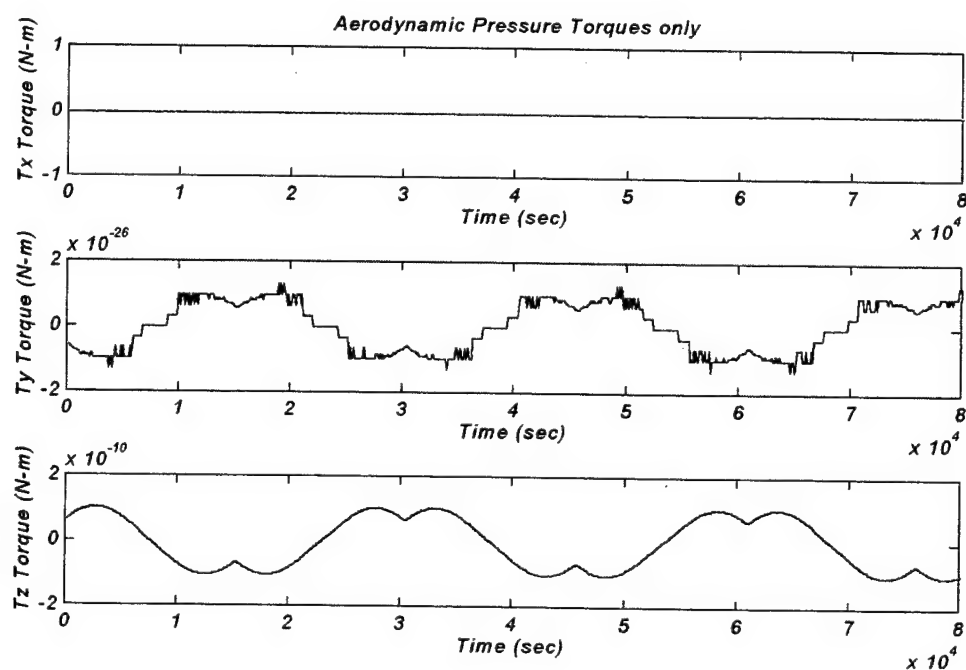


Figure 4-10: The three components of torque due to Aerodynamic Pressure as a function of time, with no control.

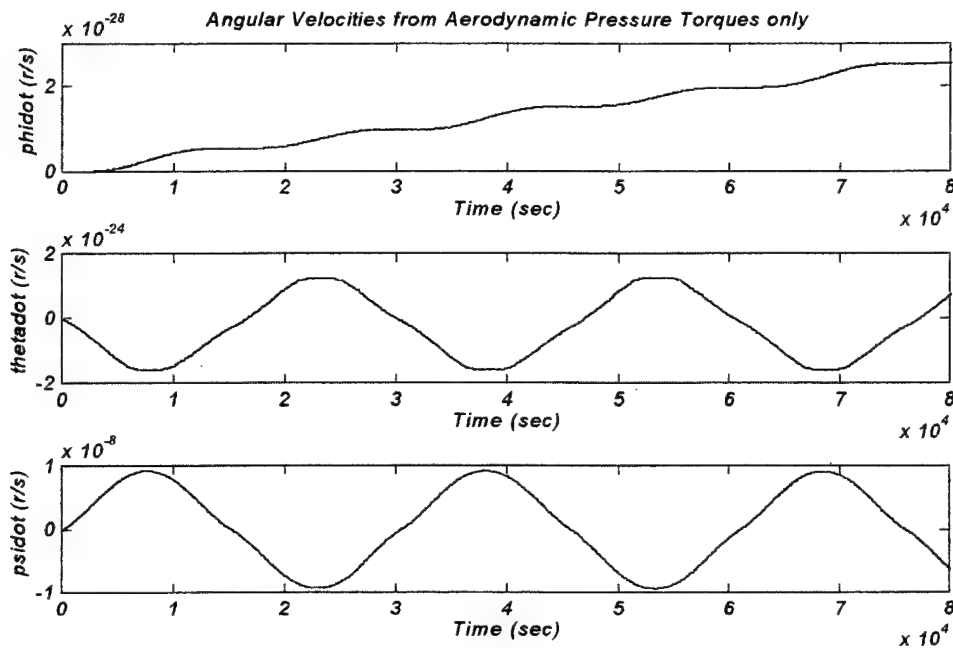


Figure 4-11: The three body components of angular velocity due to Aerodynamic Pressure as a function of time, with no control.

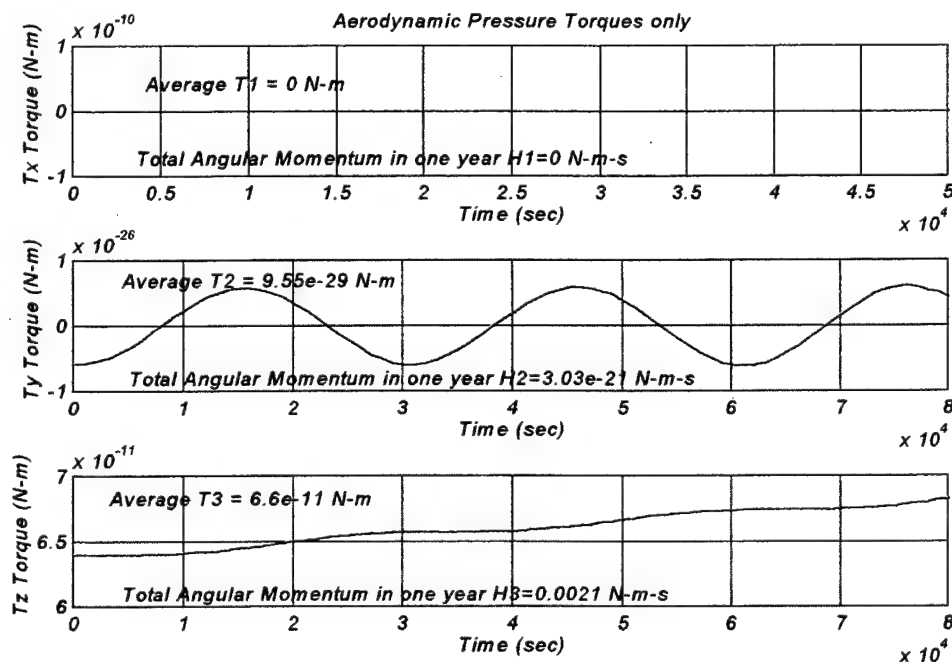


Figure 4-12: The three components of torque due to aerodynamic pressure disturbances as a function of time, with active control.

4. Combined External Disturbance Torques

Next, calculations were made for when all three torques acted on the spacecraft simultaneously. This required combining the three separate Matlab programs into one program. The motion of the spacecraft was then simulated and the sum of the environmental disturbance torques computed (see Appendix E).

Finally, an estimation of the total torque imparted to the spacecraft over one year for each of the four situations was performed. To do this for gravity gradient and aerodynamic required taking data from several orbits, then computing the average torque over that period and finally multiplying by the time expired. This method is good for gravity gradient and aerodynamic as long as data from several orbits is computed. Computing the total torque from the solar pressure is more complicated. Since the Beta angle changes with time throughout the year, several orbits will not be adequate. So, the simulation was ran for a delta t of one year, then the total torque was computed. The results can be seen in Table 4-2.

	SOLAR PRESSURE	GRAVITY GRADIENT	AERO- DYNAMIC	COMBINED
Average T_1	9.33e-10 Nm	≈ 0	≈ 0	-2.5e-6 Nm
Average T_2	1.33e-6 Nm	1.2e-6 Nm	9.55e-29 Nm	1.4e-4 Nm
Average T_3	5.03e-8 Nm	≈ 0	6.6e-11 Nm	-2.78e-6 Nm
Maximum Torque (T_{\max})	1.8e-6 Nm	1e-4 Nm	7e-11 Nm	2.2e-4 Nm
Estimated H_1 (1 year)	0.0296 Nms	≈ 0	≈ 0	0.1718 Nms
Estimated H_2 (1 year)	42.23 Nms	3155 Nms	3.03e-21 Nms	3197.23 Nms
Estimated H_3 (1 year)	1.594 Nms	≈ 0	0.0021 Nms	0.19033 Nms

Table 4-2: Summary of External Disturbance Torques and Angular Momentum Imparted to the Spacecraft

Figures 4-13 through 4-15 are the result of the calculations described above. A brief explanation of each figure follows:

a. Figure 4-13

Figure 4-13 is a graph of the three components of torque, (i.e. T_x , T_y , and T_z) acting on the spacecraft due to solar pressure, gravity gradient and aerodynamic disturbances, when the spacecraft is not being controlled by the Attitude Dynamics and Control Subsystem. Also, the torque components are with respect to the spacecraft's body fixed frame.

b. Figure 4-14

Figure 4-14 is a graph of the three components of the spacecraft's angular velocity due to solar pressure, gravity gradient and aerodynamic pressure disturbances when the spacecraft is not being controlled by the Attitude Dynamics and Control Subsystem. Also, the angular velocity components are expressed with respect to the spacecraft's body fixed frame.

c. Figure 4-15

Figures 4-15 is a graph of the three components of torque, (i.e. T_x , T_y , and T_z) acting on the spacecraft due to solar pressure, gravity gradient and aerodynamic pressure disturbances, when the spacecraft is being controlled by the Attitude Dynamics and Control Subsystem. Also, the torque components are with respect to the spacecraft body fixed frame.

It should be noted that the total torque component along the pitch axis is periodic and secular, with a period equal to the orbit period. Hence the net effect of this torque is a build up of Angular Momentum. On the other hand, the components along the other axes have cyclic components, resulting in no net change in the spacecraft angular momentum over a full orbit.

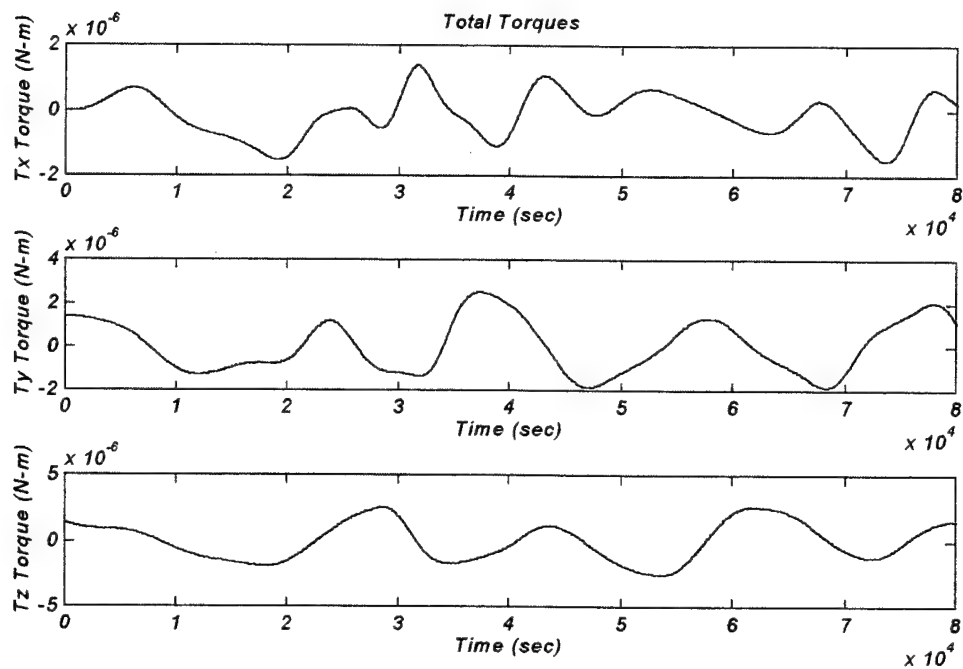


Figure 4-13: The three components of torque due to total external disturbance torques as a function of time, with no control.

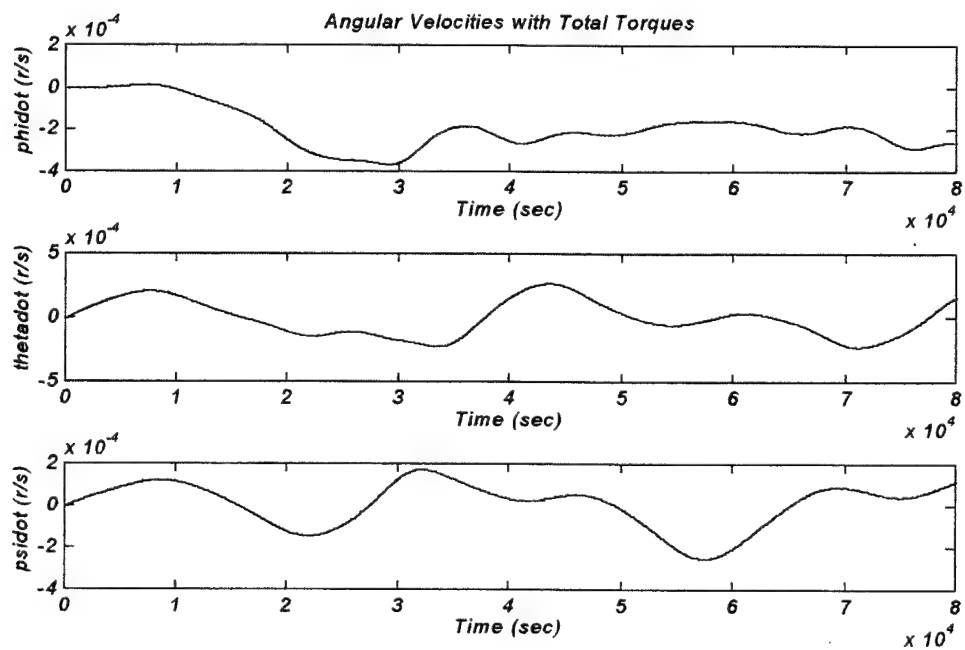


Figure 4-14: The three body components of angular velocity due to total external disturbance torques as a function of time, with no control.

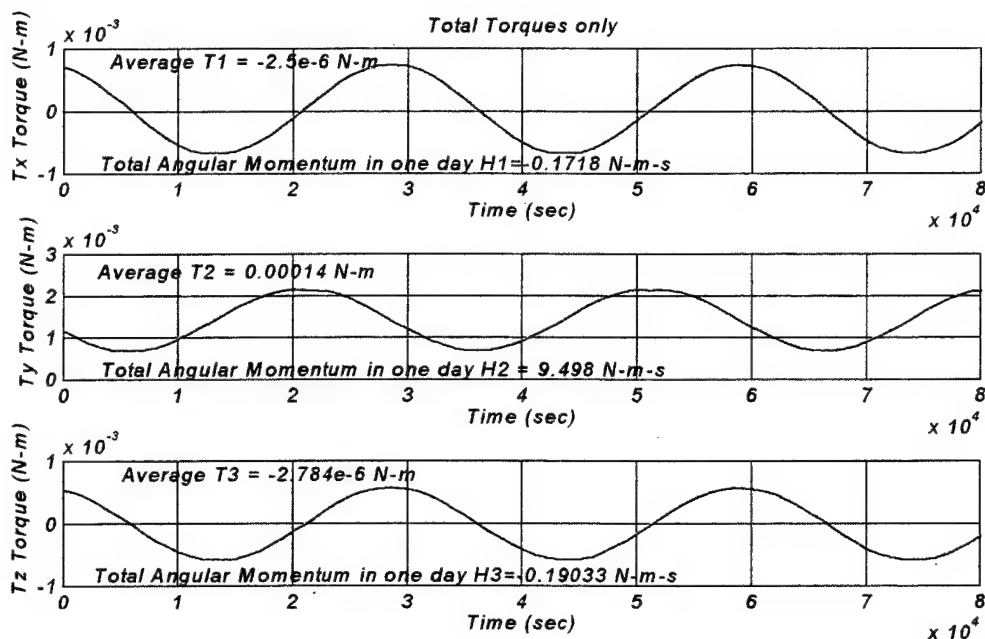


Figure 4-15: The three components of torque due to solar pressure, gravity gradients and aerodynamic pressure disturbances as a function of time, with active control.

C. INTERNAL DISTURBANCE TORQUES

There are several other kinds of disturbance torques that are internal to the spacecraft. First, these torques may be due to moving parts such as rotating wheels, circulating fluids or tracking devices. Fortunately, the ADCS designer has some control over these torques. For example, if a disturbance torque in one component is found to be much larger than the others, the component can be changed in order to meet higher specifications. However, there is a trade-off here. A change can be made to meet higher standards only at the expense of more mass and/or cost. Next, an internal torque may arise due to thruster mis-alignment with the center of gravity. This will only occur during thruster firing and will be corrected in a closed loop Attitude Dynamics and Control Subsystem. The concern here is that the disturbance will not cause the spacecraft to exceed the minimum pointing requirements. [Ref. 6: p. 352]

Of greater importance is slosh and mechanical machinery torques. They can, however, be controlled by proper selection of hardware. Table 4-3 summarizes the common internal disturbance torques. [Ref. 6: p.352]

Disturbances	Effect on Vehicle	Typical Values
Uncertainty in center of gravity (cg)	<ul style="list-style-type: none"> • Unbalanced torques during firing of coupled thrusters • Unwanted torques during translation thrusting 	1 to 3 cm
Thruster misalignment	Same as cg uncertainty	0.1° to 0.5°
Mismatch of thruster outputs	Similar to cg uncertainty	± 5%
Rotating machinery (pumps, tape recorders)	Torques that perturb both stability & accuracy	Dependent on spacecraft design; may be compensated by counter-rotating elements
Liquid sloshing	Torques due to fluid motion and variation in center of mass location	Dependent on specific design; may be controlled by bladders or baffles
Dynamics of flexible bodies	Oscillatory resonance at bending frequencies, limiting control bandwidth	Depends on spacecraft structure
Thermal shocks on flexible appendages	Attitude disturbances when entering/leaving eclipse	Depends on spacecraft structure. Worst for gravity gradient systems with long inertia booms

Table 4-3: Principal Internal Disturbance Torques which spacecraft designers have a great deal of control over.

V. ATTITUDE DYNAMICS AND CONTROL SUBSYSTEM HARDWARE SELECTION AND DESCRIPTION

A. SIZING THE ADCS REACTION WHEELS

1. Torque and Angular Momentum Requirements Due to Yaw Steering

In Chapter III the yaw steering requirements of the spacecraft were investigated and it was concluded the Yaw command angle could be stated as:

$$\psi(\beta, \delta) = \tan^{-1} \left[\frac{-\sin(\beta)}{\tan(\delta)} \right] \quad (5-1)$$

where,

β is the angle in the orbital plane between the point with minimum distance (sub-solar point) to the Sun and the satellite. And, δ is the angle between the orbital plane and the direction of the Sun (see Figure 5-1).

By looking at Figure 3-4 it is apparent that the angular velocity and angular acceleration maximums occur for the minimum value of δ . And, since our minimum δ is equal to 5° we will single this curve out and find the maximum angular velocity and maximum angular acceleration the spacecraft must perform in the yaw direction. Since this requirement is the most demanding; if we can show it will be met then any other torque and angular momentum requirement will also be satisfied.

Figure 5-1 is a graph of $\psi(\beta, 5^\circ) = \tan^{-1} \left[\frac{-\sin(\beta)}{\tan(5^\circ)} \right]$ for $\delta = 5^\circ$. It can readily be

shown that $\psi'(\beta, 5^\circ)$ which is the angular velocity is given by

$$\psi'(\beta, 5^\circ) \approx (-0.1806) * \left[\frac{\cos(2.76e - 4 * t)}{1 + 130.646 * [\sin(2.76e - 4 * t)]^2} \right] \quad (5-2)$$

and, $\psi''(\beta, 5^\circ)$ which is the angular acceleration is given by

$$\psi''(\beta, 5^\circ) \approx (4.98e-5) * \left[\frac{\sin(2.76e-4 * t)}{1 + 130.646 * [\sin(2.76e-4 * t)]^2} \right] +$$

$$(0.013) * \left[\frac{[\cos(2.76e-4 * t)]^2 * \sin(2.756e-4 * t)}{[1 + (130.646) * [\sin(2.76e-4 * t)]^2]^2} \right] \quad (5-3)$$

Figures 5-2 and 5-3 are graphs of the angular velocity and angular acceleration respectively for $\delta = 5^\circ$.

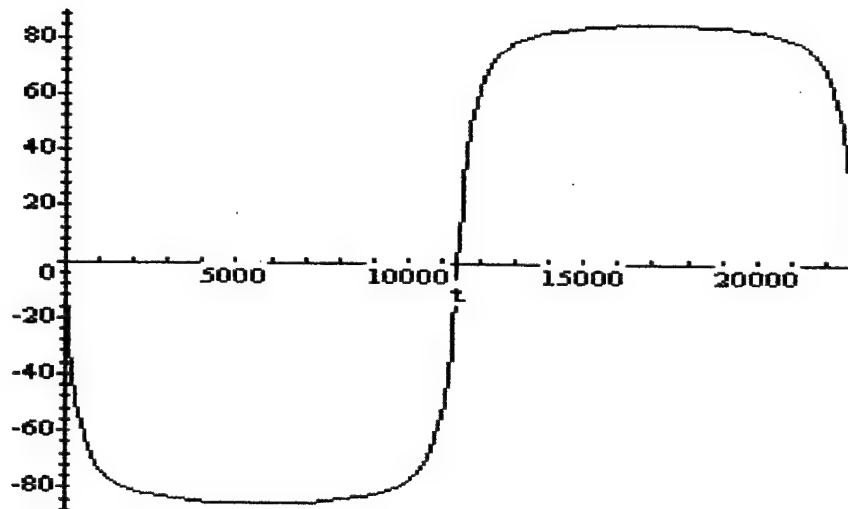


Figure 5-1: Graph of $\psi(\beta, 5^\circ)$, where ψ is in degrees and time is in seconds.

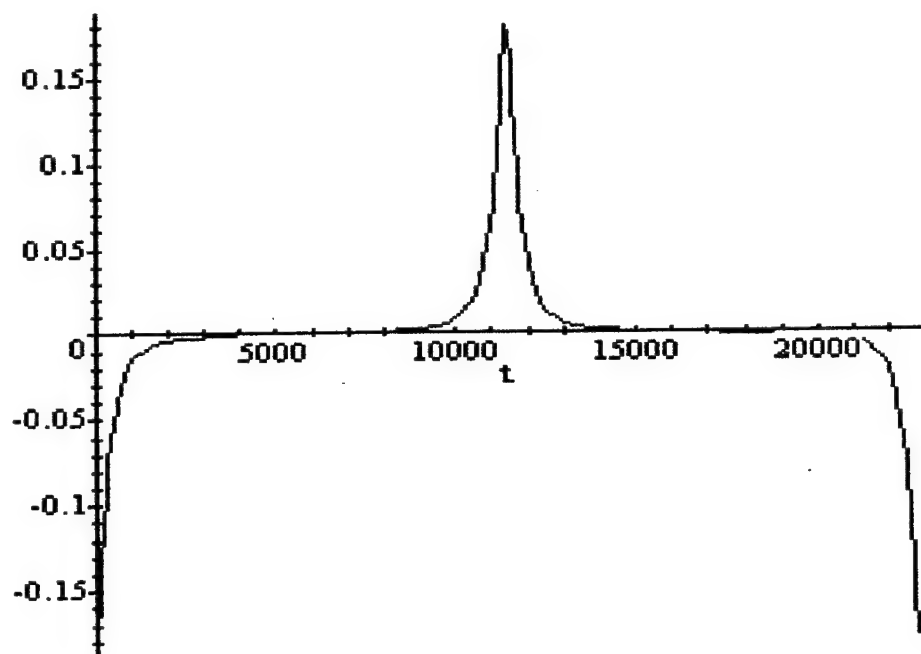


Figure 5-2: Angular Velocity in units of degrees/second.

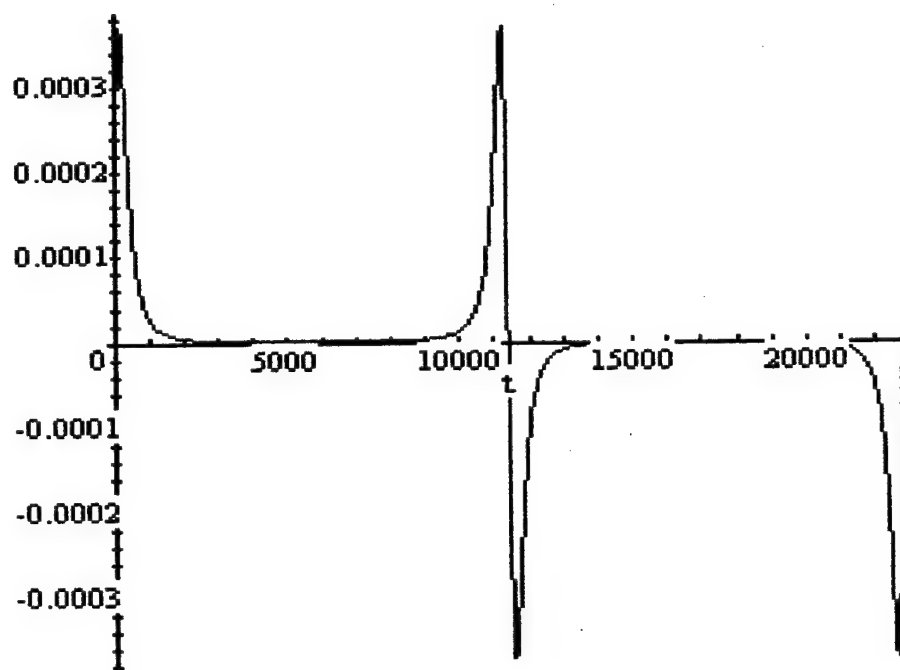


Figure 5-3: Angular Acceleration in units of degrees/second².

From the graphs it is observed that the maximum angular velocity occurs at $t=0$, 11400 and 22800 seconds and the maximum angular acceleration occurs at $t \cong 0^+$, 11400⁻, 11400⁺, and 22800⁻ seconds. The respective values are as follows:

$$\psi'(\beta, 5^\circ)_{\max} \approx 0.18^\circ / \text{sec} \approx 3.142e-3 \text{ rad} / \text{sec}$$

$$\psi''(\beta, 5^\circ)_{\max} \approx 0.00037^\circ / \text{sec}^2 \approx 6.4577e-6 \text{ rad} / \text{sec}^2$$

The maximum acceleration of the satellite has to be realized by accelerating the reaction wheel in the opposite direction. The maximum torque T_{\max} needed follows from the formula:

$$T_{\max} = I_{ZZ} * \psi''_{\max} = (14113) * (6.4577e-6 \text{ rad} / \text{sec}^2) = 0.0911 \text{ Nm} \quad (5-4)$$

And, the maximum angular momentum B_{\max} is given by:

$$B_{\max} = I_{ZZ} * \psi'_{\max} = (14113) * (3.142e-3 \text{ rad} / \text{sec}) = 44.34 \text{ Nms} \quad (5-5)$$

The total acceleration $\Delta\omega$ of the reaction wheel due to the rotation can simply be calculated with the following relation:

$$I_{ZZ} * \psi'_{\max} = I_{\omega} * \Delta\omega \quad \Rightarrow \quad \Delta\omega = \frac{I_{ZZ} * \psi'_{\max}}{I_{\omega}} \quad (5-6)$$

where, we find I_{ω} from the formula for the moment of inertia for a hollow cylinder with a relative small wall thickness, $I = mR^2$. So, for a reaction wheel with a mass of 10.5 kg and a radius of 0.1965m:

$$\Rightarrow I_{\omega} \approx 0.4054 \text{ kg m}^2$$

such that,

$$\Delta\omega = \frac{I_{ZZ} * \psi'_{\max}}{I_{\omega}} \approx 9.69 \text{ rad} / \text{sec} \approx 93 \text{ rpm}$$

In conclusion, the reaction wheel to be selected must meet these requirements for torque, momentum and acceleration.

2. Torque and Angular Momentum Requirements Due to External Disturbances

The maximum torque and angular momentum requirements due to external disturbances were calculated and found to be:

$$\begin{array}{ll} T_{1\max} = 8e-4 \text{ Nm} & H_{1\max} = 0.1718 \text{ Nms} \\ T_{2\max} = 2.2e-3 \text{ Nm} & H_{2\max} = 9.498 \text{ Nms} \\ T_{3\max} = 6e-4 \text{ Nm} & H_{3\max} = 0.19033 \text{ Nms} \end{array}$$

As can be seen, these torque and angular momentum requirements are not as demanding as those resulting from yaw steering. However, the external disturbances produce a secular torque which builds up angular momentum with time. As can be seen from Figure 4-16; a secular torque results in the T_y direction and creates a buildup of angular momentum as given by

$$(T_{y\text{avg}}) \times (1 \text{ month}) = 362 \text{ Nms}$$

over the course of one month. This build up must be dumped by either the Magnetic Acquisition / Despin system or the spacecraft thrusters. Not accounting for these secular disturbances appropriately could result in a premature mission due to unexpected demands of spacecraft fuel.

B. SIZING THE MAGNETIC TORQUERS

Magnetic torquers use the Earth's magnetic field, B , and electrical current through the torquer to create a magnetic dipole (D) that results in torque (T) on the vehicle given by:

$$D = \frac{T}{B} \quad (5-7)$$

Magnetic torquers used for momentum dumping must equal the peak disturbance plus a margin to compensate for the lack of complete directional control.

From equation 5-8 we can estimate the worst case earth magnetic field for our orbit given by using the following values:

$$r = 1.737 \text{ e}7 \text{ m}$$

$$\theta = 0^\circ$$

$$\mu_E = 8.1 \text{ e}25 \text{ g} \cdot \text{cm}^3 = 8.1 \text{ e}15 \text{ T} \cdot \text{m}^3$$

$$|\vec{B}_o| = \frac{\mu_E}{r^3} (1 + 3 \sin \theta_m)^{1/2} \quad (5-8)$$

$$\Rightarrow |B_{\max}| = 1.55 \text{ e} - 6 \text{ T}$$

Next, we calculate the torque rod's magnetic torquing ability (dipole) to counteract the worst case external disturbance;

$$T_{\max} = 2.2 \text{ e} - 3 \text{ Nm}$$

as,

$$D = \frac{T}{B} = 1419.35 \text{ A} \cdot \text{m}^2$$

which is achievable. The earth's field is cyclic at twice the orbital frequency; thus, maximum torque is available only twice per orbit. A torquer of 2500 to 3000 $\text{A} \cdot \text{m}^2$ capacity will provide sufficient margin to counteract these expected maximum disturbance torques and/or provide a momentum dumping capacity for the reaction wheels.

C. OTHER SENSOR SELECTION ISSUES

The driving requirement for the remaining sensors and actuators are the attitude knowledge and pointing requirements as stated in Chapter 6 under the system level requirements section. All sensors and actuators selected meet these requirements with a considerable margin built in.

D. HARDWARE SELECTION

1. Spacecraft Control Processor

The Satellite Control Processor unit selected is produced by Honeywell and is scheduled to be used on the International Space Station. Honeywell's Multiplexer/Demultiplexer (MDM) is a high speed interface and computer that controls sensors, effectors and other unique devices. [Ref. 29]

The MDM collects signals from sensors, effectors and subsystems; then processes the information and transmits signals and commands. For example, the MDM directs the solar arrays to point at the sun. [Ref. 29]

The MDM is rugged and adaptable to a wide range of applications. Five standard I/O circuit cards cover most applications, but this can be modified if needed. Also, the MDM size can be modified based on the number of I/O circuit cards needed. [Ref. 29]

To enhance reliability and supportability, software and hardware self-test features can detect and report 94% of all possible failure modes. In addition Honeywell can help develop I/O cards and user application programs that meet individual needs. Figure V-4 is an overview of the MDM architecture. Features of the MDM: [Ref. 29]

1. The basic MDM consists of a chassis, power supply, I/O Control Unit, I/O backplane, SX backplane and I/O circuit cards selected to meet specific requirements.
2. The I/O Control Unit includes the processor, memories, 1553 bus interface function, I/O Circuit Card Control logic, and Analog-to-Digital converter.
3. Communication is via independent, dual redundant MIL-STD-1553B channels, enabling the MDM to operate in Bus Controller, Bus Monitor or Remote Terminal mode. Firmware supports functions of each 1553 channel independently of the user application software. The MDM is capable of serial asynchronous communication via RS449 with RS485 driver/receivers and provides 16 bits of parallel I/O functionality. The MDM self-test capabilities include Built-In Test (BIT) software routines and supporting hardware Built-In Test Equipment (BITE).

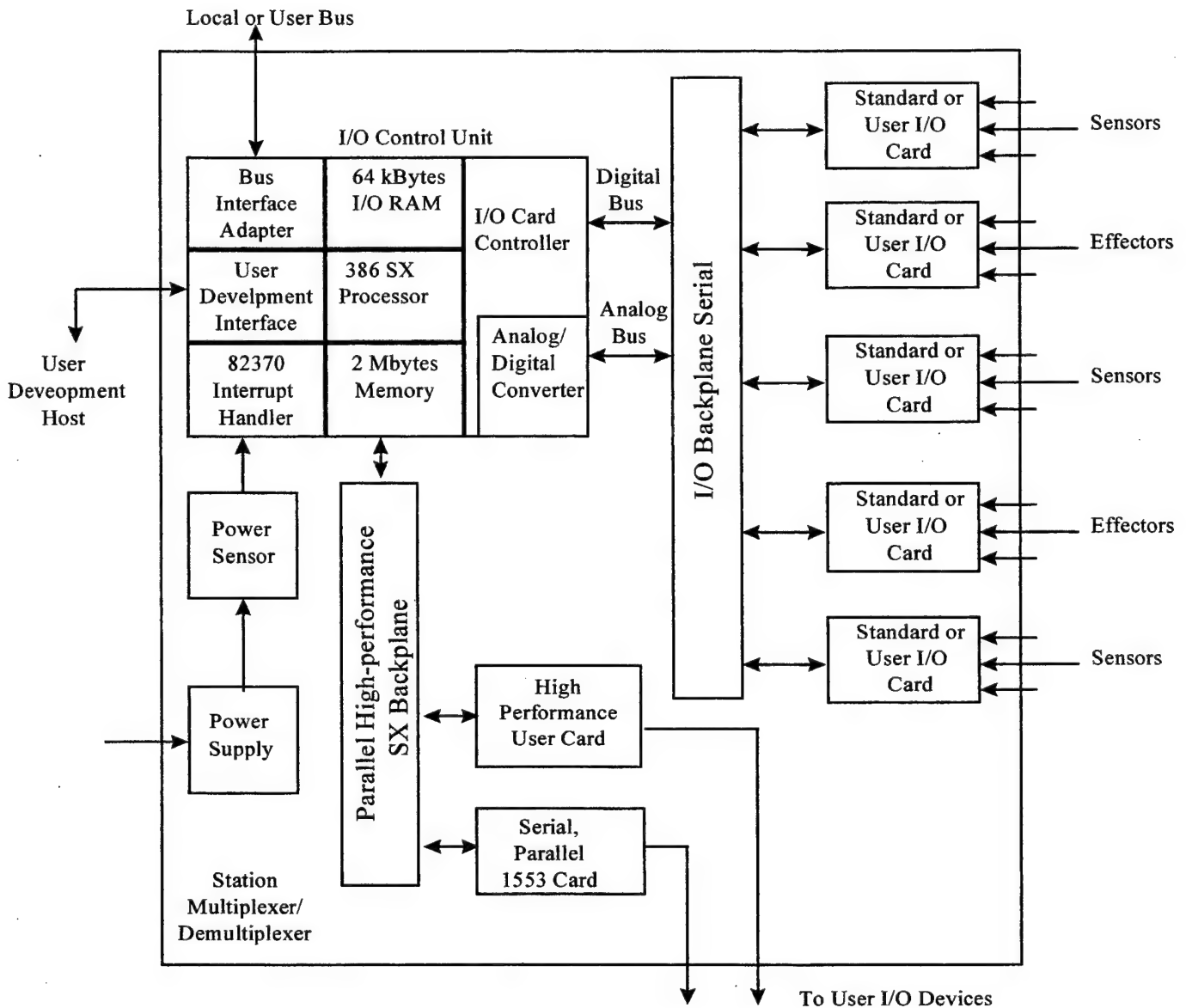


Figure 5-4: MDM Architecture

2. Magnetic Acquisition and De-spin System

The Magnetic Acquisition and Despin (MAD) system is designed for use on spacecraft for the reduction of spin rates and momentum dumping and is built and manufactured by ITHACO Space Systems. The spin rates can be encountered as a normal part of a mission or can result from ground control errors or onboard equipment failures. Under normal conditions, the launch vehicle leaves the satellite spinning at the end of orbit insertion. If the spacecraft is to be stabilized, the spin rate imparted by the launch vehicle must be corrected. The unexpected activation of a thruster or a momentum wheel failure would also result in unacceptable spin rates. Corrective action can often be taken if the vehicle rates can be reduced in some manner. The Magnetic Acquisition/Despin system performs this function. [Ref. 30, Ref. 31]

The MAD system consists of three Torque rods, an electronics controller, and a three-axis magnetometer. One Torque rod is aligned with each axis of the spacecraft and is mounted away from any instruments sensitive to magnetic fields. In addition, Torque rods are separated from one another in order to avoid cross coupling effects. The use of Torque rods allows complete momentum management of the spacecraft without consumables in almost any orbit, thus providing a clean, contamination free environment. Even in high orbits, Torque rods can make a significant contribution to the total momentum management problem. By eliminating or reducing the need for consumables, the use of Torque rods can reduce mission costs significantly. Next, the electronics controller can be mounted at any convenient location. The electronics should be accessible, however, since a trimming operation at the spacecraft level is required to compensate for the unavoidable magnetometer to torque rod coupling. The magnetometer should be mounted so that one Torque rod is aligned with each of the magnetometer axes. The magnetometer probe should be mounted as far away from the Torque rods as possible to minimize magnetic coupling. The maximum rate from which the MAD system can achieve capture depends upon the bandwidth that can be used. The maximum bandwidth in any given system depends on the amount of coupling between the Torque rods and the magnetometer. Thus, maximum separation is an advantage for the available capture capability of the MAD system. [Ref. 30, Ref. 31]

The MAD system relies upon a "minus B-dot" control law. Each Torque rod is driven to a value determined by the negative rate of change of the magnetic field along the rod. The effect is that the Torque rods behave like magnetic brakes and lock onto the Earth's magnetic grid. From this terminal state, the spacecraft's attitude control system can capture control or excess momentum can be dumped. The system specifications are as follows:

	SIZE	WEIGHT	POWER
Control Electronics	6" x 6" x 2"	0.9 kg	2.0 W
Magnetometer	2.8" x 3.8" x 4.7"	0.5 kg	0.7 W
Torque Rods	19.5 "	0.9 kg	N/A

Table 5-1: Specifications of Magnetic Acquisition / Despin System

3. Earth Sensor / Sun Sensor Assembly

a. Overview

The Earth Sensor/Sun Sensor Assembly (ES/SSA) is an innovative combined Earth horizon and two axis sun sensor which offers unprecedented performance in terms of accuracy, mass, power consumption, reliability, and automation. This sensor autonomously determines three-axis attitude information at medium earth orbits, geosynchronous, or super geosynchronous altitudes, as well as during transfer orbit. [Ref. 32]

b. Theory of Operation

The Earth Sensor portion of the ES/SSA is a scanning sensor with two sets of two infrared (IR) Fields of View which scan about the axis of rotation (scan axis) at a rate of 2 revolutions per second. Each of the four IR scans possesses a 1.5° instantaneous Field of View. As the scan progresses, each of the instantaneous Fields of View crosses the relative "cold" of space to the "warmth" of Earth and back into space. Roll attitude is derived from differences in the sensed Earth chord widths. Pitch attitude is derived from the phase angle of the sensed Earth crossings. [Ref. 32]

The sensor has also been designed to operate in transfer orbit and/or constant altitudes ranging from 11,000 km through 77,000 km. At geosynchronous

altitudes all four Earth scans cross the Earth's disc at nominally 3 and 6 degrees above the equator and 3 and 6 degrees below the equator. [Ref. 32]

The Sun Sensor portion of the ES/SSA incorporates two static, mutually orthogonal sensing (axes) arrays to detect the orientation of the sun. Each axis is comprised of a slit allowing a plane of light to pass through and intersect with an orthogonally mounted, high resolution, linear photodiode array. The point of intersection, which indicates sun angle, is obtained by reading the energy stored in the array. [Ref. 32]

Each ES/SSA is comprised of a scanning Earth sensor and a two-channel sun sensor housed in a single aluminum enclosure. Mounting is achieved by an asymmetric three point mount which allows for easy alignment and shimming if required. [Ref. 32]

The Earth sensor operates over an attitude range of $\pm 24^\circ$ in pitch and $\pm 14^\circ$ in roll, while the Sun Sensor typically operates with sun locations of $\pm 60^\circ$ in azimuth and $\pm 30^\circ$ in elevation, although fields as large as $128^\circ \times 128^\circ$ may be accommodated. All processing and calibration data utilized to derive pitch and roll output from the Earth Sensor, as well as sun azimuth and elevation from the Sun Sensor is available on-board the sensor. Output occurs over a digital interface governed by the MIL-STD-1553 data bus, EIA RS-422A, or user specified interface. Upon asserting a data request the ES/SSA outputs all Earth Sensor and Sun Sensor information including diagnostics and status information. Table 5-2 lists the Earth Sensor / Sun Sensor Assembly Specifications. [Ref. 32]

EARTH SENSOR	
Roll/Pitch Accuracy (Includes all long term & diurnally varying errors)	$\pm 0.02^\circ (3\sigma)$
Transfer Orbit Roll / Pitch Accuracy	$\pm 0.1^\circ (3\sigma)$
Attitude Range	$\pm 14^\circ$ Roll, $\pm 24^\circ$ Pitch
SUN SENSOR	
Range	Up to $128^\circ \times 128^\circ$
Accuracy	$\pm 0.01^\circ (3\sigma)$
OVERALL INSTRUMENT	
Manufacturer	ITHACO Space Systems
Power Consumption	< 5.5 Watts
Mass	< 5.5 lb (2.5 kg)
Dimensions	6.4 x 3.9 x 8.0 in
Output Data Rate	4 Hz
Data Interface Options	MIL-STD-1553, EIA RS-422A, or per User Spec
Qualification Life (Including Particle Radiation)	22.5 yrs
Qualification Temperature	-34°C to $+71^\circ$
Vibration	22.5 grms (Random)
Parts Program	S Level and MIL-STD-1547
Reliability	$< 163 \times 10^{-9}$ failures / hr
Mounting	Asymmetric 3 Point Flange Mount

Table 5-2: The Earth Sensor / Sun Sensor Assembly Specifications

4. The Reaction Wheel Assembly

a. Application

The Type E Reaction Wheel Assembly provides a reliable source of reaction torque and angular momentum storage for attitude control of medium to large spacecraft. Accelerating or decelerating a flywheel with an integral motor provides a means of controlled momentum exchange with the spacecraft, which is advantageous for a variety of attitude control schemes. [Ref. 33]

Featuring high, bi-directional torque capability, a set of Type E Reaction Wheels is ideal for agile three-axis reaction control applications. With a momentum storage capacity of 50 N-m-s and an available reaction torque of up to 0.3 N-m, the Type E Reaction Wheel can satisfy a broad range of spacecraft requirements. [Ref. 33]

b. Design Description

1. Structure

The Type E Reaction Wheel consists of a precision balanced solid flywheel suspended on ball bearings and driven by a brushless DC motor. The aluminum housing is vented to space to eliminate viscous drag torque from the flywheel due to windage. Removable domed covers provide access to the wheel interior for inspection with the flywheel installed. [Ref. 33]

2. Suspension

The flywheel is suspended on high capacity angular contact ball bearings. A low vapor pressure lubricant synthesized specifically for high vacuum spaceflight applications is used to lubricate the bearings, which incorporates a flight proven extreme pressure additive to prevent bearing wear while operating at low speeds below 50 rpm when an EHD film is insufficient to prevent ball to race contact. Labyrinth seals and barrier film coatings ensure long life operation by preventing loss of lubricant from the bearings due to evaporation and surface migration. A life test of the Reaction Wheel in a bi-directional reaction wheel application frequently crossing through zero speed has been operating successfully since April 1994. In addition, ITHACO is offering an On-orbit grease replenishment design for all their Reaction Wheels in order to reliably increase minimum ball bearing operating lifetime from eight to fifteen years. The newly developed device utilizes a Kapton heater and a simple thermostat circuit to drive a sealed grease reservoir to a specific temperature. The high thermal expansion coefficient of the grease results in the injection of a controlled amount of grease from the reservoir directly into the bearing. The system is unpressurized and contains no active moving parts, resulting in reliable, fail-safe performance. [Ref. 33, Ref. 34]

3. Motor

A discretely commutated, ironless armature brushless DC torque motor drives the flywheel in the Reaction Wheel. Maximum inertia to weight ratio is realized with the large diameter motor components and the unique feature of the ironless armature

design which strategically places all of the mass of the iron and magnets on the rotor. The ironless armature design also eliminates cogging for smooth transitions during direction reversals. Hall sensors integrated directly into the armature sense the alternating flux field from the permanent magnets to provide commutation information for the motor driver, as well as a high resolution tachometer signal for speed and direction of rotation information. [Ref. 33]

4. Motor Driver

The motor driver responds proportional to an analog torque command and provides linear motor torque to the flywheel over the entire speed range. A digital interface per MIL-STD-1553 or other custom interface can be easily incorporated in the existing board space. Analog and digital tachometers are provided to accommodate a variety of user needs. Due to the high torque and current in the Reaction Wheel, the motor driver is packaged in a separate enclosed electronics box for flexible thermal management. The motor drivers are designed to minimize electrical interference, and have demonstrated superb electromagnetic compatibility by meeting the requirements of MIL-STD-461 and MIL-STD-462. [Ref. 33]

5. Specifications

The performance specifications for the Reaction Wheel (E - Wheel) are presented here in tabular and graphical form. Higher angular momentum capacities and higher torque versions can be made available as non-standard designs. Within the present Reaction Wheel case sizes, higher reaction torque can be accommodated with a rescaled motor driver. [Ref. 33]

ITHACO "E WHEEL" REACTION WHEEL ASSEMBLY	
Speed Range (rpm)	0 to \pm 3850
Angular Momentum Capability	50 N-m-s (36.8 ft-lb-sec)
Reaction Torque	300 mN-m (42 oz-in)
Weight of Wheel Assembly	10.5 kg (23.1 lb)
Weight of Driver Assembly	3.63 kg (8.0 lb)
Dimensions of Wheel Assembly	39.3 dia x 16.6 cm (15.5 x 6.6 in)
Dimensions of Driver Assembly	17.8 x 17.8 x 10.2 cm (7.0 x 7.0 x 4.0 in)
Tachometer (Pulses per revolution)	72
Static Imbalance	3.6 gram-cm (0.05 oz-in)
Dynamic Imbalance	120 gram-cm ² (oz-in ²)
Estimated Lifetime	15 years

Table 5-3: Ithaco Reaction Wheel Specifications

5. The Satellite Inertial Reference System

a. Heritage

Honeywell has been involved in many successful space programs including launch vehicles, satellites, space probes and manned space flight. Recent experiences have included the TOS, Centaur launch systems, MSX and Space Station Freedom.

The Miniature Inertial Measurement Unit (MIMU) product is an integration of components from several Honeywell programs into a standard product. These other programs have provided the hardware and software knowledge and experience to develop a family of systems consisting of three axis rotation sensors and optional three axis linear acceleration sensors in a small, lightweight radiation hardened product. The MIMU uses the Honeywell GG 1320 ring laser gyroscope which is in high volume production the their Minneapolis ring laser gyro production facility.

b. Miniature Inertial Measurement Unit

The MIMU family was designed to be a low cost, low risk radiation hardened product, to be used as the inertial measurement system in a broad range of satellite applications. The system contains three GG 1320 ring laser gyros mounted orthogonally as the rotation sensors and three optional Allied Signal QA 3000 accelerometers as the linear acceleration sensors. A block diagram of the MIMU is shown in Figure 5-5. [Ref. 35]

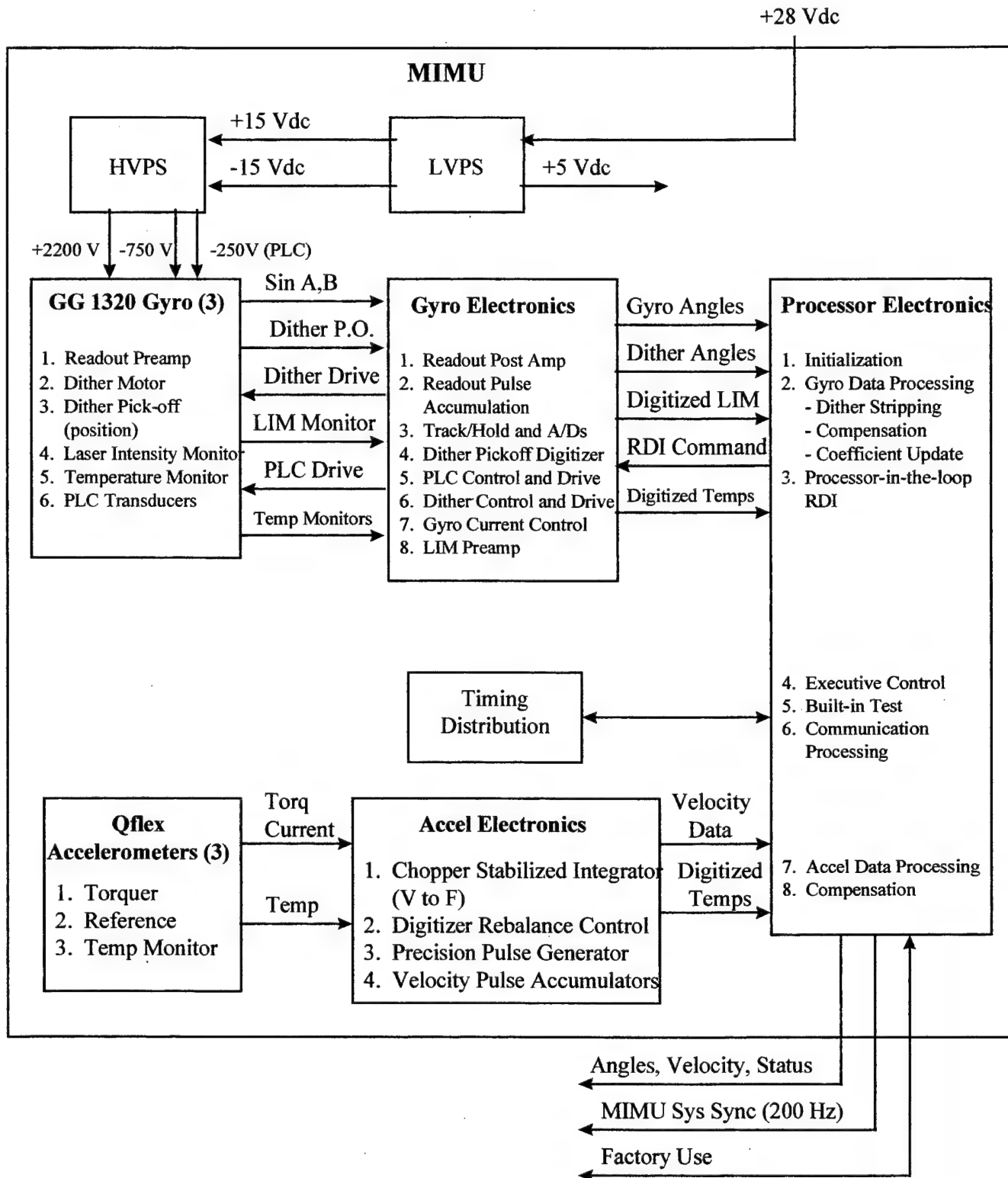


Figure 5-5: The Miniature Inertial Measurement Unit

The Honeywell MIMU Model YG9666 B	
Size	250 in ³
Weight (w/o magnetic shield)	7.6 lb
Power	33.7 Watts
Rate Capability (deg/sec)	± 375
Acceleration	25 g
Life (yrs, operation dependent)	15
Gyro-GG1320	
Bias Stability (1σ, deg/hr; short term)	0.008
Angular Random Walk (deg/√hr)	0.005
Scale Factor Error (1σ, ppm; short term)	5
Readout Noise (μrad, 1σ)	5
Accelerometer	QA 3000
Bias Stability (1σ, mg; short term)	0.04
Scale Factor Error (1σ, ppm; short term)	80
Output Data	
Angle LSB (μrad)	1.0
Velocity LSB (mm/sec)	0.0753
Temperature	
Operating (°C)	-30 to +70
Non-Operating (°C)	-45 to +75
Radiation (krads total dose)	100

Table 5-4: The MIMU Performance Parameters

The MIMU offers excellent long term stability, very high reliability and a wide dynamic range. Recent reliability studies of field life data has shown the life of the gyroscope to be in excess of 300,000 hours. This gives the MIMU a high probability of success for missions of 15 years or more. [Ref. 35]

The processor electronics assembly consists of the Honeywell radiation hardened GVSC, RH-1750 processor, a 16 bit processor utilizing the full MIL-STD-1750A instruction set. The software performs the functional control as shown in the block diagram of Figure 5-6. This assembly also contains a standard RS422 interface operating at a 200 Hz data rate. MIMU can also be configured to use an optional MIL-STD-1553B interface. [Ref. 35]

The standard RS422 interface consists of ten 16-bit data words. These data words are shown in Table V-5.

Word 1	Frame Timer (MSH)
Word 2	Frame Timer (LSH)
Word 3	X Compensated Gyro Angle
Word 4	Y Compensated Gyro
Word 5	Z Compensated Gyro Angle
Word 6	X Compensated Velocity
Word 7	Y Compensated Velocity
Word 8	Z Compensated Velocity
Word 9	Multiplexed BIT Status
Word 10	Checksum

Table 5-5: MIMU Output Data Message

The data rate is 1 Mbit/sec. The multiplexed BIT Status word consists of 256 words multiplexed at one word output each 200 Hz period. The BIT status word is identified by the LSH of the frame timer word. [Ref. 35]

The accelerometer electronics are also located on the processor assembly. The QA3000 Q-Flex accelerometer is a torque-rebalance sensor with fused quartz flexures with a permanent magnetic torquer, a capacitive pickoff system, and self-contained servo electronics. The accelerometer outputs a current proportional to the acceleration. The accelerometer electronics on the processor assembly digitizes this current (three channels) which is then read by the processor. Mathematical modeling of bias, scale factor, and axis misalignment is performed over the temperature range to enhance the performance. [Ref. 35]

The gyro electronics assembly contains the electronics for control of the three Ring Laser Gyros. The RLG readout post amplifier provides the gain to amplify the gyroscope's photodetector outputs to levels which can be digitized. These readout pulses

are then accumulated and are read by the processor. Pulses are accumulated for positive angular rotation and for negative angular rotation. Net rotation is then calculated by the processor. [Ref. 35]

To overcome a lock-in mechanism at low rates, the gyro is dithered, which involves subjecting the gyroscope to a small angular oscillation through a controlled mechanical resonance. The MIMU gyros are oscillated at three separate frequencies (nominally 525, 575, and 625 Hz). The baseline means of removing the dither oscillation from the gyro signal is through a procedure called "dither stripping". The procedure involves measuring the angle between the gyro block and the gyro mounting base and subtracting this angle from the gyro output signal. The output of a piezoelectric sensor attached to the dither spring is passed through an A/D converter to the digital processor, scaled and corrected for phase, and subtracted from the gyro signal. The result is a wide bandwidth signal with the content at the dither frequency removed. An alternate means of removing dither is filtering. Filtering is used when low readout noise is required, and the corresponding latency penalty can be tolerated. The dither control electronics are also located on the gyro electronics assembly. [Ref. 35]

The gyro electronics assembly also contains the path length control (PLC) circuitry. In order to maintain the RLG laser at its peak operating point (peak power), PLC is utilized by using a PZT which converts a voltage input to a path length distance. The lasing power is at maximum when the laser beam path length is equal to an integral number of wavelengths. [Ref. 35]

The gyro electronics assembly also contains the RLG current control circuitry. The current in each leg of the RLG is precisely controlled to minimize temperature and gas flow induced bias changes. [Ref. 35]

The Low Voltage Power Supply modules convert the spacecraft +28 Vdc to the isolated secondary voltages required for operations (+5 Vdc, +15 Vdc, and -15 Vdc). [Ref. 35]

The High Voltage Power Supply (HVPS) module provides +2200 Vdc to the gyroscope cathodes during startup. After startup the HVPS provides -750 Vdc to maintain the laser currents. The PLC circuitry requires +250 Vdc provided the HVPS. [Ref. 35]

6. HD-1003 Star Tracker

The HD-1003 Star Tracker, produced by Hughes Danbury Optical Systems, Inc. is designed to meet current and future needs for a lightweight, reliable and accurate star tracker. A simple optical system, ASIC based electronics and high throughput firmware

architecture make the HD-1003 mission adaptable, even while in operational orbit. [Ref. 36]

The HD-1003 attitude determination system provides continuous three-axis attitude data over the entire orbit. An autonomous all-stellar attitude determination system is available, minimizing spacecraft computation and ground support. Since the HD-1003 has no moving parts, high reliability and long life are achieved. Further, since the HD-1003 system can provide multiple star updates every one tenth of a second for LOS rates up to 1.0 deg/sec, reliance on the inertial reference unit can be reduced or eliminated. [Ref. 36]

Some key features of the HD-1003 include:

A. Performance

1. Six-star tracking capability
2. Six arc-sec rms per star
3. Two arc-sec rms multi-star average
4. 10 Hz update rate
5. 8 x 8 9 or 20 degree circular FOV
6. Parts count has been reduced by 5 times.

B. Growth

1. 12 MIPS throughput with 50% margin
2. Expandable memory
3. Uplinkable code
4. Small or large space-craft compatible

C. Survivability

1. All electronic parts are hardened to 100 Krad or higher
2. Built-in radiation shielding
3. Space qualified proton/debris rejection software
4. Expected life on orbit is 15 to 18 years
5. HDOS has completed a 2 year test program to verify the HD-1003's performance in high radiation environments.
6. Test results and design have been independently verified by Lockheed Martin, Aerospace and the Naval Research Lab.

D. Producibility

1. Modular design
2. ASIC-based electronics
3. No moving parts, sun safe
4. Safety engineered

The HD-1003 Star Tracker benefits from over Twenty years of experience in leading attitude determination technology. Hughes Danbury produced the world's first CCD-based star sensor to be qualified in space, the first "multi-star" tracker, and the first CCD upgrade to NASA's Standard Fixed Head Star Tracker. The Hughes Danbury team continues to satisfy evolving demands by utilizing the latest technology and innovative packaging. [Ref. 36]

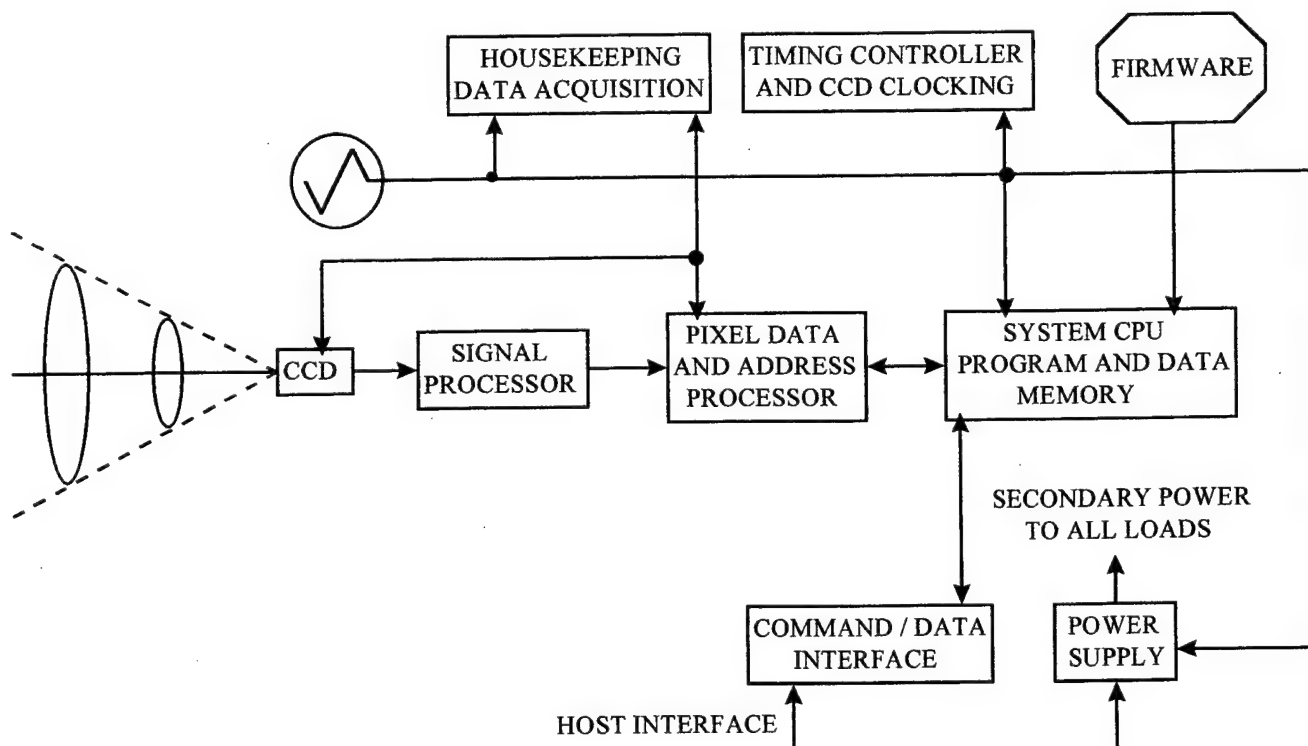


Figure 5-6: CCD Focal Plane and Microprocessor Controller Sample and Centroid up to Six Star Images Simultaneously.

Performance Category	HD-1003 Narrow FOV	HD-1003 Wide FOV
Size (with light shade) (L x W x H)	16 x 6.2 x 4.4 in.	7 x 6.2 x 4.4 in
Weight (with light shade)	8.0 lb	7.1 lb
Power (average at 28 Vdc)	9 Watts	9 Watts
Communication Interface	MIL-STD-1553B	MIL-STD-1553B
Field of View (deg)	8° x 8°	20° circular
Sensitivity (5000 K star) (m_v)	+6.0	+4.7
Overall Accuracy, Each Axis		
* Pitch / Yaw (per star) (arc-sec, rms)	6 2	30 10
* Multi-star average (arc-sec, rms)	40	50
* Roll (5-stars) (arc-sec, rms)	0.25	0.25
* Magnitude (\pm)		
Update (frame) Rate (Hz)	10	4
Stars Simultaneously Tracked	6	6
Bright Object Rejection Angle**		
* Sun (deg)	35°	40°
* Earth (deg)	25°	30°
* Moon (deg)	25°	25°
Acquisition Time (6 stars) (sec. 1-sigma)	6	6
Mean Time Between Failures (Hours)	1,000,000 hr	1,000,000 hr
Environments:		
Temperature		
* Nominal (°C)	-5 to +45	-5 to +45
* Survival (°C)	-15 to +55	-15 to +55
Vibration (Random) (g rms)	12.2	12.2
EMC Level	MIL-STD-461C	MIL-STD-461C
** Light shade is modular to accommodate various mission requirements		

Table 5-6: HD-1003 Star Tracker Performance Capability

7. Global Positioning System

A Global Positioning System receiver is required to provide the spacecraft with an autonomous capability to accurately determine its position. The Motorola GPS Spaceborne Receiver system was selected for this mission. This system is capable of determining the spacecraft's position to within 15 meters for Autonomous Position and 2 to 5 meters for Differential Position; provided that the Selective Availability is not implemented. This system also provides the ability to determine spacecraft attitude to accuracies of 0.1° in pitch, roll and yaw. In addition, the system can determine pitch, roll and yaw rates to accuracies of $0.5^\circ/\text{second}$. These accuracies are not sufficient to meet the crosslink pointing knowledge requirements but are suitable to provide a backup source of attitude information for basic spacecraft control functions in the event of failures in the primary. Table 5-7 identifies the characteristics of the Motorola GPS Spaceborne Receiver.

Additional key features of the Motorola GPS Spaceborne Receiver include:

1. Space qualified digital design.
2. Full spaceborne doppler capability.
3. Autonomous operation with doppler capability at 1 second rate.
4. Non-destruct doppler measurements at 1 second rate.
5. Radiation hardened 1 PPS clock output synchronized to GPS time.

Multiple Configurations Available	
* L1, C/A and P-code	
* L1/L2, C/A and P-code	
* Y-code-Anti-Spoof and Selective Availability	
* Multiple Antennas	
* 6 to 18 channels	
Physical / Environment	
Size	6.0" x 5.2" x 2.7"
Weight	3.7 lb
DC Power	7 Watts
Vibration	25 grms
Shock	3000 g at 10 kHz
Temperature	-20° C to +75° C
Performance Characteristics	
Receiver Accuracies (over C/N₀ Range of 32 to 42 dB/Hz):	
Pseudo-Range (10 sec)	0.2 m
Pseudo-Range Interchannel Bias	< 0.1 m
Carrier Phase (1 sec)	0.01 m
Navigation Solution Accuracy (GDOP = 3, Selective Availability not implemented):	
Autonomous Position	< 15 m (1 σ)
Differential Position	2 to 5 m (1 σ)
Time Offset	100 ns
Time-to-First-Fix	
Mean TTFF	< 60 sec
Maximum TTFF (P _f > 0.9)	< 90 sec
User S/C Ephemeris	< 10 km, 10 m/s
User Clock Error	< 1 x 10 ⁻⁷
Orbital Dynamics (typical / spacecraft orbit):	
Velocity	8,000 m/s
Acceleration	10 m/s ²

Table 5-7: Characteristics of the Motorola GPS Spaceborne Receiver

8. Sun Sensor

a. Overview

Two Sun sensors will be used; one on each solar array substrate assembly. These two sun sensors will be the primary method for determining the yaw angle and solar array rotation angle required to maintain solar tracking. The Sun Sensor Assembly selected is a two axis digital sun sensor which offers unprecedented performance in terms of accuracy, mass, power consumption, reliability and automation. The sensor autonomously determines two-axis attitude information with respect to the sun line from low Earth through super geosynchronous orbits.

b. Theory of Operation

The Sun Sensor Assembly incorporates two static, mutually orthogonal sensing (axes) arrays to detect the orientation of the sun. Each axis is comprised of a slit allowing a plane of light to pass through it intersecting with an orthogonally mounted, high resolution, linear photodiode array. The point of intersection, which indicates sun angle, is obtained by reading the energy stored in the array.

The Sun Sensor Assembly typically operates with sun locations of $\pm 64^\circ$ in azimuth and $\pm 64^\circ$ in elevation. All processing and calibration data utilized to derive sun azimuth and elevation from the Sun Sensor Assembly occurs on board the sensor. Output occurs over a digital interface governed by the MIL-STD-1553 data bus, EIA RS-422A, or user specified interface. Upon asserting a data request the SSA outputs all SSA information including diagnostics and status information. Units have been provided for the MSTI, APEX, and Sea Star Programs.

Unit	Description	Quantity	Size (ea)	Mass (ea)	Avg Pwr	Peak Pwr
ADCS Control Processor	P. 3-3	2	305 x 102 x 152 mm	5.7 kg (ea)	25 W	*** Unknown
Control Electronics	ITHACO Catalog	1	152.4 x 152.4 x 50.8 mm	0.9 kg	2.0 W	*** Unknown
Magnetometer	ITHACO Catalog	1	71.12 x 96.52 x 119.38 mm	0.5 kg	0.7 W	*** Unknown
Torqrods	ITHACO Catalog	3	495.3 mm	0.9 kg (ea)	N/A	N/A
Reaction Wheel	Honeywell HR-60	1	125.9 x 407 x 407 mm	14.3 kg (ea)	28 W	280 W
Reaction Wheel	ITHACO Catalog	3	**	10.5 kg	30 W	280 W
Star Trackers	Hughes Catalog	3	406.4 x 157.48 x 11.76 mm	3.63 kg	9 W	*** Unknown
Inertial Reference Unit	Honeywell/AAS Paper	2	4096.77 cm ³	3.45 kg	34 W	N/A
Sun Sensor	Ithaco	2	5 x 5 cm	0.64 kg	1 W	N/A
GPS	Motorola	2	15.24 x 13.21 x 6.86 cm	1.68 kg	7 W	7 W
GPS Antenna	Motorola	4	5 cm x 7 cm triangle plate	0.2kg	N/A	N/A
Earth/Sun sensor assembly	ITHACO Space Systems	2	162.56 x 99.06 x 203.2 mm	2.5 kg	5.5 W	5.5 W

Table 5-8: Components selected for the MUS satellite

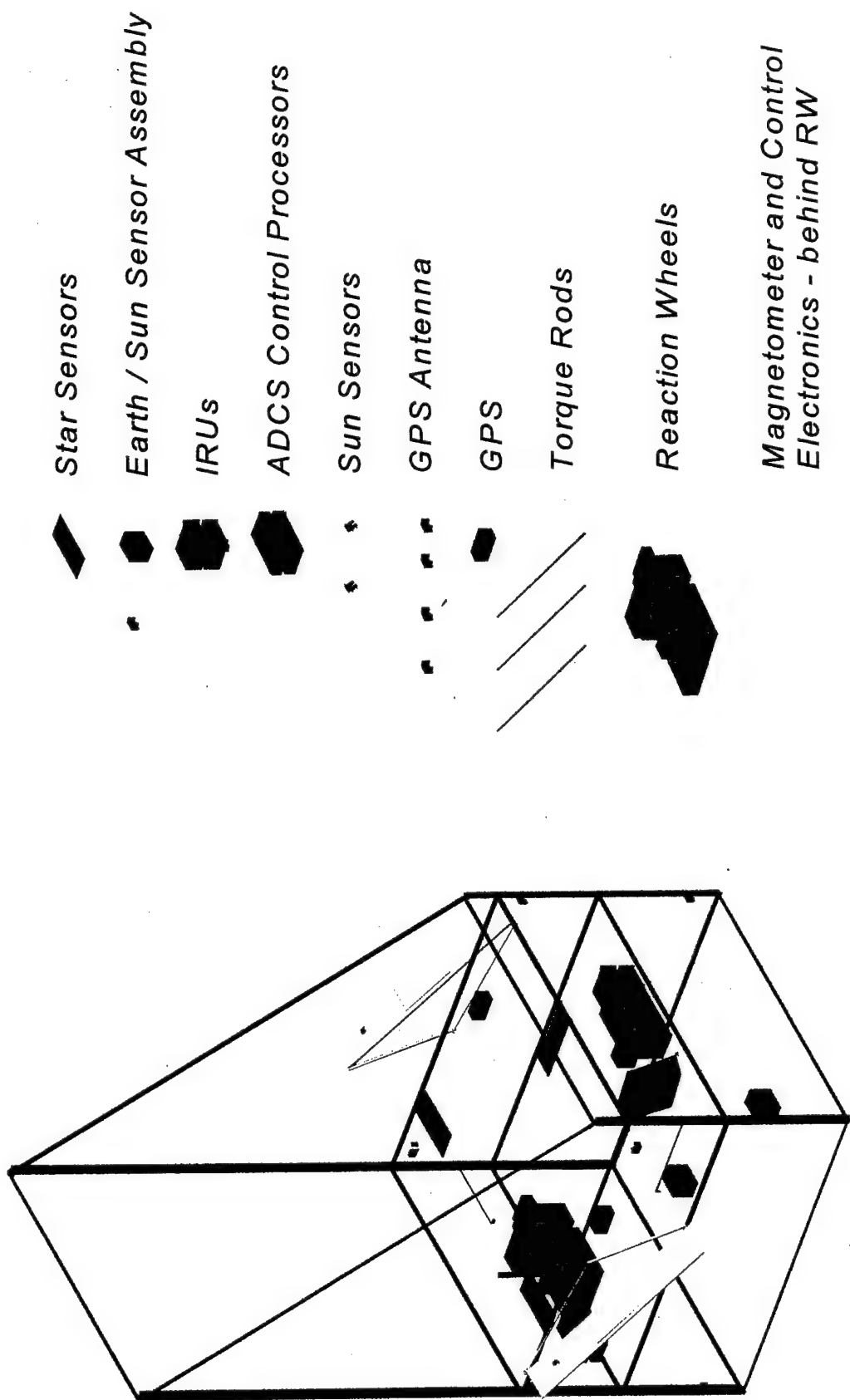


Figure 5-7: ADCS Component Lay-out

VI. YAW CONTROLLING

On orbit pointing control utilizes three reaction wheels to provide roll, pitch and yaw attitude control. An earth sensor provides two axis attitude data for roll and pitch and a sun sensor provides one axis attitude data for yaw. The yaw control is similar to both roll and pitch except that it must utilize additional information in order to maintain solar array sun tracking. Also, changes in yaw do not adversely effect the communications payload as long as pointing error limits about the roll and pitch axis are maintained. In this section the peculiarities of yaw steering will be discussed.

A. YAW DISTURBANCES

Due to secular disturbances, momentum accumulates in the wheel, and wheel speeds will build up with time. In normal operations these secular torques in the yaw direction will be compensated by operation of the magnetic torque rods. In the back-up mode momentum would be dumped through a series of minimum impulse thruster pulses.

B. SUN AND NADIR POINTING GEOMETRY

Figure 6-1 illustrates the Sun and Nadir pointing geometry for the MUS spacecraft. β represents the azimuth and δ the elevation of the sun line relative to the spacecraft orbit plane. β is referenced to the X axis. The X - axis coincides with the velocity vector in the local geodetic reference frame (i.e. orbit nominal frame). The commanded yaw and array angles vary as a function of β and δ due to the effects of the space vehicles orbital motion, precession of the orbit plane, and movement of the sun in the earth centered inertial frame. These commands maintain the normal to the solar panels directed toward the sun and the sun in the spacecraft roll/yaw plane. Except for very low sun angles, when $\delta < 5.0^\circ$, the -X side of the spacecraft is always oriented towards the sun. [Ref. 27: p. 458]

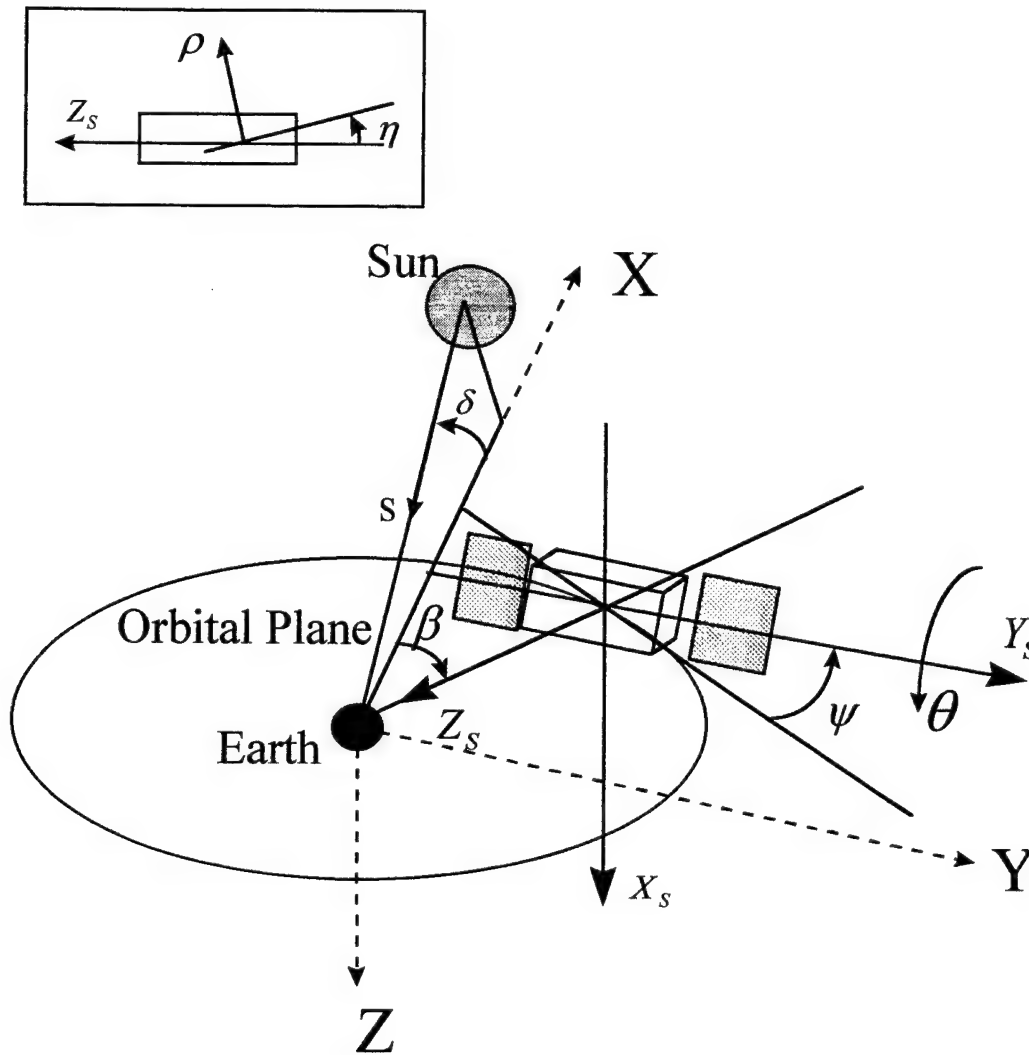


Figure 6-1: Pointing Geometry

C. SUN AND NADIR YAW POINTING STRATEGY

The Attitude Dynamics and Control Subsystem is designed to track the nominal sun/nadir yaw trajectory for sun angles (δ) greater than 5.0° from the orbit plane. The closed loop controller uses sun sensor data as the yaw attitude reference. When the spacecraft is in the sun/earth co-linearity region, defined when δ is less than 15° and the projection of the sun line in the orbit plane is within 15° of the nadir vector, yaw sensing is restricted due to either poor geometry or an eclipse condition. In these regions, a yaw momentum tracking tach loop is used to track an ideal yaw momentum profile. Predicted Euler coupling torques are fed forward to achieve a high degree of accuracy, minimizing yaw pointing error at exit from the region. [Ref. 27: p. 460]

When the sun is within 5.0°, nominal, of the orbit plane, the ADCS enters a constant yaw mode which maintains the pitch (array rotational) axis on the orbit normal and an orbit rate rotation about the pitch axis. The constant yaw mode minimizes Reaction Wheel torque and momentum demand while maintaining specified yaw pointing. Table 6-1 summarizes the sun and nadir yaw pointing strategy. [Ref. 27: p. 460]

Yaw Tracking Mode	Sun Rotation Angle β(deg)	Sun to Orbit Plane Angle (δ)	Yaw Control Reference	Remarks
Ideal Yaw Tracking Mode	All β angles	$ \delta \geq 15^\circ$	ST/Yaw SS Output Null Position	Closed loop yaw control using Star Trackers (ST) / SS derived yaw & yaw rate
	$ \beta - 90^\circ \geq 15^\circ$ and $ \beta - 270^\circ \geq 15^\circ$	$15^\circ > \delta \geq 5.0^\circ$	ST/Yaw SS output null position	Closed loop yaw control using ST/SS derived yaw & yaw rate
	$ \beta - 90^\circ < 15^\circ$ or $ \beta - 270^\circ < 15^\circ$	$15^\circ > \delta \geq 5.0^\circ$	ST/Calculated yaw cmd, no SS yaw sensing	Poor yaw signal from SS when $ \delta < 15^\circ$ due to array position or no SS output due to eclipse
Constant yaw tracking mode	$ \beta - 90^\circ \geq 15^\circ$ and $ \beta - 270^\circ \geq 15^\circ$	$ \delta < 5.0^\circ$	ST/Yaw SS output biased at δ	Constant pitch rate control; Closed loop yaw control using ST/SS derived yaw and yaw rate.
	$ \beta - 90^\circ < 15^\circ$ or $ \beta - 270^\circ < 15^\circ$	$ \delta < 5.0^\circ$	ST/Zero yaw angle; no SS yaw sensing	Constant pitch rate control; Feed forward tach loop yaw rate tracking control; Poor SS yaw signal when $ \beta < 15^\circ$ due to array position or no SS output due to eclipse; Minimum yaw control torque required.

Table 6-1: Sun and Nadir Yaw Pointing Strategy

D. SUN AND NADIR ARRAY CONTROL STRATEGY

The ADCS is designed to track the nominal sun/nadir array trajectory for sun angles (δ) greater than 5.0° from the orbit plane. The closed loop controller uses course sun sensor data as the array loop null reference. When the spacecraft is in eclipse, a calculated nominal array trajectory drives the array loop with position feedback provided by the measured array angle. When the sun is within 5.0° , nominal, of the orbit plane, the ADCS enters a constant yaw mode. The array control strategy is unchanged, but the constant yaw geometry results in an orbital rate rotation of the array. The transition into and out of the constant yaw mode is limited to the segment of the orbit with sun rotation angles between 120° and 240° ; i.e. between 2pm and 10pm spacecraft local time, precluding the need for yaw inversion maneuvers. Table 6-2 describes the sun/nadir array control strategy. [Ref. 27: p. 462]

Solar Array Tracking Mode	Eclipse Condition	Sun to Orbit Plane angle δ	Array Control Reference	Remarks
Ideal Sun-Nadir Array Tracking	No eclipse	$ \delta \geq 5.0^\circ$	ST/Pitch SS output null position	No eclipse will occur when $ \delta > 15^\circ$
	Eclipse	$15^\circ \geq \delta \geq 5.0^\circ$	Calculated ideal array angle command	The error between measured array position and command reference is used for control
Constant Array Rate Tracking	No eclipse	$ \delta < 5.0^\circ$	ST/Pitch SS output null position	Array sun pointing error δ
	Eclipse	$ \delta < 5.0^\circ$	Calculated array angle command for constant yaw tracking	Measured array position used for control; sun pointing error equals δ

Table 6-2: Sun and Nadir Array Control Strategy

E. NORMAL, ON-STATION CONTROL FUNCTIONAL BLOCK DIAGRAM

The Attitude Dynamics and Control Subsystem provides fully autonomous three axis attitude determination and control throughout the Space Vehicle's operational lifetime. Three of four redundant reaction wheels control body attitude, and redundant magnetic torquing coils control system momentum. There is no thruster utilization for the Normal, On-Station mode of operation. Thrusters are used primarily to provide ΔV and control actuation during stationkeeping maneuvers, but also provide backup momentum unloading in the event of a failure of the magnetic system. Also, control loop compensation is provided in the attitude control software for Euler coupling torques, magnetic and thruster desaturation torques, and wheel friction torques to optimize pointing and reduce jitter. [Ref. 27: p. 266]

While the system is fully autonomous, the Control Segment has full override access to the ADCS equipment configuration and operating mode. The internal state of all software flags is available in telemetry and any control mode or functions may be either inhibited or forced by a ground override of the appropriate flag(s). Any control algorithm may also be reprogrammed by ground command. The system is capable of operation for periods of at least 210 days with no ground intervention. Figure 6-2 illustrates the Normal, On-Station Functional Block Diagram. [Ref. 27: p. 466]

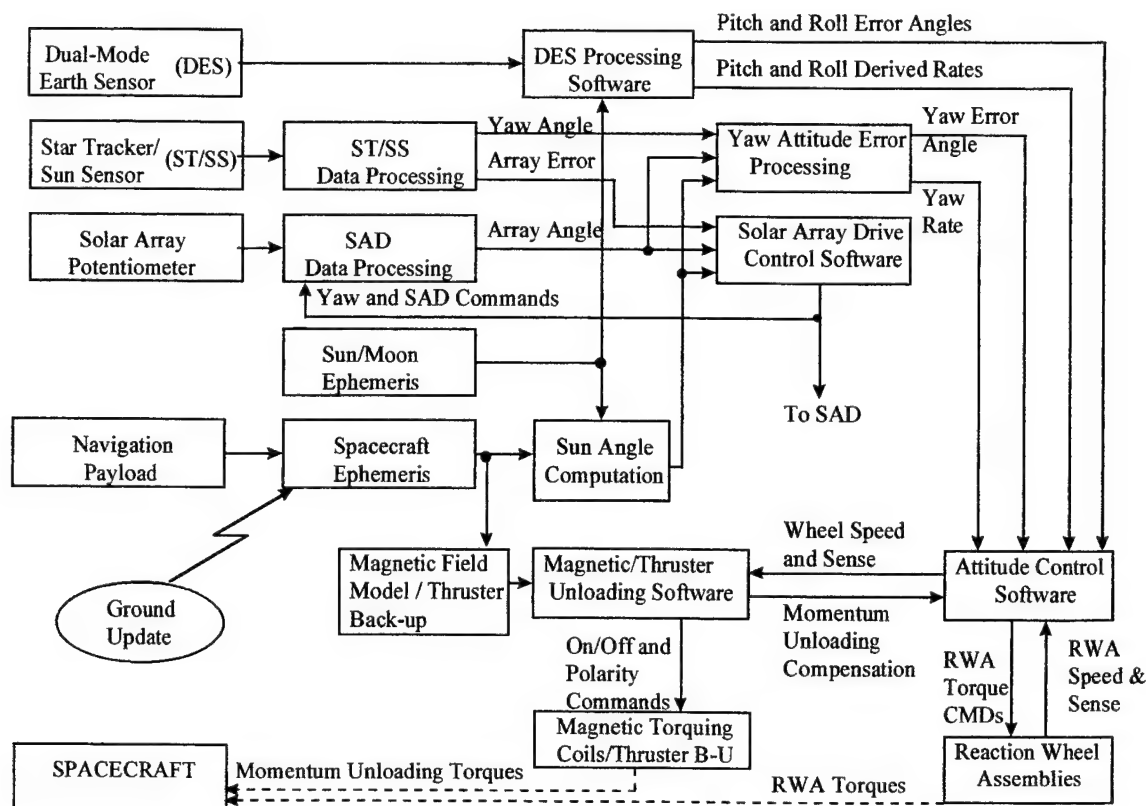


Figure 6-2: Normal, On-Station Functional Block Diagram

F. ATTITUDE DETERMINATION SOFTWARE FUNCTIONAL OVERVIEW

The attitude determination software comprises two primary functions; namely, attitude sensor data processing and payload ephemeris data processing. The attitude sensor processing conditions the raw data input from the various attitude sensors, processes the data to derive three-axis spacecraft attitude and attitude rate, and generates the yaw and solar array drive reference commands to drive the respective control loops in the co-linearity regions and for low sun angles ($\delta \leq 5.0^\circ$). The ephemeris processing, which uses Navigation Payload data as the primary reference and ground uplink data as the backup reference, generates sun angle data for sun/nadir pointing mode operation, sun/moon interference predictions for earth sensor processing, and a magnetic field model for the momentum unloading software. Figure 6-3 is a Functional Overview of the Attitude Determination Software. [Ref. 27: p. 468]

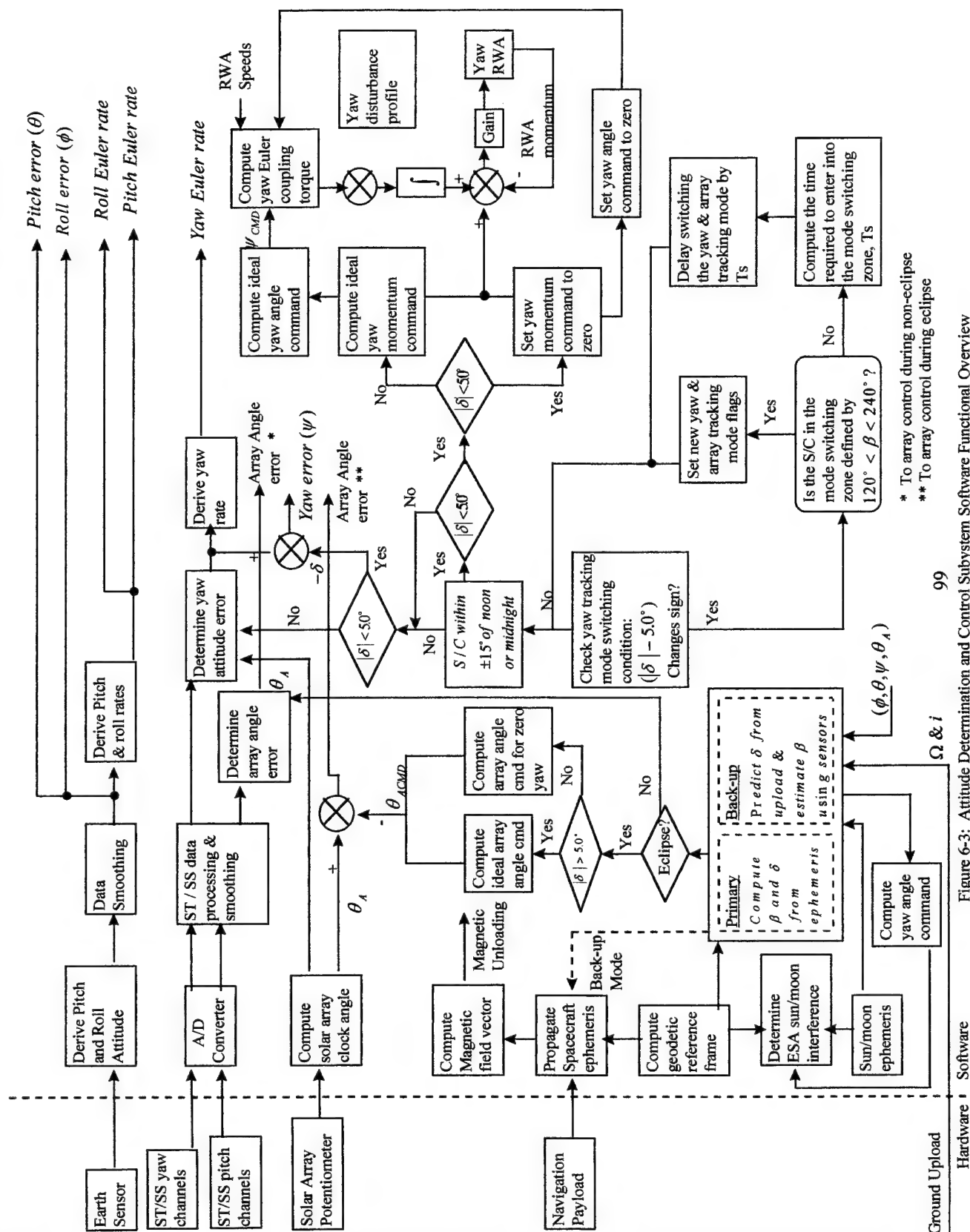


Figure 6-3: Attitude Determination and Control Subsystem Software Functional Overview

G. SUN ANGLE ESTIMATION (β AND δ)

The ADCS processes both Navigation payload data as well as ground uploaded ephemeris to provide a reliable basis for sun/nadir pointing. The spacecraft ephemeris obtained from the on-board navigation payload and the sun ephemeris generated on-board are used to compute the sun rotation (azimuth) angle (β) and the out-of orbit plane sun angle (δ) from which eclipses times and yaw/array control phase is determined. [Ref. 27: p. 470]

The backup mode determines δ using the orbit right ascension of ascending node, Ω , and the orbit inclination, i , along with the on-board generated sun ephemeris. β is estimated from the calculated δ angle and the array position when the array position relative to the yaw axis is suitable and attitude pointing is within tolerance. Yearly variations of Ω and i are represented by an on-board model, thus each upload covers a time span of one year. To satisfy the autonomy requirements, however, uploads are required every few months. The backup estimator is run at all times, but the estimated β and δ are only used when payload data is unavailable or invalid. Figure 6-4 is the flow diagram for the estimation of Sun angles β and δ . [Ref. 27: p. 470]

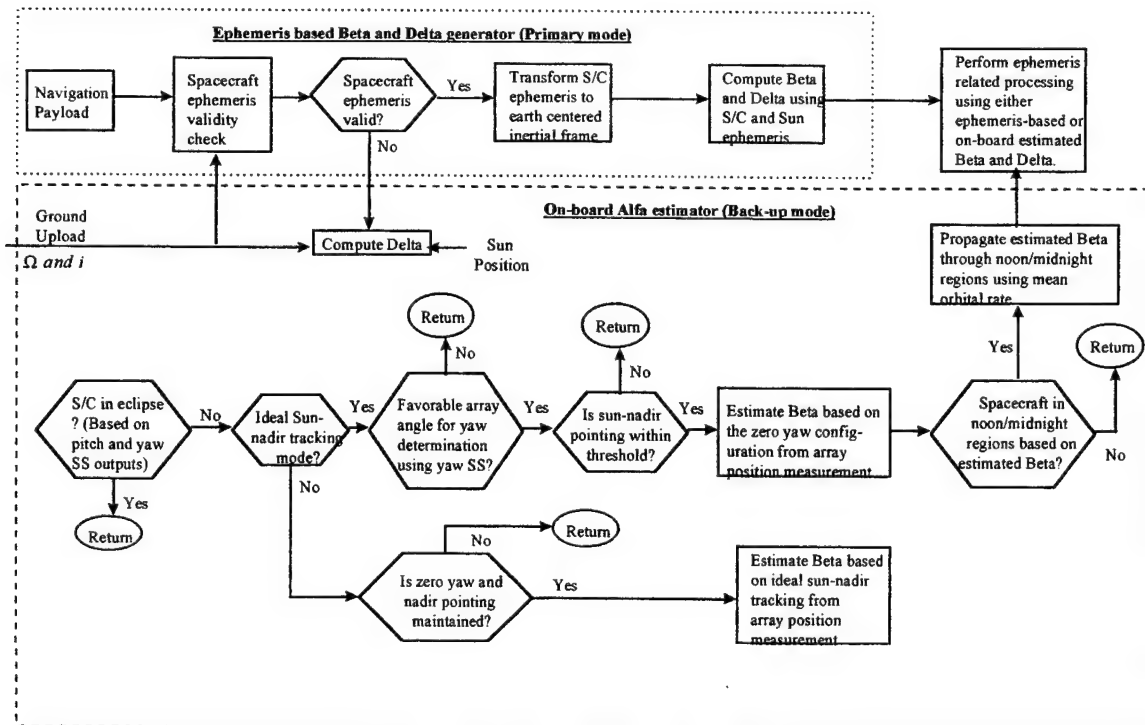


Figure 6-4: Sun Angle Estimation

H. YAW DATA PROCESSING

The ADCS utilizes a two-axis sun sensor for yaw attitude control and solar array drive control. The Sun sensor is comprised of two sensing units, one located on each solar array, which provide redundant detector sets and processing electronics for each sensing axis. Data from the two detector units is differenced to provide a measurement that is linear on each axis over approximately $\pm 40^\circ$ and covers a full range of $\pm 125^\circ$, minimum, per axis. For yaw determination, the sensor data must be weighted as a function of the solar array orientation. [Ref. 27: p. 472]

This Page Intentionally Left Blank

VII. SIMULATION OF THE ATTITUDE DYNAMICS AND CONTROL SUBSYSTEM

A. PROBLEM STATEMENT

The MUS spacecraft is a Medium Earth Orbit satellite which has the following moments of inertia of:

$$I_{roll} = 13,337.7 \text{ kg} \cdot \text{m}^2$$

$$I_{pitch} = 14,083.6 \text{ kg} \cdot \text{m}^2$$

$$I_{yaw} = 14,113.7 \text{ kg} \cdot \text{m}^2$$

The pointing accuracy for the spacecraft is:

a) 0.1° for Roll and Pitch

b) 1.0° for Yaw

The disturbance torques on the spacecraft are primarily due to solar pressure, and can be approximated by:

$$T_x = T_{roll} = (1 \times 10^{-3}) * \cos(\omega_o t) \quad N \cdot m$$

$$T_y = T_{pitch} = (1.5 \times 10^{-3}) * \cos(\omega_o t) \quad N \cdot m$$

$$T_z = T_{yaw} = (1 \times 10^{-3}) * \cos(\omega_o t) \quad N \cdot m$$

The thruster misalignment torque about any axis can be approximated by:

$$T_F = 1 \times 10^{-4} \quad N \cdot m$$

Finally, the design of the attitude control system for the spacecraft must meet the given specifications when the environmental torques are imposed on the spacecraft.

B. THREE AXIS STABILIZATION

The control torques along the axes of three-axis-stabilization systems are provided by various combinations of momentum wheels, reaction wheels, and thrusters. Broadly, however, there are two types of three-axis-stabilization systems: a momentum biased system with a momentum wheel along the pitch axis, and a zero-momentum system with a reaction wheel along each axis. [Ref. 25: p. 130]

In momentum wheel systems, the angular momentum along the pitch axis provides gyroscopic stiffness. In these systems, the pitch and roll axes are controlled directly and the yaw axis is controlled indirectly due to a yaw sensor. In reaction wheel systems, all three axes are controlled independently, thus requiring a yaw sensor also. The momentum wheel can be fixed or gimballed about one or two axes. The control torque along the pitch axis is provided by the change in the speed of the momentum wheel. The torque along the roll axis is provided by thrusters, a reaction wheel, or by changing the gimbal angles in the gimballed momentum wheel. [Ref. 25: p. 130]

1. Small Angle Approximation

When the satellite's body frame orientation remains very close to the orbit nominal frame, a small angle approximation is achievable as well as being able to disregard higher order terms. This greatly simplifies the problem. A linearized analysis of the three-axis-stabilization system is given in this section. The linearized equations of motion of a three-axis-stabilized spacecraft are derived first. The angular velocities of the spacecraft can be expressed in terms of the orbital rate, ω_o , and the attitude error angles, ψ , θ , and ϕ , which are known as yaw, pitch, and roll errors, respectively, as follows:

$$\bar{\omega} = \begin{Bmatrix} \omega_x \\ \omega_y \\ \omega_z \end{Bmatrix} = \begin{bmatrix} 1 & 0 & -\sin(\theta) \\ 0 & \cos(\phi) & \cos(\theta)\sin(\phi) \\ 0 & -\sin(\phi) & \cos(\theta)\cos(\phi) \end{bmatrix} \begin{Bmatrix} \dot{\phi} \\ \dot{\theta} \\ \dot{\psi} \end{Bmatrix} - \omega_o \begin{Bmatrix} \cos(\theta)\sin(\psi) \\ \cos(\phi)\cos(\psi) + \sin(\phi)\sin(\theta)\sin(\psi) \\ -\sin(\phi)\cos(\psi) + \cos(\phi)\sin(\theta)\sin(\psi) \end{Bmatrix} \cong \begin{Bmatrix} \dot{\phi} - \omega_o\psi \\ \dot{\theta} - \omega_o \\ \dot{\psi} + \omega_o\phi \end{Bmatrix} \quad (7-1)$$

The angular momentum of the system can be written in the form

$$\vec{H} = \vec{H}_w + \vec{H}_b \quad (7-2)$$

where,

$$\begin{aligned} \vec{H}_w &= [h_x \quad h_y \quad h_z]^T \\ \vec{H}_b &= [I_{xx}\omega_x \quad I_{yy}\omega_y \quad I_{zz}\omega_z]^T \end{aligned} \quad (7-3)$$

are the angular momentum of the wheels and of the spacecraft, respectively, where I_{xx} , I_{yy} , and I_{zz} are the principal moments of inertia of the spacecraft and ω_x , ω_y , and ω_z are the angular velocity components of axes x, y, and z as given by Eq. (7-1). Introducing Eq. (7-2), in conjunction with Eqs. (7-3) and (7-1) into $\vec{M}_c = \vec{H}_{c\text{rel}} + \bar{\omega} \times \vec{H}_c$ and ignoring nonlinear terms, we obtain the moment equation in the form

$$\vec{M} \cong \begin{Bmatrix} \dot{h}_x + I_{xx}(\ddot{\phi} - \omega_o\dot{\psi}) + h_z(\dot{\theta} - \omega_o) - h_y(\dot{\psi} + \omega_o\phi) - (I_{zz} - I_{yy})\omega_o(\dot{\psi} + \omega_o\phi) \\ \dot{h}_y + I_{yy}\ddot{\theta} + h_x(\dot{\psi} + \omega_o\phi) - h_z(\dot{\phi} - \omega_o\psi) \\ \dot{h}_z + I_{zz}(\ddot{\psi} + \omega_o\dot{\phi}) + h_y(\dot{\phi} - \omega_o\psi) - h_x(\dot{\theta} - \omega_o) - (I_{yy} - I_{xx})\omega_o(\dot{\phi} - \omega_o\psi) \end{Bmatrix} \quad (7-4)$$

2. Large Angle Requirements

Unfortunately, the yaw steering requirements of the satellite does not allow us to either make small angle approximations or to disregard higher order terms. This greatly complicates the equations of motion which are presented below. As previously discussed, the angular velocities of the spacecraft can be expressed in terms of the orbital rate, ω_o , and the attitude angles, ϕ , θ , and ψ , which are known as roll, pitch, and yaw respectively, as follows:

$$\begin{aligned} \bar{\omega} = \begin{Bmatrix} \omega_x \\ \omega_y \\ \omega_z \end{Bmatrix} &= \begin{bmatrix} 1 & 0 & -\sin(\theta) \\ 0 & \cos(\phi) & \cos(\theta)\sin(\phi) \\ 0 & -\sin(\phi) & \cos(\theta)\cos(\phi) \end{bmatrix} \begin{Bmatrix} \dot{\phi} \\ \dot{\theta} \\ \dot{\psi} \end{Bmatrix} - \\ &\quad \omega_o \begin{Bmatrix} \cos(\theta)\sin(\psi) \\ \cos(\phi)\cos(\psi) + \sin(\phi)\sin(\theta)\sin(\psi) \\ -\sin(\phi)\cos(\psi) + \cos(\phi)\sin(\theta)\sin(\psi) \end{Bmatrix} \\ &= \begin{Bmatrix} \dot{\phi} - \dot{\psi}\sin(\theta) - \omega_o\cos(\theta)\sin(\psi) \\ \dot{\theta}\cos(\phi) + \dot{\psi}\cos(\theta)\sin(\phi) - \omega_o\cos(\phi)\cos(\psi) - \omega_o\sin(\phi)\sin(\theta)\sin(\psi) \\ -\dot{\theta}\sin(\phi) + \dot{\psi}\cos(\theta)\cos(\phi) + \omega_o\sin(\phi)\cos(\psi) - \omega_o\cos(\phi)\sin(\theta)\sin(\psi) \end{Bmatrix} \quad (7-5) \end{aligned}$$

The angular momentum of the system can again be written as stated in Eq. (7-2)

$$\bar{H} = \bar{H}_w + \bar{H}_b \quad (7-2)$$

where,

$$\begin{aligned} \bar{H}_w &= [h_x \quad h_y \quad h_z]^T \\ \bar{H}_b &= [I_{xx}\omega_x \quad I_{yy}\omega_y \quad I_{zz}\omega_z]^T \end{aligned} \quad (7-3)$$

are the angular momentum of the wheels and of the spacecraft, respectively, where I_{xx} , I_{yy} , and I_{zz} are the principal moments of inertia of the spacecraft and ω_x , ω_y , and ω_z are the angular velocity components of axes x, y, and z as given by Eq. (7-5). Introducing Eq. (7-2), in conjunction with Eqs. (7-3) and (7-5) into

$\vec{M}_c = \vec{H}_{c\text{rel}} + \vec{\omega} \times \vec{H}_c$ and keeping all terms, we obtain the moment equations in the form:

$$\vec{M} = \left\{ \begin{array}{l} \dot{h}_x + I_{xx}\ddot{\phi} + \dot{\theta}\cos(\phi)h_z + \dot{\theta}\cos(\phi)I_{zz}\dot{\psi} + \dot{\psi}\cos(\theta)\sin(\phi)h_z + \dot{\psi}^2\cos(\theta)\sin(\phi)I_{zz} - \\ \omega_o\cos(\phi)\cos(\psi)h_z - \omega_o\cos(\phi)\cos(\psi)I_{zz}\dot{\psi} - \omega_o\sin(\phi)\sin(\theta)\sin(\psi)h_z - \\ \omega_o\sin(\phi)\sin(\theta)\sin(\psi)I_{zz}\dot{\psi} + \dot{\theta}\sin(\phi)h_y + \dot{\theta}^2\sin(\phi)I_{yy} - \dot{\psi}\cos(\theta)\cos(\phi)h_y - \\ \dot{\psi}\cos(\theta)\cos(\phi)I_{yy}\dot{\theta} - \omega_o\sin(\phi)\cos(\psi)h_y - \omega_o\sin(\phi)\cos(\psi)I_{yy}\dot{\theta} \\ + \omega_o\cos(\phi)\sin(\theta)\sin(\psi)h_y + \omega_o\cos(\phi)\sin(\theta)\sin(\psi)I_{yy}\dot{\theta} \\ \\ \dot{h}_y + I_{yy}\ddot{\theta} - \dot{\theta}\sin(\phi)h_x - \dot{\theta}\sin(\phi)I_{xx}\dot{\phi} + \dot{\psi}\cos(\theta)\cos(\phi)h_x + \dot{\psi}\cos(\theta)\cos(\phi)I_{xx}\dot{\phi} \\ + \omega_o\sin(\phi)\cos(\psi)h_x + \omega_o\sin(\phi)\cos(\psi)I_{xx}\dot{\phi} - \omega_o\cos(\phi)\sin(\theta)\sin(\psi)h_x - \\ \omega_o\cos(\phi)\sin(\theta)\sin(\psi)I_{xx}\dot{\phi} - \dot{\phi}h_z - \dot{\phi}I_{zz}\dot{\psi} + \dot{\psi}\sin(\theta)h_z + \dot{\psi}^2\sin(\theta)I_{zz} + \\ \omega_o\cos(\theta)\sin(\psi)h_z + \omega_o\cos(\theta)\sin(\psi)I_{zz}\dot{\psi} \\ \\ \dot{h}_z + I_{zz}\ddot{\psi} + \dot{\phi}h_y + \dot{\phi}I_{yy}\dot{\theta} - \dot{\psi}\sin(\theta)h_y - \dot{\psi}\sin(\theta)I_{yy}\dot{\theta} - \omega_o\cos(\theta)\sin(\psi)h_y - \\ \omega_o\cos(\theta)\sin(\psi)I_{yy}\dot{\theta} - \dot{\theta}\cos(\phi)h_x - \dot{\theta}\cos(\phi)I_{xx}\dot{\phi} - \dot{\psi}\cos(\theta)\sin(\phi)h_x - \\ \dot{\psi}\cos(\theta)\sin(\phi)I_{xx}\dot{\phi} + \omega_o\cos(\phi)\cos(\psi)h_x + \omega_o\cos(\phi)\cos(\psi)I_{xx}\dot{\phi} + \\ \omega_o\sin(\phi)\sin(\theta)\sin(\psi)h_x + \omega_o\sin(\phi)\sin(\theta)\sin(\psi)I_{xx}\dot{\phi} \end{array} \right\} \quad (7-6)$$

The external moments arise from three major sources: the gravitational gradient, the solar radiation pressure, and the control moments from actuators. Denoting the individual torques by \vec{M}_G , \vec{M}_s , and \vec{M}_c , respectively, we can write

$$\vec{M} = \vec{M}_G + \vec{M}_s + \vec{M}_c. \quad (7-7)$$

where,

$$\bar{M}_G \cong 3\omega_o^2 \begin{Bmatrix} \phi(I_{zz} - I_{yy}) \\ \theta(I_{xx} - I_{zz}) \\ 0 \end{Bmatrix} \quad (7-8)$$

Different types of active control systems have different key parameters and algorithms. Frequently, three-axis control can be decoupled into three independent axes. The most basic design parameter in each axis is its position gain, K_p . This is the amount of control torque which results from a unit attitude error and can be expressed in Nm/deg or Nm/rad. The position gain is selected by the designer and must be high enough to provide the required attitude control accuracy in the presence of disturbances, or $K_p \geq T_d / \theta_\varepsilon$, where K_p is position gain, T_d is peak disturbance torque, and θ_ε is allowable attitude error. In its simplest form, a spacecraft attitude control system can be represented in the s-domain as a $1/s^2$ plant and may be controlled by a proportional plus derivative (PD) controller where $T_c \equiv K_p \theta_\varepsilon + K_r \dot{\theta}_\varepsilon$. The position gain, K_p , controls system bandwidth and the rate gain, K_r , controls damping. [Ref. 6: p. 364]

The value of the position gain also determines the attitude control system bandwidth and speed-of-response. The bandwidth is given by $\omega_n = (K_p / I)^{1/2}$, where I is the spacecraft moment of inertia. The bandwidth defines the frequency at which control authority begins to diminish. Attitude control and disturbance rejection are effective from 0 frequency (d.c.) up to the bandwidth. Speed of response is approximately the reciprocal of bandwidth. Note that position gain is inversely proportional to allowable error and bandwidth is proportional to the square root of position gain. Therefore, high accuracy implies high position gain and high bandwidth. However, high bandwidth may cause bending resonances to affect control system performance. [Ref. 6: p. 365]

With the relations given, the system designer can estimate required position gain from his estimates of disturbance torque and accuracy requirements. He can use this estimate to compute control system bandwidth. This allows him to specify minimum bending frequencies as discussed below. [Ref. 6: p. 365]

In defining algorithms for the control system, we must also consider whether the vehicle will have flexible-body effects that can make the vehicle unstable. Spacecraft with flexible appendages such as antennas, booms, and solar panels may produce slight warping at their natural frequencies. Control torques and external-disturbance torques will cause structural vibrations, in some cases close to or within the control system's bandwidth. The lowest natural frequencies of flexible components should be at least an order of magnitude greater than the rigid body frequencies before we can neglect flexibility.

C. THREE-AXIS REACTION WHEEL SYSTEM

A three-axis reaction wheel system can be considered as a combination of three independent roll, pitch, and yaw control systems, see Figure 7-1. Each axis is controlled by varying the speed of the reaction wheel in response to the attitude error. The system requires a reaction wheel with zero nominal angular momentum and an attitude sensor for each axis. [Ref. 25: p. 149]

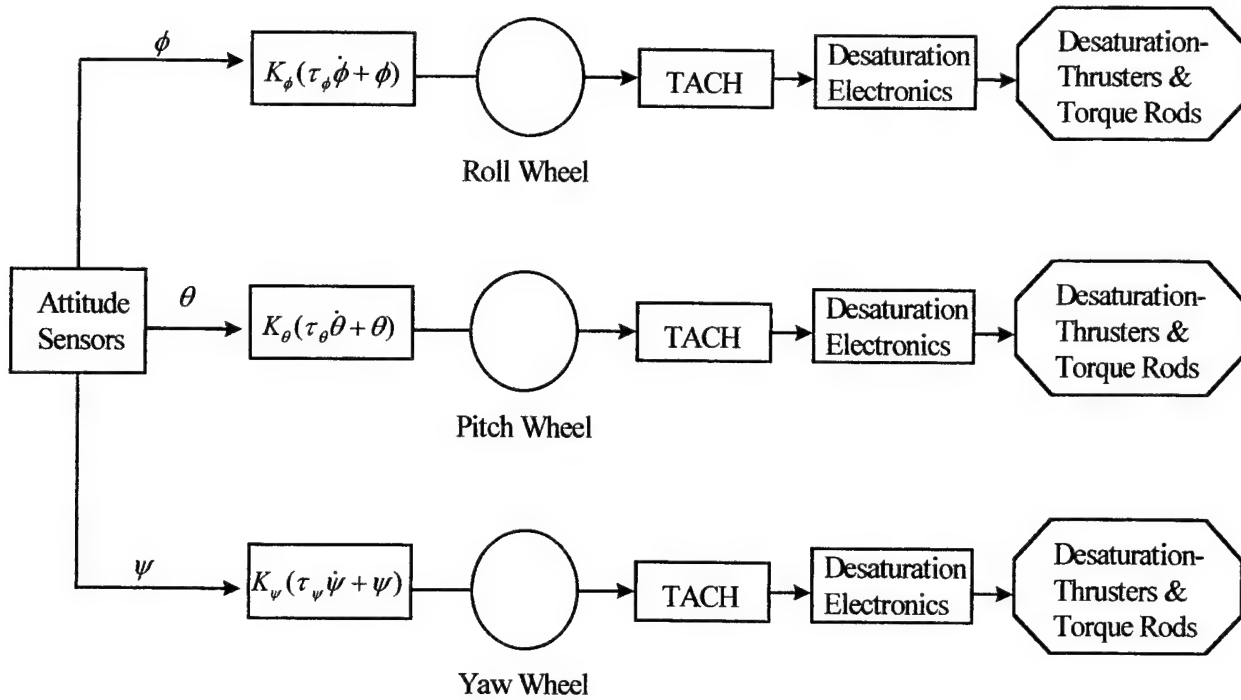


Figure 7-1: Block diagram of a three-axis reaction control system

1. Small Angle Approximation

In this section the control of the spacecraft is explored when small angle approximations are made which would be the case if yaw steering was not being performed.

Introducing Eqs. (7-4) and (7-8) into Eq. (7-7) and neglecting the transverse inertia of the wheel, the equations of motion for a three-axis reaction wheel system are

$$\begin{aligned}
 M_{cx} + M_{sx} &= I_{xx}\ddot{\phi} + \left[4\omega_o^2(I_{yy} - I_{zz}) - \omega_o h_y\right]\phi + \left[-h_y - \omega_o(I_{xx} - I_{yy} + I_{zz})\right]\dot{\psi} \\
 &\quad + \dot{\theta}h_z - \omega_o h_z + \dot{h}_x \\
 M_{cy} + M_{sy} &= I_{yy}\ddot{\theta} + 3\omega_o^2\theta(I_{xx} - I_{zz}) + \omega_o h_x\phi - h_z\dot{\phi} + \omega_o h_z\psi + h_x\dot{\psi}_x + \dot{h}_y \\
 M_{cz} + M_{sz} &= I_{zz}\ddot{\psi} + \left[\omega_o^2(I_{yy} - I_{xx}) - \omega_o h_y\right]\psi + \left[h_y + \omega_o(I_{xx} + I_{zz} - I_{yy})\right]\dot{\phi} \\
 &\quad - h_x\dot{\theta} + \omega_o h_x + \dot{h}_z
 \end{aligned} \tag{7-9}$$

Although Eqs. (7-9) are coupled, because h_x, h_y, h_z , and ω_o are small, the coupling terms are small. If the coupling terms are neglected, the equations of motion about the pitch, roll, and yaw axes become independent, and hence they can be controlled independently. Therefore, the equations of motion become:

$$\begin{aligned} M_{cx} + M_{sx} &= I_{xx}\ddot{\phi} + \dot{h}_x = T_x \\ M_{cy} + M_{sy} &= I_{yy}\ddot{\theta} + \dot{h}_y = T_y \\ M_{cz} + M_{sz} &= I_{zz}\ddot{\psi} + \dot{h}_z = T_z \end{aligned} \quad (7-10)$$

Then, the control torques are applied by letting the rates of change of the angular moment of the reaction wheels have

$$\begin{aligned} \dot{h}_x &= K_\phi(\tau_\phi\dot{\phi} + \phi) \\ \dot{h}_y &= K_\theta(\tau_\theta\dot{\theta} + \theta) \\ \dot{h}_z &= K_\psi(\tau_\psi\dot{\psi} + \psi) \end{aligned} \quad (7-11)$$

Making the appropriate substitution leads to the following:

$$\begin{aligned} T_x &= I_{xx}\ddot{\phi} + K_x[\tau_x\dot{\phi} + \phi] \\ T_y &= I_{yy}\ddot{\theta} + K_y[\tau_y\dot{\theta} + \theta] \\ T_z &= I_{zz}\ddot{\psi} + K_z[\tau_z\dot{\psi} + \psi] \end{aligned} \quad (7-12)$$

Next, entering the Laplace domain yields:

$$\begin{aligned}
\phi(s) &= \frac{T_x(s)}{[I_{xx}s^2 + K_r\tau_r s + K_r]} \\
\theta(s) &= \frac{T_y(s)}{[I_{yy}s^2 + K_p\tau_p s + K_p]} \\
\psi(s) &= \frac{T_z(s)}{[I_{zz}s^2 + K_y\tau_y s + K_y]}
\end{aligned} \tag{7-13}$$

The next step is to determine the position gains and the time constants. For the roll axis we can say:

$$\omega_r = \sqrt{\frac{K_r}{I_{xx}}} \quad \zeta_r = \left[\frac{\tau_r}{2} \right] \omega_r \tag{7-14}$$

Then, using the final value theorem, $\phi_{ss} = \lim_{s \rightarrow 0} [s\phi(s)]$, we can state

$$\phi_{ss} = \frac{(2 \times 10^{-4})}{K_r},$$

and since, $\phi_{ss} < 0.001745 \text{ rad} \Rightarrow K_r > 0.1146$. Therefore, we can let $K_r = 0.5$.

Next, since $\omega_r = \sqrt{\frac{K_r}{I_{xx}}} = 0.0061227 \text{ rad/sec} = 9.7446e-4 \text{ hz}$,

and, since $\tau_r = \frac{2\zeta_r}{\omega_r} \Rightarrow \tau_r = 2060$.

In a similar manner the remaining values were determined and are listed in Table 7-1.

ROLL	PITCH	YAW
$K_r = 0.5$	$K_p = 0.3$	$K_y = 0.1$
$\omega_r = 0.0061$ rad/sec	$\omega_p = 0.0046$ rad/sec	$\omega_y = 0.00266$ rad/sec
$\zeta_r = 1$	$\zeta_p = 1$	$\zeta_y = 1$
$\tau_r = 2060$ sec	$\tau_p = 433$ sec	$\tau_y = 751$

Table 7-1: Control Law Values

The final step is to code in Matlab and simulink. The Laplace equations I used for this simulation are as follows:

$$\begin{aligned}
T_x(s) - K_r[\tau_r s + 1]\phi(s) + \omega_o[I_{xx} - I_{yy} + I_{zz}]s\psi(s) &= [I_{xx}s^2 + 4\omega_o^2(I_{yy} - I_{zz})]\phi(s) \\
T_y(s) - K_p[\tau_p s + 1]\theta(s) &= [I_{yy}s^2 + 3\omega_o^2(I_{xx} - I_{zz})]\theta(s) \\
T_z(s) - K_y[\tau_y s + 1]\psi(s) - \omega_o(I_{xx} + I_{zz} - I_{yy})s\phi(s) &= [I_{zz}s^2 + \omega_o^2(I_{yy} - I_{xx})]\psi(s)
\end{aligned}
\tag{7-15}$$

For the computer simulation I used Matlab and Simulink. I considered three situations. First, a step input due to thruster misalignment. Second, the sinusoidal input due to solar pressure torques; and third, an impulse input of approximately one order of magnitude larger than the others; see simulink diagrams and Matlab code in Appendix F.

The first simulation was the pitch response due to a step input. As can be seen from Figure 7-2, a step input occurred at time, $t=100$. Then, the control system was able to counterbalance the input with in 1300 seconds and remain with in a pointing tolerance of 0.1° . But, this requires a continual supply of angular momentum from the reaction wheel. A momentum dump will need to occur after 850,000 seconds or every 9.8 days for the momentum wheels selected. Next, with a sinusoidal torque input the system remained within pointing accuracy and fluctuated between $\pm 0.05^\circ$. Finally, with an impulse input of approximately one order of magnitude larger than the other torques the system stabled out after 1600 seconds and also remained within the required pointing accuracy, see Figure 7-4.

The second simulation was of the roll and yaw components, which are coupled (see Appendix F). Other than the coupling difference the simulation process was the same as for the pitch. Graphs of the simulation can be seen in Figures 7-5 through 7-8. For the sinusoidal input for roll the angular momentum did not increase with time but instead was sinusoidal. This is significant because a momentum dump will not be required. For the sinusoidal input for yaw a momentum dump must occur every 800,000 seconds or every 9.25 days.

The final simulation was that for the contingency mode of operation which simulated a yaw control failure (see Appendix F). For this I just used a fourth reaction wheel canted between the roll and yaw directions. Then, I ran all three inputs to show that the system was able to control the spacecraft and remain within pointing accuracies. This information is displayed in Figures 7-9 through 7-12.

Finally, in estimating the fuel required for momentum dumping I tended to be conservative. For the estimation I am assuming that both pitch and yaw angular momentum must be dumped every 10.5 days and 9.25 days respectively. Therefore, we will need approximately 80 pulses in a year.

Next, from the following relationships we can determine the amount of propellant mass used in each burn:

$$F = \frac{H}{Lt}$$

$$M_p = \frac{Ft}{I_{sp}g}$$
7-16

Therefore, the total propellant mass used in one year for thruster only momentum dumping is estimated to be 1.5 kg.

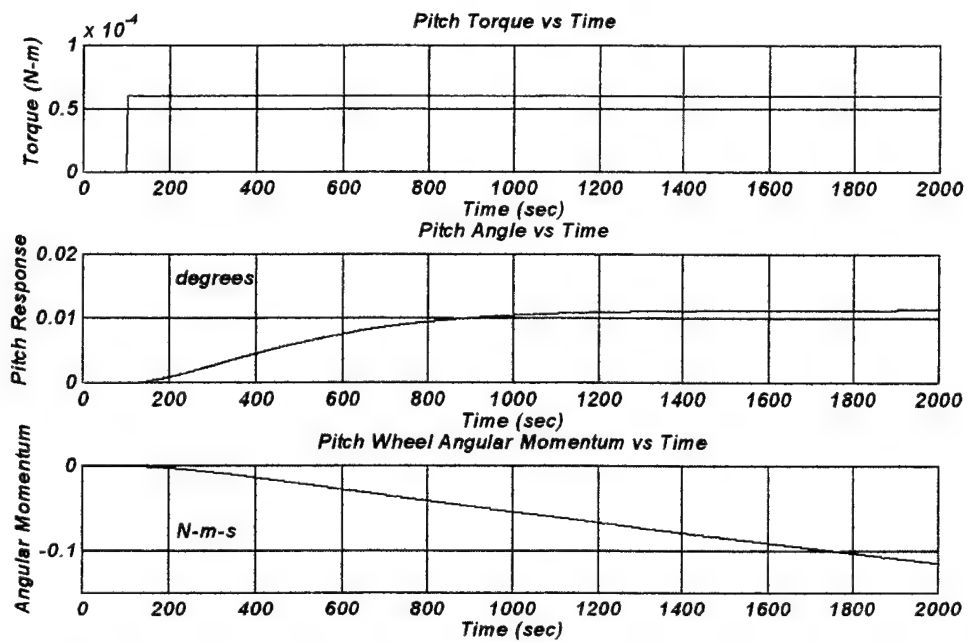


Figure 7-2: Pitch Response Due to a Step Input Disturbance Torque.

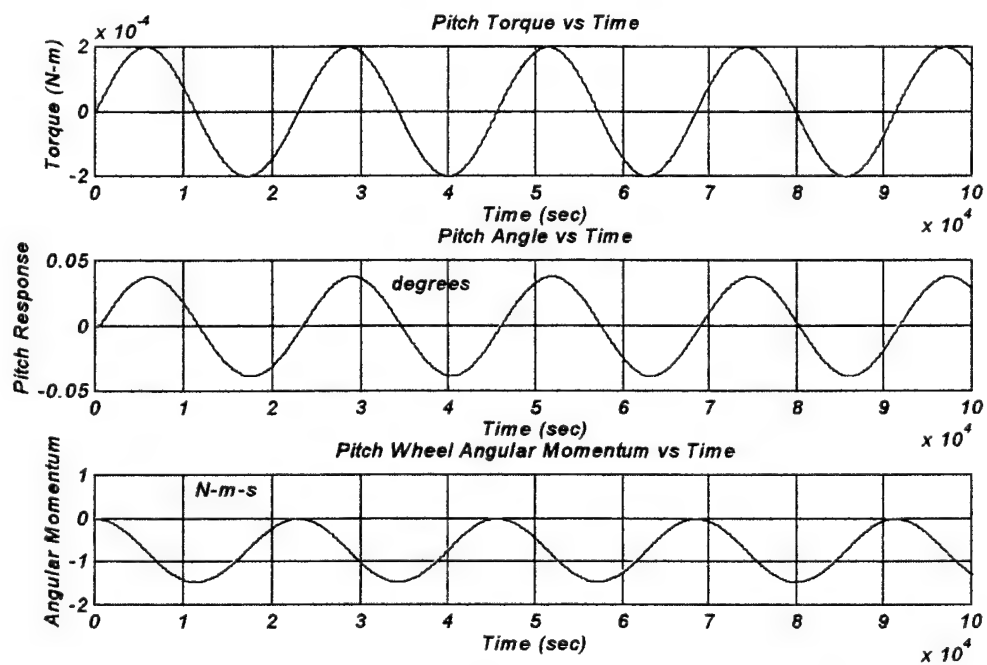


Figure 7-3: Pitch Response Due to a Sinusoidal Disturbance Torque.

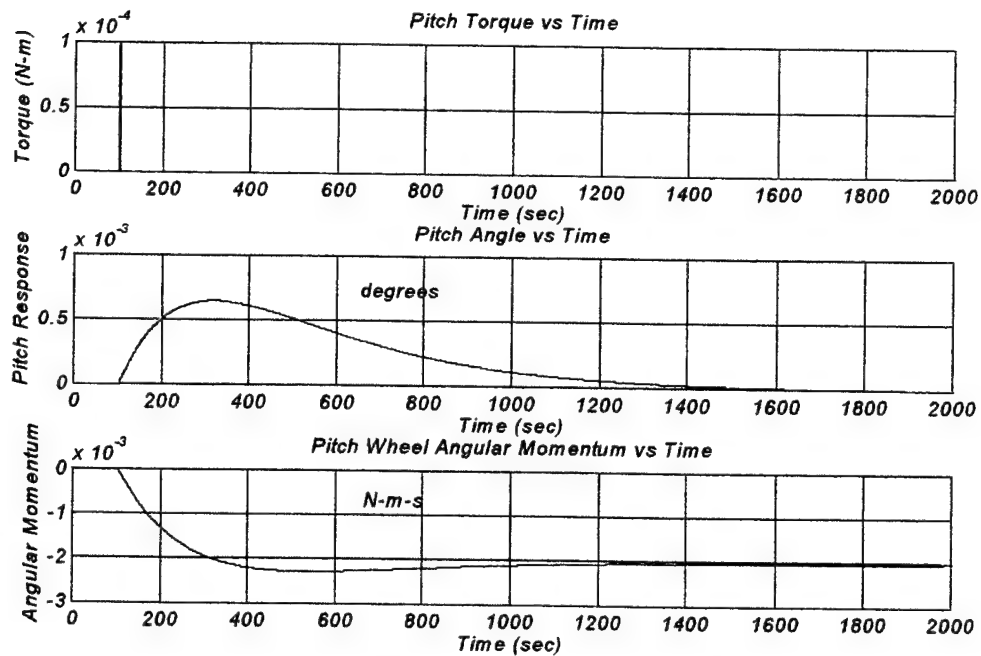


Figure 7-4: Pitch Response Due to an Impulse Disturbance Torque.

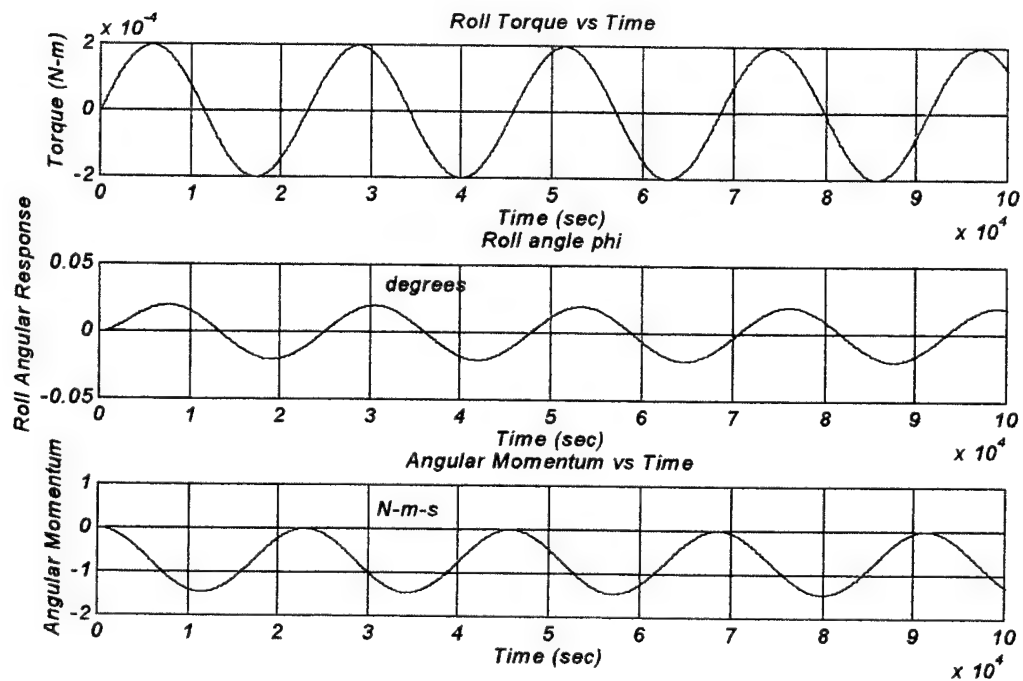


Figure 7-5: Roll Response Due to a Sinusoidal Disturbance Torque.

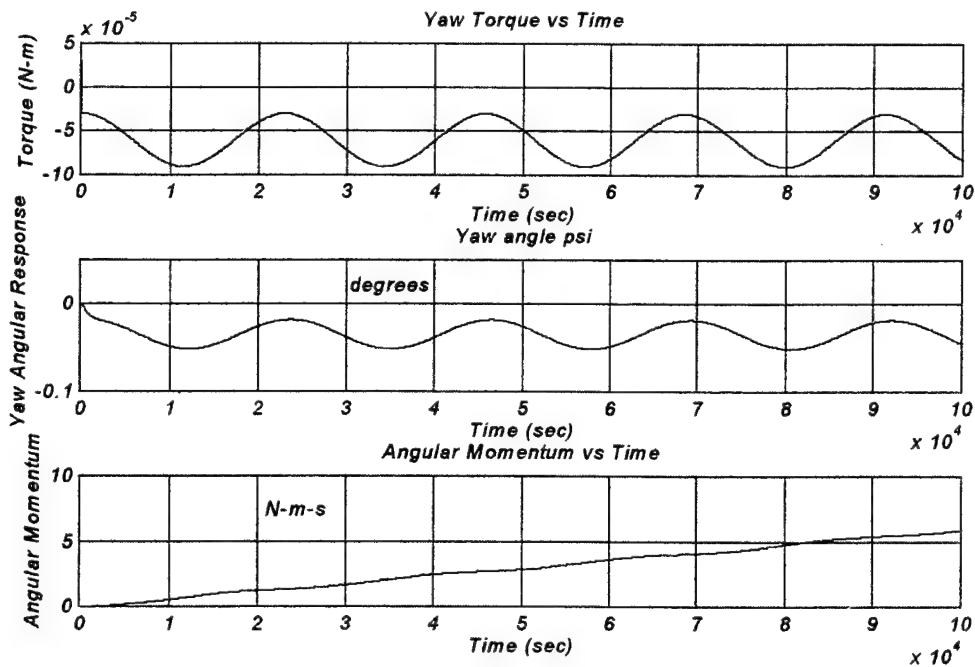


Figure 7-6: Yaw Response Due to a Sinusoidal Disturbance Torque.

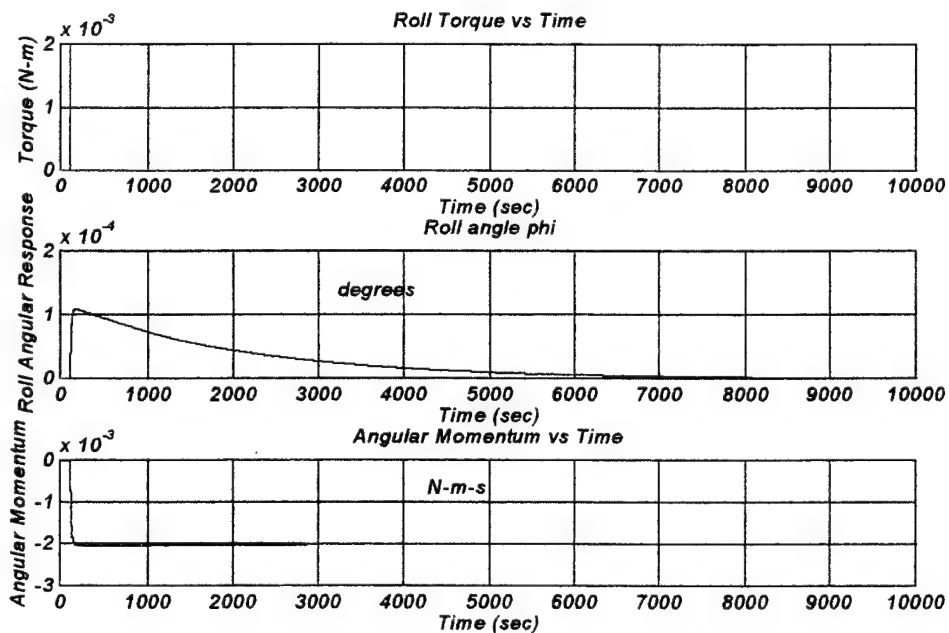


Figure 7-7: Roll Response Due to an Impulse Disturbance Torque.

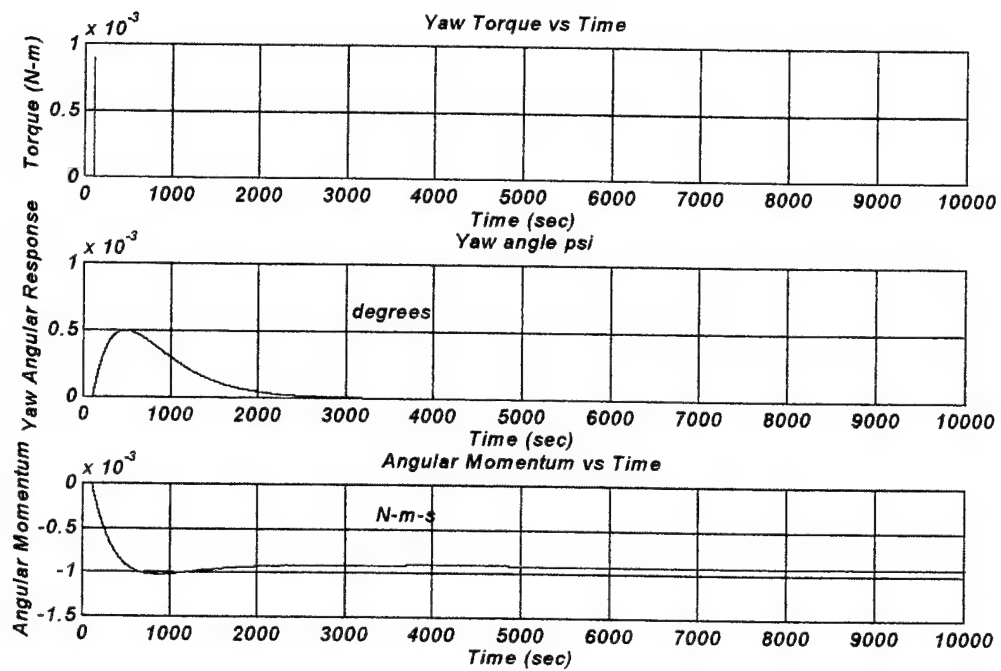


Figure 7-8: Yaw Response Due to an Impulse Disturbance Torque.

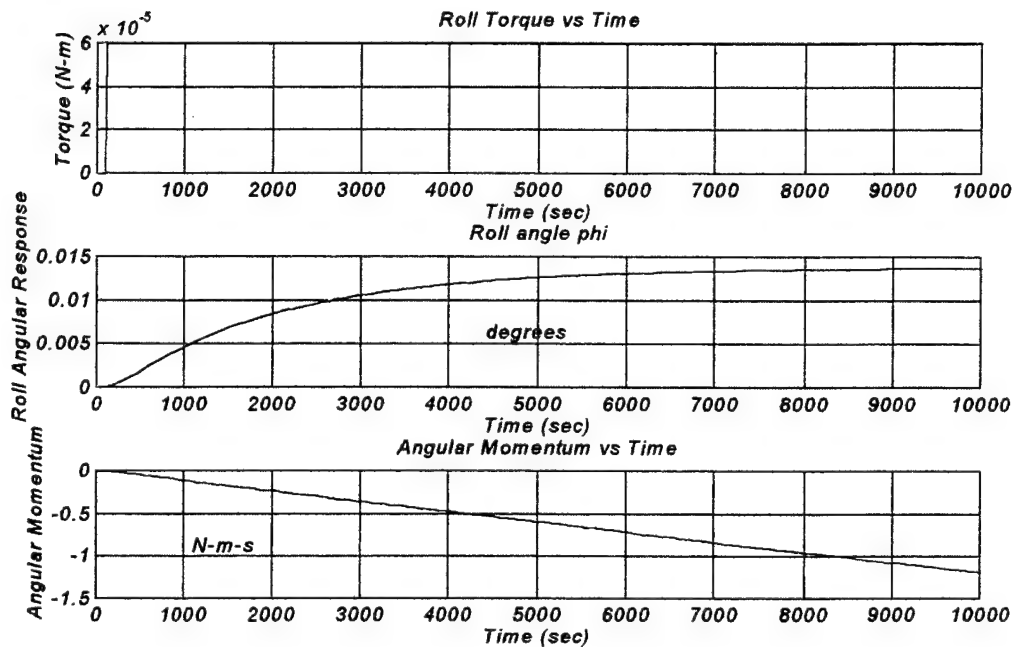


Figure 7-9: Roll Response Due to a Step Input Disturbance Torque - Back Up System.

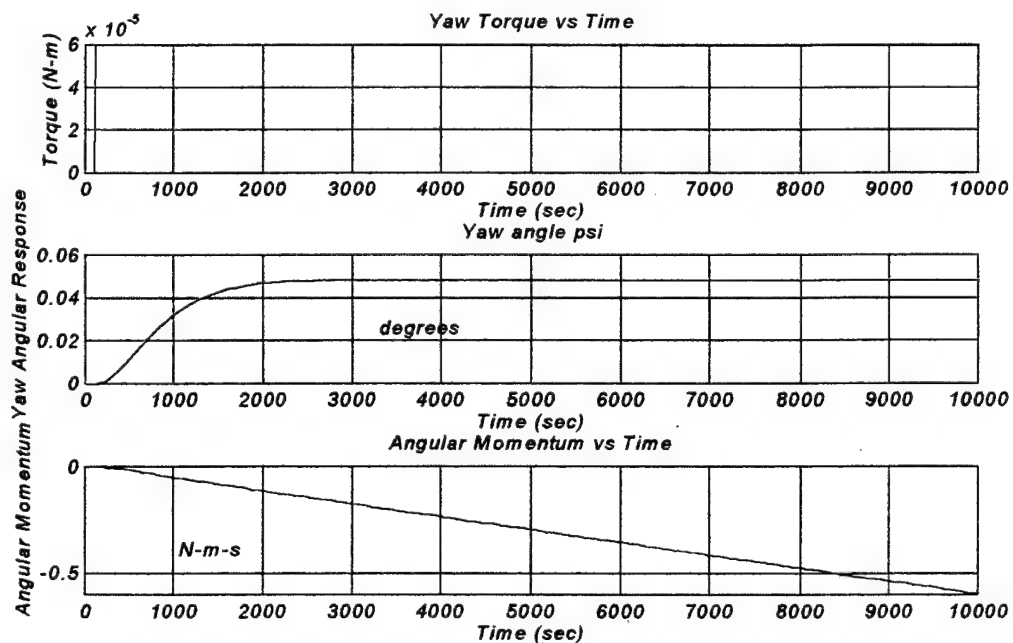


Figure 7-10: Yaw Response Due to a Step Input Disturbance Torque - Back Up System.

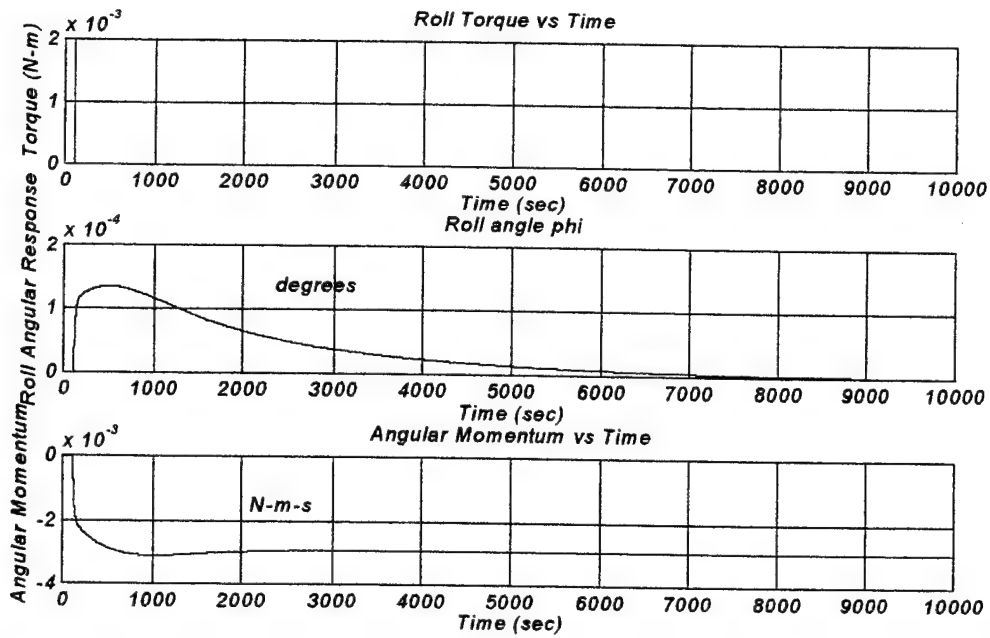


Figure 7-11: Roll Response Due to an Impulse Disturbance Torque - Back Up System.

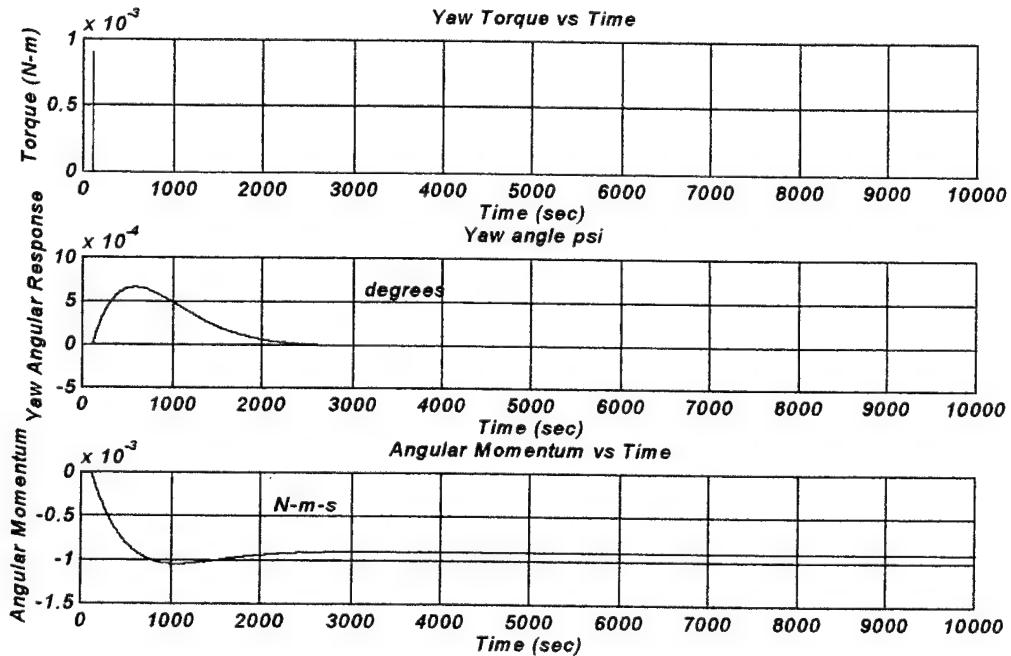


Figure 7-12: Yaw Response Due to an Impulse Disturbance Torque - Back Up System.

2. Yaw Steering Requirements

In this section the attitude dynamics and control of the spacecraft is explored when small angle approximations are not made and all higher order terms are included in the equations of motion. This is a complexity that is a result of the requirements for yaw steering.

Introducing Eqs. (7-6) and (7-8) into Eq. (7-7), the equations of motion for a three axis reaction wheel system are

$$\begin{aligned}
 M_{cx} + M_{sx} = & I_{xx}\ddot{\phi} + \dot{\theta}\cos(\phi)I_{zz}\dot{\psi} + \dot{\psi}^2\cos(\theta)\sin(\phi)I_{zz} - \omega_o\cos(\phi)\cos(\psi)I_{zz}\dot{\psi} - \\
 & \omega_o\sin(\phi)\sin(\theta)\sin(\psi)I_{zz}\dot{\psi} + \dot{\theta}^2\sin(\phi)I_{yy} - \dot{\psi}\cos(\theta)\cos(\phi)I_{yy}\dot{\theta} - \\
 & \omega_o\sin(\phi)\cos(\psi)I_{yy}\dot{\theta} + \omega_o\cos(\phi)\sin(\theta)\sin(\psi)I_{yy}\dot{\theta} - \\
 & 3\omega_o^2\sin(\phi)\cos(\phi)[\cos(\theta)]^2I_{zz} + 3\omega_o^2\sin(\phi)\cos(\phi)[\cos(\theta)]^2I_{yy} + \dot{h}_x \\
 & + \dot{\theta}\cos(\phi)h_z + \dot{\psi}\cos(\theta)\sin(\phi)h_z - \omega_o\cos(\phi)\cos(\psi)h_z - \\
 & \omega_o\sin(\phi)\sin(\theta)\sin(\psi)h_z + \dot{\theta}\sin(\phi)h_y - \dot{\psi}\cos(\theta)\cos(\phi)h_y - \\
 & \omega_o\sin(\phi)\cos(\psi)h_y + \omega_o\cos(\phi)\sin(\theta)\sin(\psi)h_y \\
 \\
 M_{cy} + M_{sy} = & I_{yy}\ddot{\theta} - \dot{\theta}\sin(\phi)I_{xx}\dot{\phi} + \dot{\psi}\cos(\theta)\cos(\phi)I_{xx}\dot{\phi} + \omega_o\sin(\phi)\cos(\psi)I_{xx}\dot{\phi} - \\
 & - \omega_o\cos(\phi)\sin(\theta)\sin(\psi)I_{xx}\dot{\phi} - \dot{\phi}I_{zz}\dot{\psi} + \dot{\psi}^2\sin(\theta)I_{zz} + \\
 & \omega_o\cos(\theta)\sin(\psi)I_{zz}\dot{\psi} - 3\omega_o^2\sin(\theta)\cos(\theta)\cos(\phi)I_{zz} + \\
 & 3\omega_o^2\sin(\theta)\cos(\theta)\cos(\phi)I_{xx} + \dot{h}_y - \dot{\theta}\sin(\phi)h_x + \dot{\psi}\cos(\theta)\cos(\phi)h_x + \\
 & \omega_o\sin(\phi)\cos(\psi)h_x - \omega_o\cos(\phi)\sin(\theta)\sin(\psi)h_x - \dot{\phi}h_z + \dot{\psi}\sin(\theta)h_z + \\
 & \omega_o\cos(\theta)\sin(\psi)h_z
 \end{aligned}
 \tag{7-17}$$

$$\begin{aligned}
 M_{cz} + M_{sz} = & I_{zz}\ddot{\psi} + \dot{\phi}I_{yy}\dot{\theta} - \dot{\psi}\sin(\theta)I_{yy}\dot{\theta} - \omega_o\cos(\theta)\sin(\psi)I_{yy}\dot{\theta} - \dot{\theta}\cos(\phi)I_{xx}\dot{\phi} - \\
 & \dot{\psi}\cos(\theta)\sin(\phi)I_{xx}\dot{\phi} + \omega_o\cos(\phi)\cos(\psi)I_{xx}\dot{\phi} + \omega_o\sin(\phi)\sin(\theta)\sin(\psi)I_{xx}\dot{\phi} \\
 & - 3\omega_o^2\sin(\theta)\cos(\theta)\sin(\phi)I_{xx} + 3\omega_o^2\sin(\theta)\cos(\theta)\sin(\phi)I_{yy} + \dot{h}_z + \dot{\phi}h_y - \\
 & \dot{\psi}\sin(\theta)h_y - \omega_o\cos(\theta)\sin(\psi)h_y - \dot{\theta}\cos(\phi)h_x - \dot{\psi}\cos(\theta)\sin(\phi)h_x + \\
 & \omega_o\cos(\phi)\cos(\psi)h_x + \omega_o\sin(\phi)\sin(\theta)\sin(\psi)h_x
 \end{aligned}$$

These equations of motion are somewhat overwhelming. In the process of developing a control law the first step was to transform these equations of motion into a

state space formulation and develop a Matlab/Simulink model for the motion of the spacecraft with no control. The state space formulation used was the following:

$$\begin{aligned}x_1 &= \phi \\x_2 &= \dot{x}_1 = \dot{\phi} \\x_3 &= \theta \\x_4 &= \dot{x}_3 = \dot{\theta} \\x_5 &= \psi \\x_6 &= \dot{x}_5 = \dot{\psi}\end{aligned}$$

$$\begin{aligned}\dot{x}_1 &= x_2 \\ \dot{x}_2 = \ddot{x}_1 = \ddot{\phi} &= \left[\frac{-1}{I_{xx}} \right] (\dot{\theta} \cos(\phi) I_{zz} \dot{\psi} + \dot{\psi}^2 \cos(\theta) \sin(\phi) I_{zz} - \omega_o \cos(\phi) \cos(\psi) I_{zz} \dot{\psi} - \\ &\quad \omega_o \sin(\phi) \sin(\theta) \sin(\psi) I_{zz} \dot{\psi} + \dot{\theta}^2 \sin(\phi) I_{yy} - \dot{\psi} \cos(\theta) \cos(\phi) I_{yy} \dot{\theta} - \\ &\quad \omega_o \sin(\phi) \cos(\psi) I_{yy} \dot{\theta} + \omega_o \cos(\phi) \sin(\theta) \sin(\psi) I_{yy} \dot{\theta} - \\ &\quad 3\omega_o^2 \sin(\phi) \cos(\phi) [\cos(\theta)]^2 I_{zz} + 3\omega_o^2 \sin(\phi) \cos(\phi) [\cos(\theta)]^2 I_{yy} \\ &\quad + \dot{h}_x + \dot{\theta} \cos(\phi) h_z + \dot{\psi} \cos(\theta) \sin(\phi) h_z - \omega_o \cos(\phi) \cos(\psi) h_z - \\ &\quad \omega_o \sin(\phi) \sin(\theta) \sin(\psi) h_z + \dot{\theta} \sin(\phi) h_y - \dot{\psi} \cos(\theta) \cos(\phi) h_y - \\ &\quad \omega_o \sin(\phi) \cos(\psi) h_y + \omega_o \cos(\phi) \sin(\theta) \sin(\psi) h_y - M_{1d})\end{aligned}$$

$$\dot{x}_3 = x_4 \tag{7-18}$$

$$\begin{aligned}\dot{x}_4 = \ddot{x}_3 = \ddot{\theta} &= \left[\frac{-1}{I_{yy}} \right] (-\dot{\theta} \sin(\phi) I_{xx} \dot{\phi} + \dot{\psi} \cos(\theta) \cos(\phi) I_{xx} \dot{\phi} + \omega_o \sin(\phi) \cos(\psi) I_{xx} \dot{\phi} - \\ &\quad \omega_o \cos(\phi) \sin(\theta) \sin(\psi) I_{xx} \dot{\phi} - \dot{\phi} I_{zz} \dot{\psi} + \omega_o \cos(\theta) \sin(\psi) I_{zz} \dot{\psi} - \dot{\phi} h_z \\ &\quad - 3\omega_o^2 \sin(\theta) \cos(\theta) \cos(\phi) I_{zz} + 3\omega_o^2 \sin(\theta) \cos(\theta) \cos(\phi) I_{xx} + \dot{h}_y \\ &\quad - \dot{\theta} \sin(\phi) h_x + \dot{\psi} \cos(\theta) \cos(\phi) h_x + \omega_o \sin(\phi) \cos(\psi) h_x + \dot{\psi}^2 \sin(\theta) I_{zz} - \\ &\quad \omega_o \cos(\phi) \sin(\theta) \sin(\psi) h_x + \dot{\psi} \sin(\theta) h_z + \omega_o \cos(\theta) \sin(\psi) h_z - M_{2d})\end{aligned}$$

$$\dot{x}_5 = x_6$$

$$\dot{x}_6 = \ddot{x}_5 = \ddot{\psi} = \left[\frac{-1}{I_{zz}} \right] (\dot{\phi} I_{yy} \dot{\theta} - \dot{\psi} \sin(\theta) I_{yy} \dot{\theta} - \omega_o \cos(\theta) \sin(\psi) I_{yy} \dot{\theta} - \dot{\theta} \cos(\phi) I_{xx} \dot{\phi} - \dot{\psi} \cos(\theta) \sin(\phi) I_{xx} \dot{\phi} + \omega_o \cos(\phi) \cos(\psi) I_{xx} \dot{\phi} + \omega_o \sin(\phi) \sin(\theta) \sin(\psi) I_{xx} \dot{\phi} - 3\omega_o^2 \sin(\theta) \cos(\theta) \sin(\phi) I_{xx} + 3\omega_o^2 \sin(\theta) \cos(\theta) \sin(\phi) I_{yy} + \dot{h}_z + \dot{\phi} h_y - \dot{\psi} \sin(\theta) h_y - \omega_o \cos(\theta) \sin(\psi) h_y - \dot{\theta} \cos(\phi) h_x - \dot{\psi} \cos(\theta) \sin(\phi) h_x + \omega_o \cos(\phi) \cos(\psi) h_x + \omega_o \sin(\phi) \sin(\theta) \sin(\psi) h_x - M_{3d})$$

Then, after developing the simulink model, I analyzed the dynamics of the spacecraft as a function of time when a disturbance torque was applied. This can be seen in Figures 7-13 through 7-15; also, see Appendix G. Note that without control the spacecraft will become unstable very quickly.

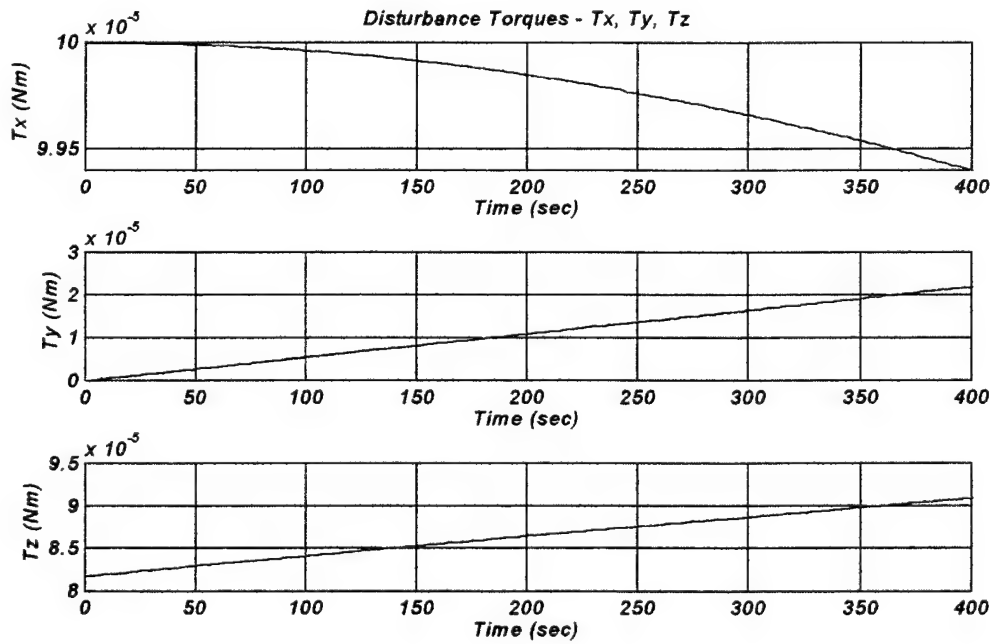


Figure 7-13: Disturbance Torques Applied to the Spacecraft - Large Angle Scenario.

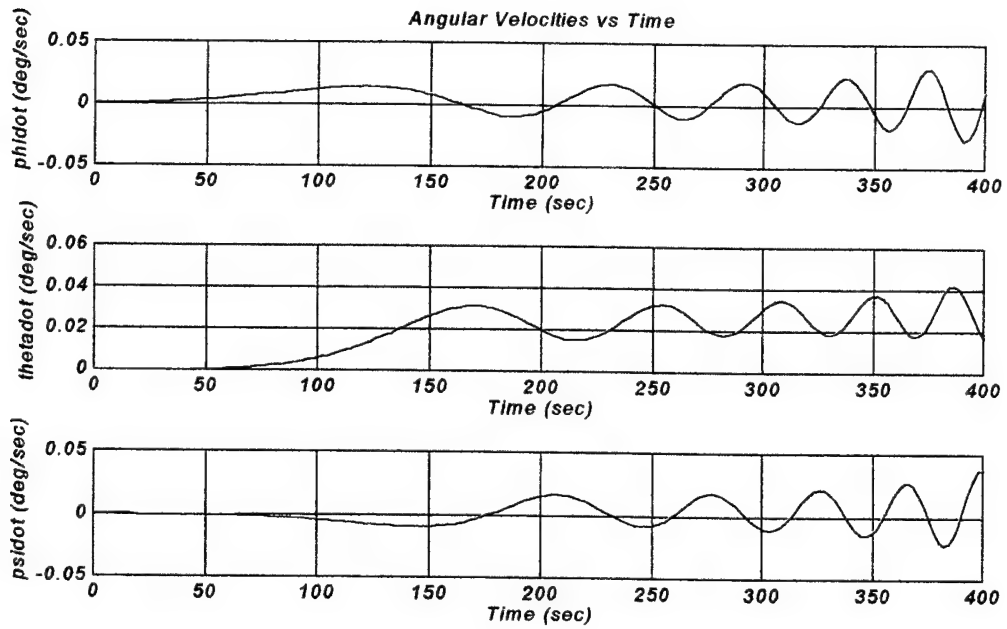


Figure 7-14: The three body components of angular velocity due to a disturbance torque with no control - Large Angle Scenario.

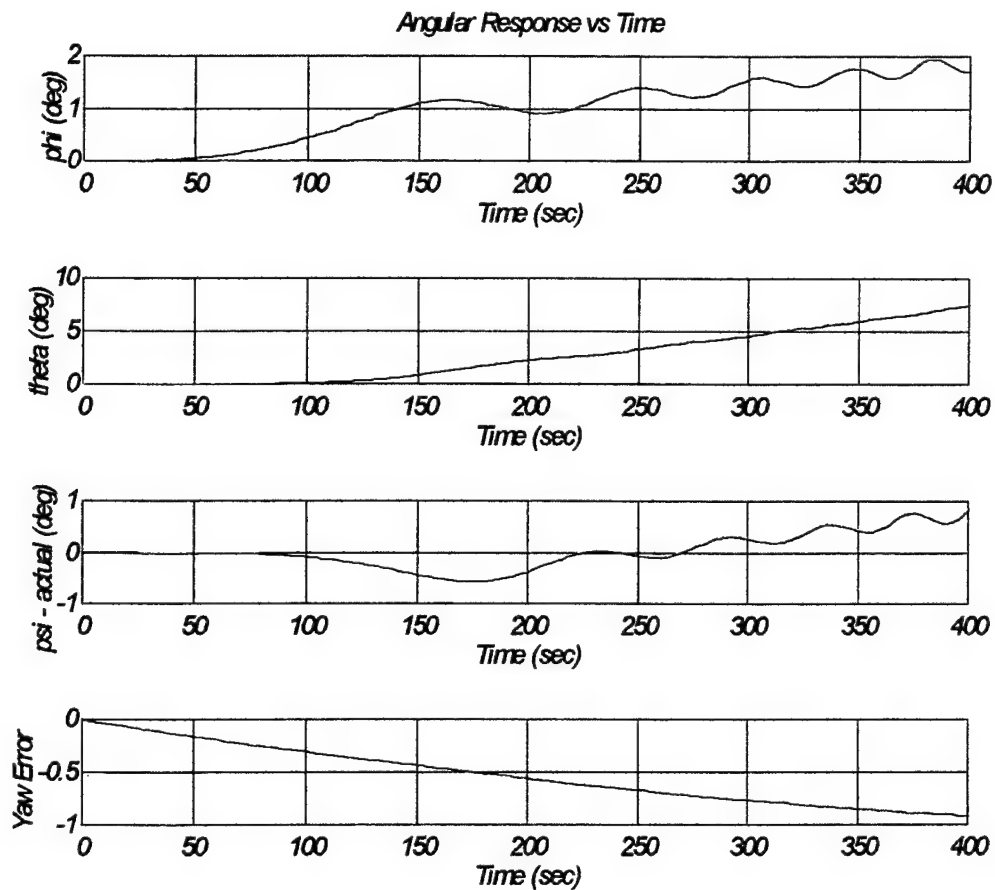


Figure 7-15: Spacecraft Angular Response Due to Disturbance Torque - Large Angle Scenario.

D. ADCS CONTROL AND PERFORMANCE ANALYSIS - YAW STEERING

In order to keep the antenna beam pointing accuracy and the solar array panel pointing accuracy between acceptable limits (0.1° and 1° respectively), a control system must determine the required movements of the reaction wheel. This controller (control loop) could be developed in many different ways. In our case the angle and the angular speed measured by the sensors are used. In this way the system corrects the deviation based on the actual deviation and the rotation speed. The control loop is given in Figure 7-16.

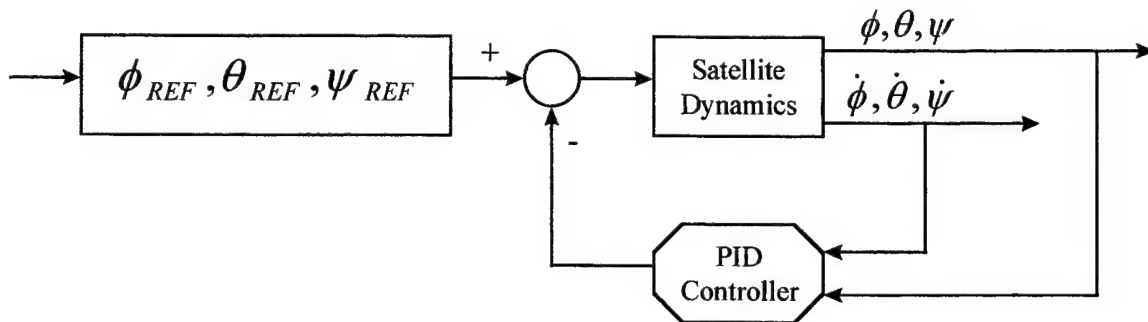


Figure 7-16: The Control Loop

The block scheme of the system model is shown in Figure 7-17. The satellite dynamics are described by the equations 7-16. The BAPTA controller controls the actions of the BAPTA, which again influences the motions about the y-axis. There are three RW controllers each controlling a reaction wheel. The OBC has two sensor inputs, the orbital angle β and the angle between the orbital plane and the Sun-Earth-vector δ .

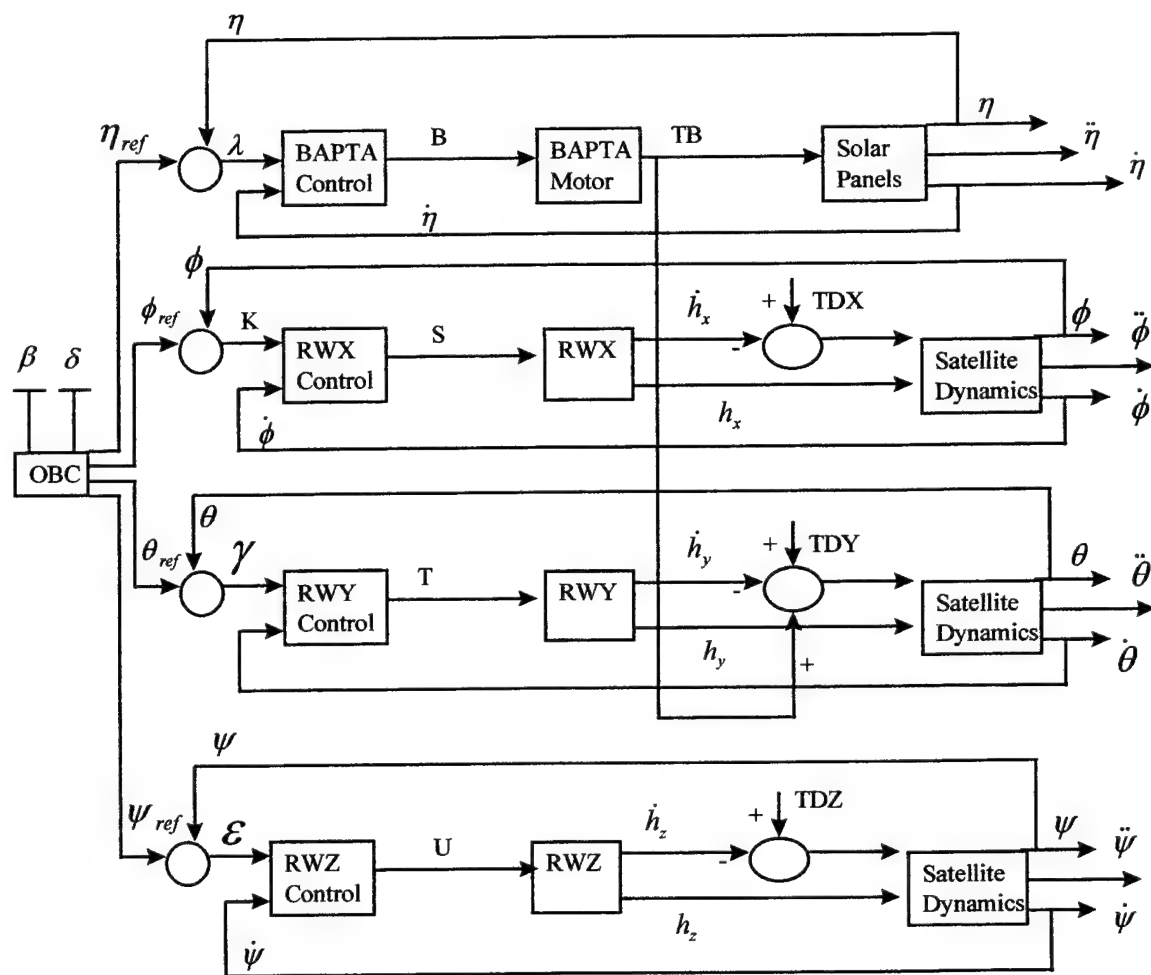


Figure 7-17: System Model

For the computer simulation Matlab and Simulink were used (see Appendix G). And, three situations were considered. First, a step input due to thruster misalignment. Second, the sinusoidal input due to solar pressure torques; and third, an impulse input of approximately one order of magnitude larger than the others (see simulink diagrams and Matlab code in Appendix G). Several combinations of the three scenarios were also tested. When modeling the simulations, disturbance torque values and scenarios were used that rarely would occur on the satellite. This was done in an effort to show the robustness of the satellite control. In general, we are trying to look at the worst case scenarios. Also, the control values selected are indicated in Table 7-2.

ROLL	PITCH	YAW
$K_r = 8.5$	$K_p = 9.0$	$K_y = 1$
$\tau_r = 2060$	$\tau_p = 2000$	$\tau_y = 751$

Table 7-2: Control Law Values

The first simulation imparted impulse torques along the roll, pitch and yaw axes. The magnitudes selected were greater than those expected to actually occur on orbit and it would be extremely unlikely to have 3 simultaneous impulse torques. As can be seen in Figure 7-18, the impulse torques occurred at time, $t=100$ seconds. Figure 7-20 illustrates the angular responses for roll, pitch, and yaw. A thorough study of the responses reveal the greatest error occurs from the effects of yaw steering and not the impulse torques. And, the required pointing accuracies have been maintained throughout the orbit. Next, with a step input along all three axes, the angular responses were evaluated and found to be within operational limitations. It should be noted that the greatest error occurs during this scenario. This is because the step disturbance is occurring at the same time the yaw inversion is taking place. So in effect, we have an additive disturbance among the two. Then, a sinusoidal disturbance torque was applied along all three axis simultaneously. This can be seen in Figures 7-21 through 7-23. And, once again the pointing accuracies fell within limits. Finally, a simulation of sinusoidal, impulse, and step disturbance torques were applied along the roll, pitch, and yaw axes respectively. And, in this scenario all pointing accuracy requirements were maintained.

Throughout the simulations the maximum error occurred when the yaw inversion took place. It is at this point that the yaw angular velocity is greatest. This is due to the fact that the yaw angle and angular rate are coupled into the roll and pitch. So, when yaw rate of change is greatest we see our greatest error along all three attitude axes. Also, the yaw angular velocity and angular acceleration is not continuous at their maximum and minimum values. This in turn creates a rapid change condition which then allows for more error to be introduced.

The final simulation was a sinusoidal input along the pitch axis and was performed to illustrate the value of disturbance torque that would cause the system to exceed

pointing accuracy requirements. As can be seen in Figures 7-24 through 7-26, a sinusoidal input of 0.01 N-m caused the pitch axis pointing accuracy to exceed 0.1° . Recall that the maximum disturbance torque anticipated is 0.001 N-m. Therefore a built in safety margin exists.

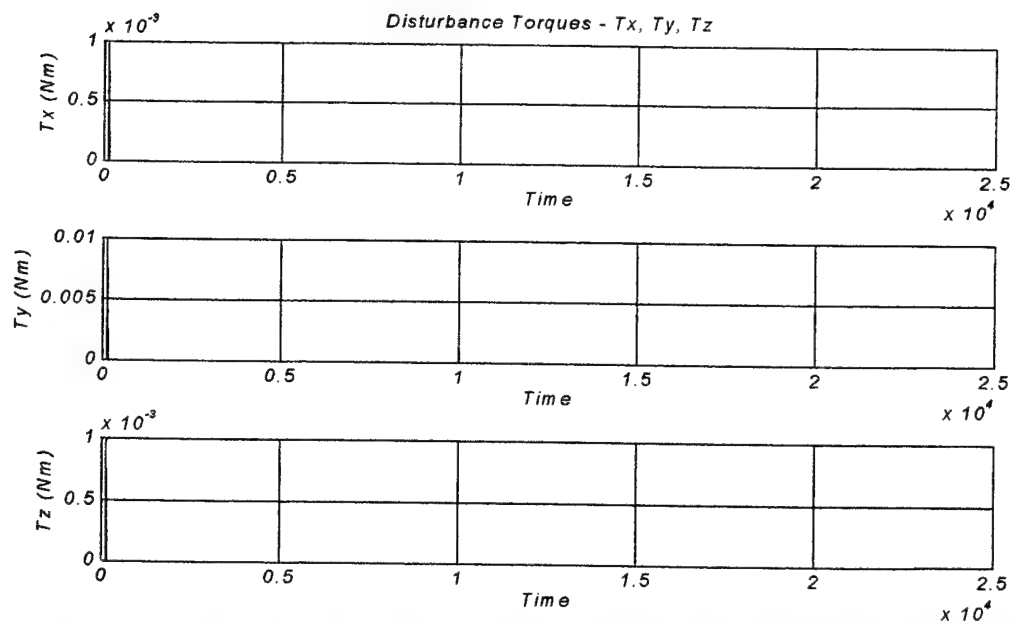


Figure 7-18: Impulse Disturbance Torque for Control of Yaw Steering Scenario #1
(Time in seconds).

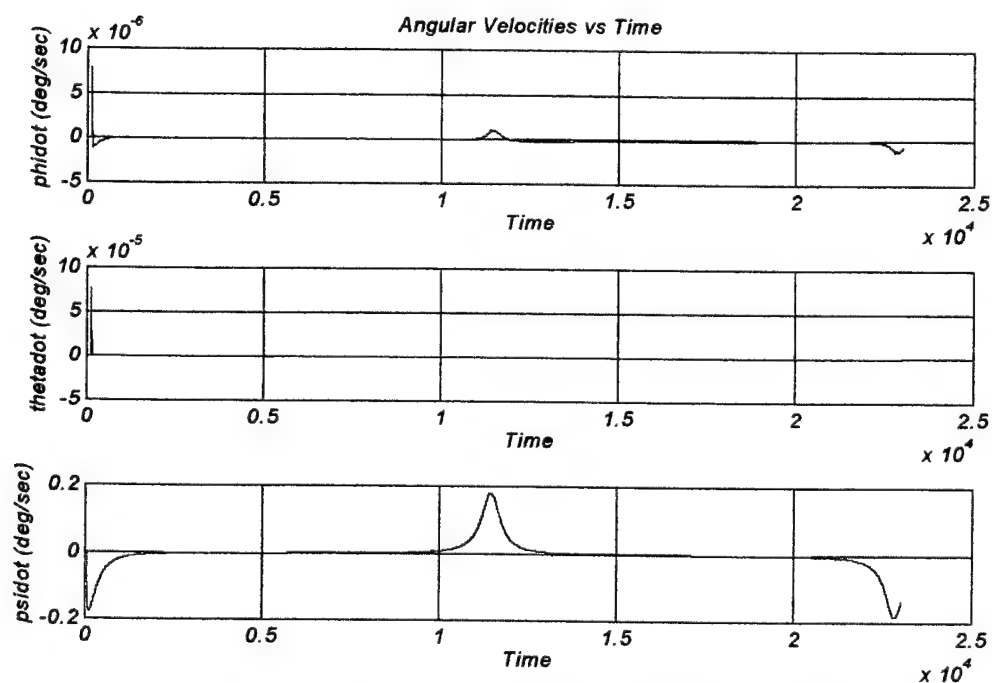


Figure 7-19: Spacecraft Angular Velocities During the Control of Yaw Steering Scenario #1 (Time in seconds).

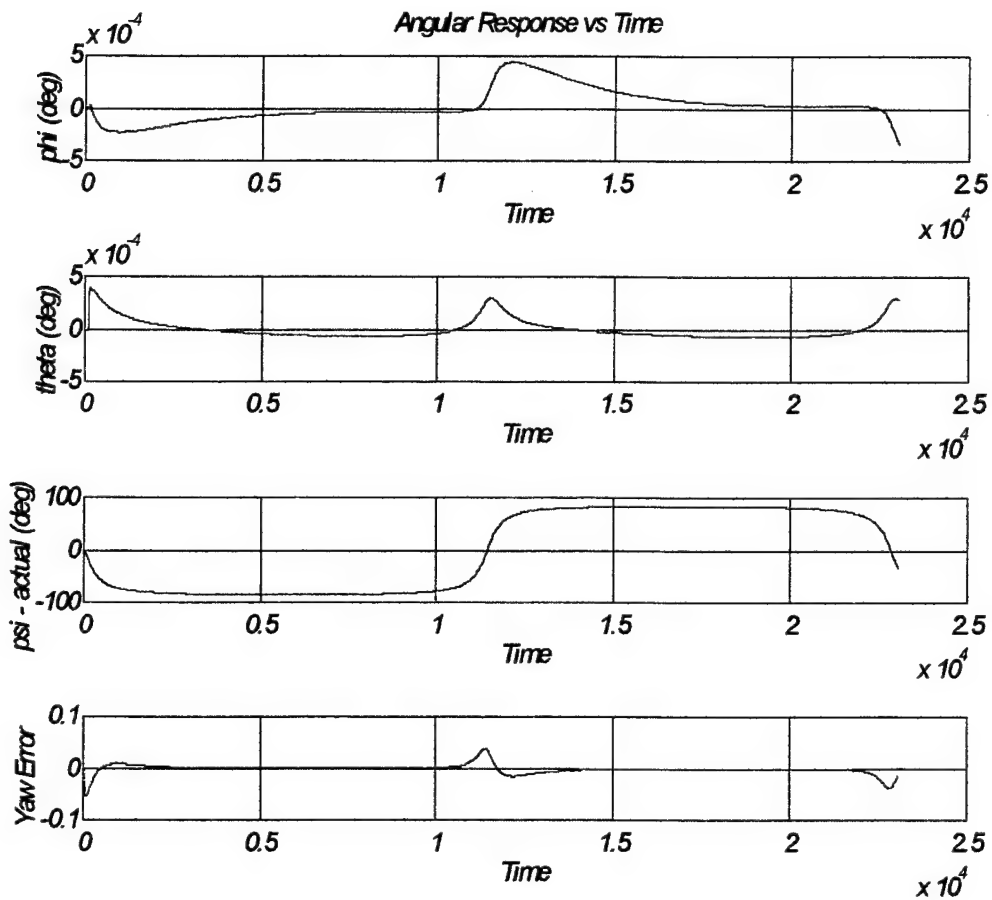


Figure 7-20: Spacecraft Angular Response Due to Impulse Disturbance Torque - Yaw Steering Scenario #1 (Time in seconds).

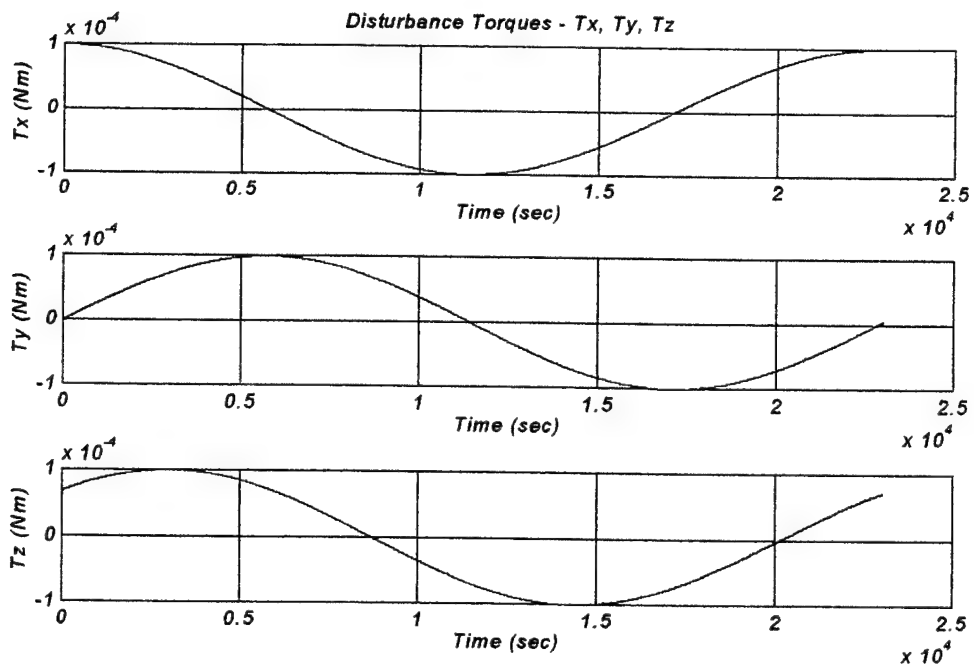


Figure 7-21: Sinusoidal Disturbance Torque for Yaw Steering Scenario #2.

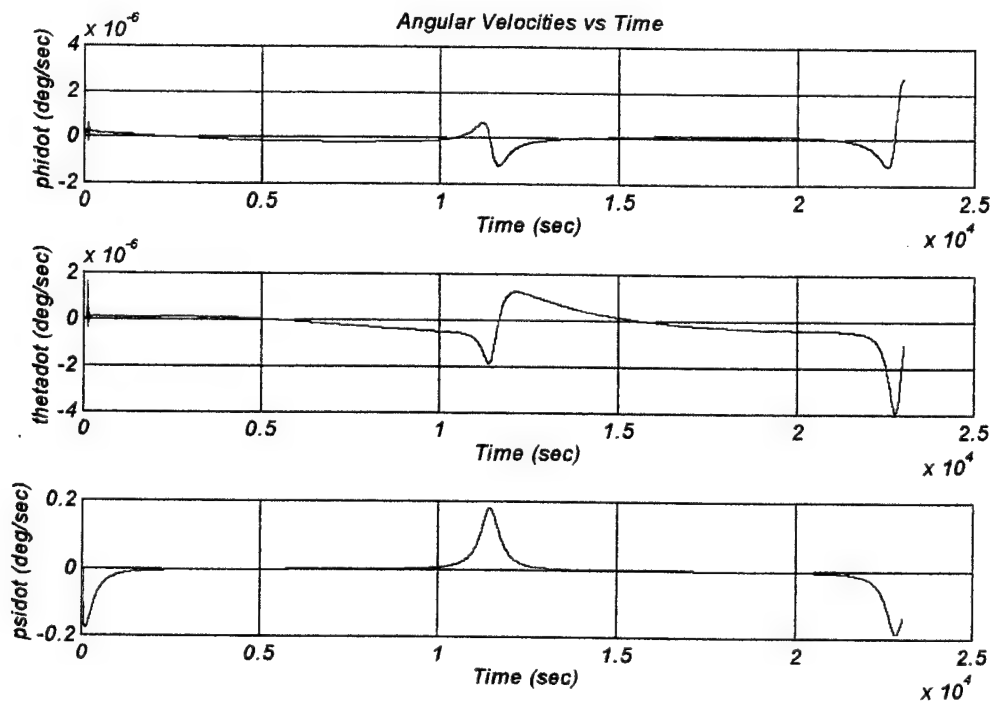


Figure 7-22: Spacecraft Angular Velocities During the Control of Yaw Steering Scenario #2.

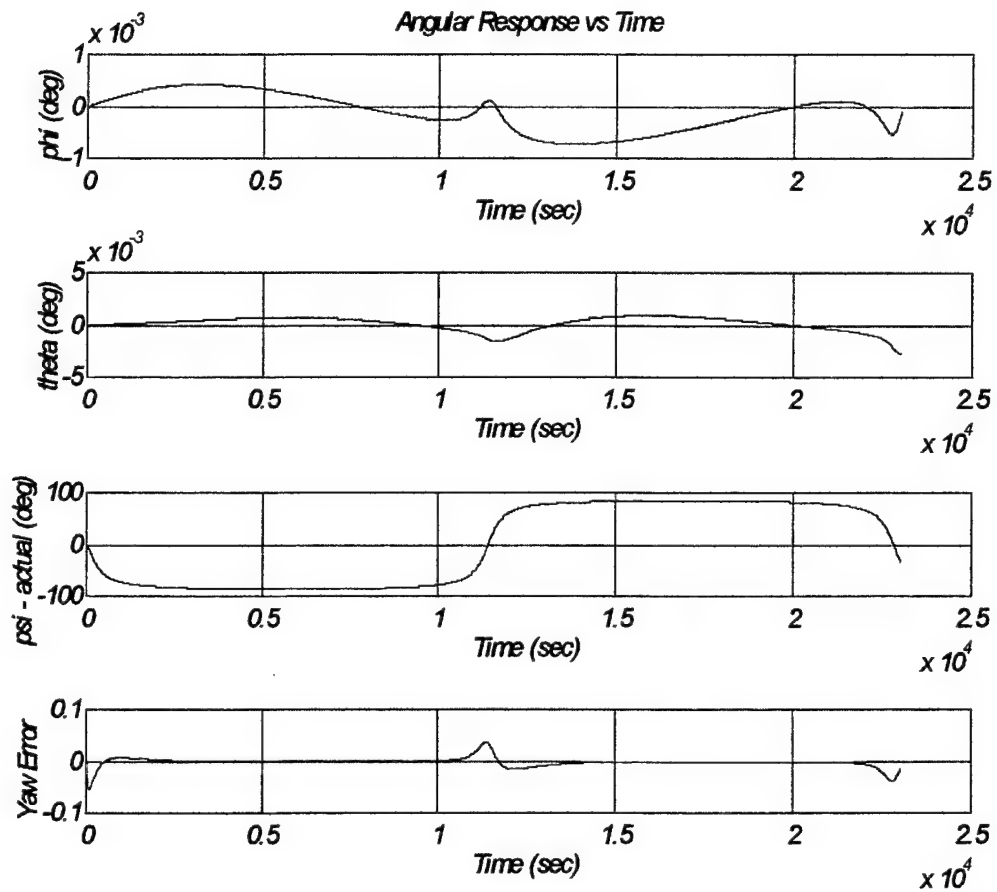


Figure 7-23: Spacecraft Angular Response Due to Sinusoidal Disturbance Torque - Yaw Steering Scenario #2.

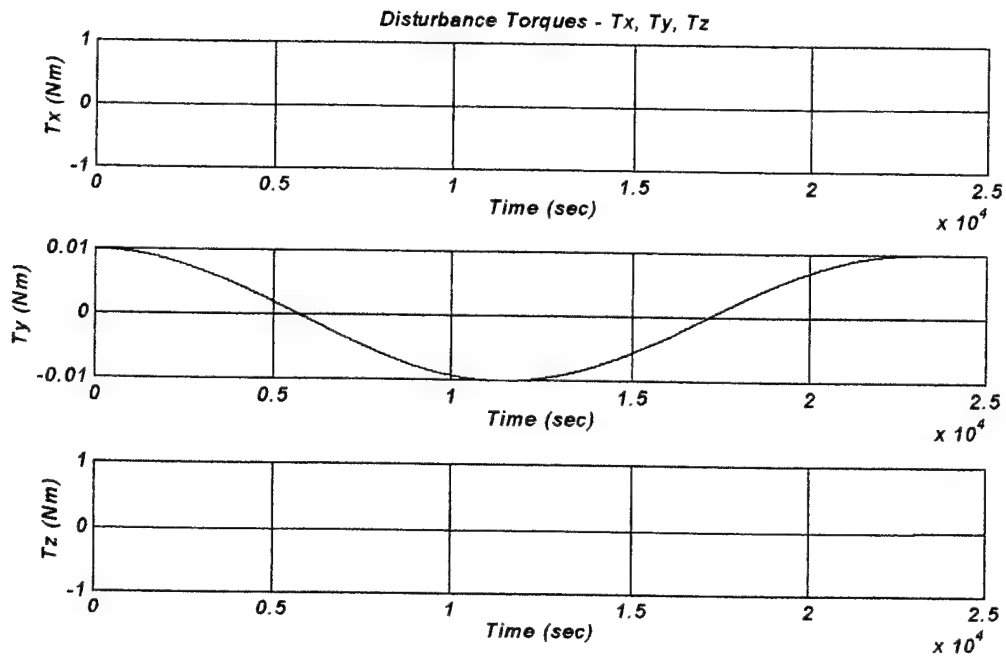


Figure 7-24: Sinusoidal Disturbance Torque for Yaw Steering Scenario #3.

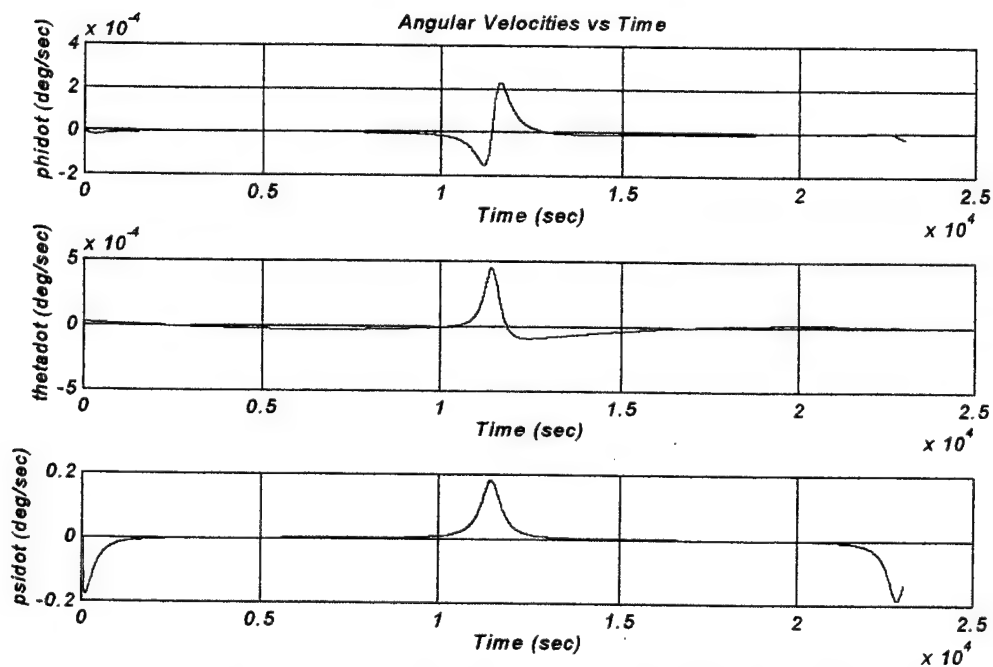


Figure 7-25: Spacecraft Angular Velocities During the Control of Yaw Steering Scenario #3.

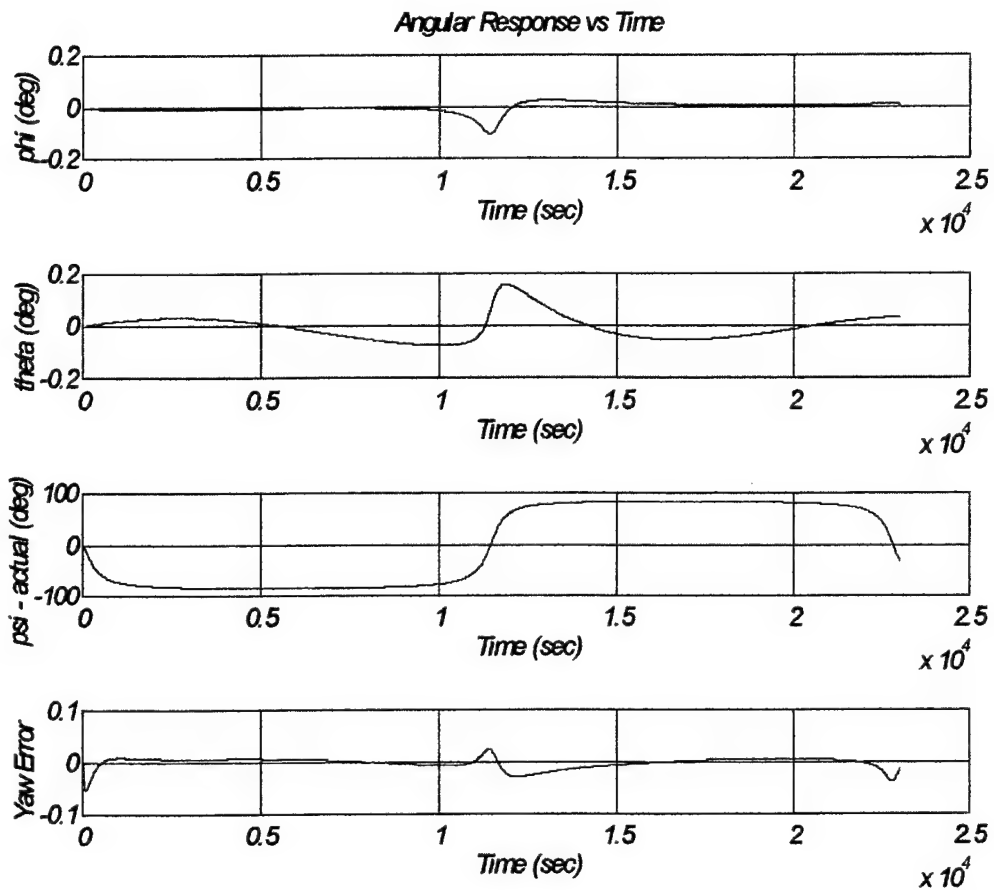


Figure 7-26: Spacecraft Angular Response Due to Sinusoidal Disturbance Torque - Yaw Steering Scenario #3.

This Page Intentionally Left Blank

VIII. CONCLUSION

A. SUMMARY OF DESIGN PROCESS

In this thesis the preliminary design of an Attitude Dynamics and Control Subsystem for a Medium Earth Orbit communications satellite was performed. The process focused on the six critical steps in designing an ADCS which are stated as follows:

1. Design control modes.
2. Define or derive system level requirements.
3. Select type of spacecraft control by attitude control mode.
4. Quantify the disturbance environment.
5. Select and size ADCS hardware.
6. Define determination and control algorithms.

Also presented was the important aspect of how the ADCS is inter-related with the other spacecraft subsystems. And, how many of the requirements and design drivers of the ADCS originate in the other spacecraft subsystems.

The highlights and conclusions of the ADCS design process are summarized as follows. First, the control modes of the spacecraft were determined and defined. The control modes determined to be most appropriate for our satellite were the following:

1. Orbit insertion mode
2. Acquisition mode
3. Sun acquisition/sun hold mode
4. Earth acquisition mode
5. Normal mode
6. Slew mode
7. Contingency mode
8. Orbit transition mode

The second design milestone was the determination of system level requirements. Ten ADCS requirements were presented which are summarized below as follows:

1. The ADCS must be fully operational without the aid of ground base control.
2. The operational lifetime of the ADCS must meet or exceed ten years.
3. The ADCS must maintain a UHF antenna beam pointing accuracy of less than or equal to 0.1° .
4. The ADCS must have the capability to provide continuous yaw steering and solar array tracking such that the solar array pointing accuracy is better than or equal to 5° .
5. The spacecraft must be fully operational during eclipse.
6. The spacecraft must be stabilized and under control during all phases of the mission.
7. The ADCS system should have system redundancy such that there are no single point failures.
8. The ADCS should have a ground override capability.
9. The spacecraft must have a cross-link antenna pointing accuracy of 0.07° which requires a spacecraft attitude knowledge requirement of 0.02° in roll, pitch, and yaw.
10. The ADCS must have a positional knowledge requirement of ± 350 meters.

The next design milestone was determining the type of spacecraft control by attitude control mode and presenting a functional description of the ADCS. During this stage we determined what kind of sensors and actuators were to be used and then showed how they were to be used in each mode of operation. Also introduced in this stage of the design was the motion of the satellite and solar arrays due to the yaw steering requirement.

Then, the design focused on quantifying the disturbance environment. In this process the derivation of the Moments due to solar pressure, gravity gradient, aerodynamic and geomagnetic were presented. And, an estimated disturbance value was attained. Next, the selection of the ADCS hardware was performed. Each sensor and

actuator was described and the reasons for selection of each component were given. The sensor and actuator selection was driven solely by the requirements initially stated.

The final step in the design process was to define determination and control algorithms. Chapter VI examined yaw controlling and presented explanations dealing with control strategy and control software. Then, in chapter VII several simulations of the ADCS were presented and the development of the control law was explained.

B. SUMMARY OF SPACECRAFT ADCS DESIGN

The ADCS chosen for the MUS satellite was a Zero Momentum three axis system which can provide any combination of slew maneuvers in the roll, pitch, and yaw directions. The ADCS can maintain Nadir pointing accuracies to within 0.1° . At the same time it can continuously rotate in the yaw direction while the solar arrays are simultaneously rotating in order to keep a perpendicular orientation towards the sun. This will greatly decrease the complexity of the solar array control mechanisms and reduce spacecraft mass.

As previously mentioned the spacecraft ADCS has eight control modes. Each control mode has peculiar operating characteristics which enable the spacecraft to maintain operations for ten or more years. The operational requirements of the control modes were satisfied by the utilization of various ADCS components as presented in Figure 8-1.

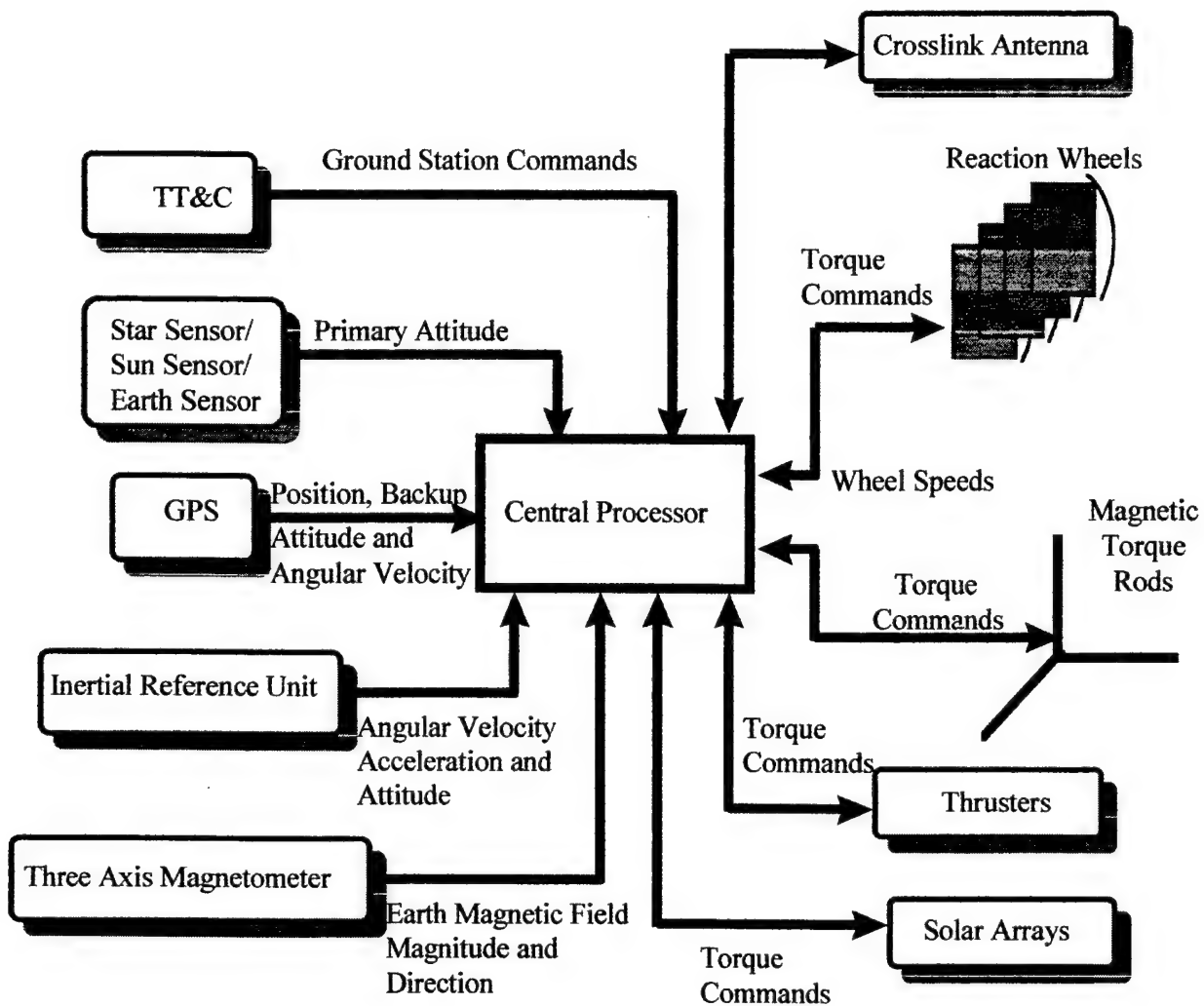


Figure 8-1: Block Diagram of the Attitude Dynamics and Control Subsystem

The ADCS components selected were those that satisfied the subsystem requirements as stated in the previous section. The components selected for the MUS spacecraft are listed in Table 8-1.

Unit	Quantity	Mass (ea)	Avg Power
ADCS Control Processor	2	5.7 kg	25 W
Control Electronics	1	0.9 kg	2.0 W
Magnetometer	1	0.5 kg	0.7 W
Torque Rods	3	0.9 kg	---
Reaction Wheel	1	14.3 kg	28 W
Reaction Wheel	3	10.5 kg	30 W
Star Trackers	3	3.63 kg	9 W
Inertial Reference Unit	2	3.45 kg	34 W
Sun Sensor	2	0.64 kg	1 W
GPS	2	1.68 kg	7 W
GPS Antenna	4	0.2 kg	---
Earth/Sun Sensor	2	2.5 kg	5.5 W

Table 8-1: Spacecraft ADCS Components

After the ADCS component selection had taken place, the satellite bus design was able to proceed by incorporating the equipment. The final ADCS configuration for the MUS design is shown in Figure 8-2.

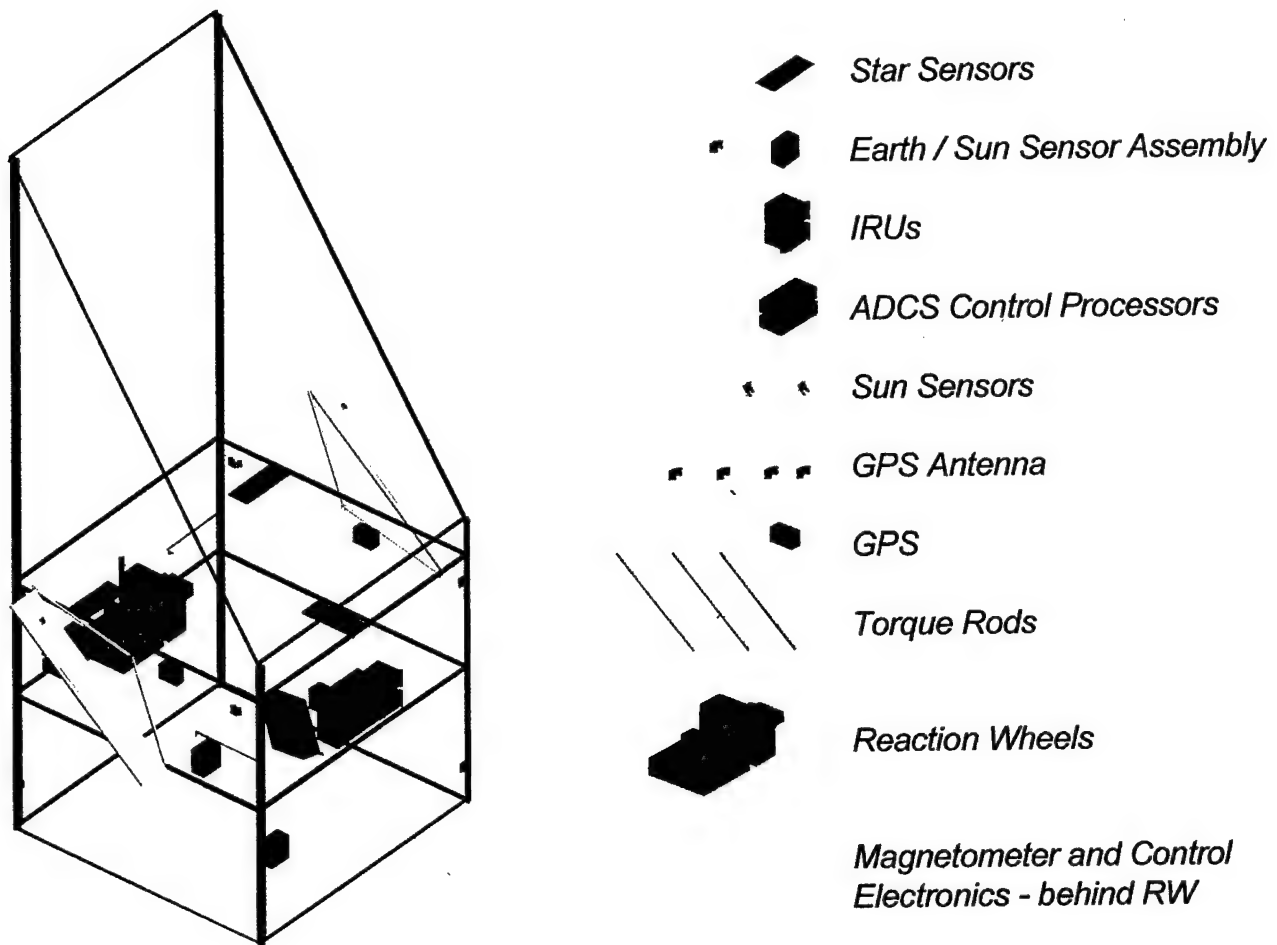


Figure 8-2: ADCS Component Layout

Finally, a simulation of the spacecraft control was performed. When expected disturbance torques and yaw steering requirements were imposed on the model; pointing accuracy requirements were maintained. The limits of the subsystem were tested and it was concluded that it would require disturbance torques approximately one order of magnitude larger than what was expected to cause spacecraft operating limits to be exceeded.

APPENDIX A

ACRONYMS

ADCS	Attitude Dynamics and Control System
AFSCN	Air Force Satellite Control Network
BAPTA	Bearing and Power Transfer Assembly
CG	Center of Gravity
CMG	Control Moment Gyro
CPU	Central Processing Unit
COTS	Commercial Off The Shelf
dB	Decibels
DoD	Department of Defense
DT	Disturbance Torque
DSCS	Defense Satellite Communications System
DuSD - Space	Deputy Undersecretary of Defense for Space
EHF	Extremely High Frequency
EPS	Electrical Power Subsystem
ES	Earth Sensor
ES/SSA	Earth Sensor / Sun Sensor Assembly
GEO	Geostationary Earth Orbit
GG	Gravity Gradient
GHz	Gigahertz
GPS	Global Positioning System
HF	High Frequency
IRU	Inertial Reference Unit
Kbps	Kilobits per second
LEO	Low Earth Orbit
MEO	Medium Earth Orbit
MHz	Megahertz
MILSATCOM	Military Satellite Communication
MOI	Moments of Inertia
MSS	Mobile Satellite Services
MUS	Mobile Users Subscribers
Nm	Newton Meter
Nms	Newton Meter Second
PMOI	Principal Moments of Inertia
Pri	Primary
RF	Radio Frequency
RW	Reaction Wheel
SA	Solar Arrays
SCOC	Satellite Control Operations Center
Sec	Secondary
SHF	Super High Frequency
SOCC	Satellite Operational Control Center

SS	Sun Sensor/Star Sensor
TT&C	Telemetry, Tracking and Control
UFO	UFH Follow On
UHF	Ultra High Frequency
VHF	Very High Frequency

APPENDIX B

GLOSSARY

Angular Momentum. The vector product of the position vector and linear velocity of a particle in motion relative to an axis.

Cyclic Torque. Torque that repeats itself in cycles such that a build up of angular momentum does not occur.

Desaturation. The process of removing built up angular momentum from the reaction wheels.

Disturbance Torque. A torque applied to the spacecraft such that its attitude is disturbed.

Geostationary Orbit. A geosynchronous orbit with an inclination of 0° or near 0° , positioning the satellite directly above the equator. [Ref. 16: p. 2]

Geosynchronous Orbit. An orbit with a period equal to the earth's rotational period of 1,436 minutes and an altitude above the earth of ~ 19300 nm. Most geosynchronous satellites move in near circular, near equatorial orbits. [Ref. 16: p. 2]

Global Coverage. Coverage of all latitudes and longitudes, 90° N to 90° S.

ICO. A medium earth orbit constellation consisting of 10 active satellites and 2 on orbit spares, which will operate at 10,400 km, providing worldwide coverage. The system will consist of 2 orbital planes with an inclination of 45° . Proposed by ICO Global Communications, IOC for the system is planned for the 4th quarter of 1999, with FOC scheduled for the 3rd quarter of 2000. ICO, which will use TDMA for modulation, will support 4,500 simultaneous handheld users per satellite, and can also support aeronautical, fixed, mobile and pager users. Satellite service life is projected at 10 years. The system will operate in S-band and C-band, supporting data rates of 2.4 or 4.8 kbps. Space segment cost is estimated to be 2.6 Billion (including 7 earth stations and 3 gateway switches), estimated handset cost is \$1,000, and projected operating cost is \$1.00-\$2.00/minute in addition to a \$40.00 per month access charge. [Ref. 16: p. 3]

Low Data Rate. For the purposes of the Mobile User Study, 64 Kbps and below. [Ref. 16: p. 4]

Medium Earth Orbit. Implies an orbital altitude between Low Earth Orbit (LEO ~ 100 nm to 540nm) and Geosynchronous Orbit (GEO ~ 18225 nm). Orbit of choice for many proposed Mobile Satellite Systems. [Ref. 16: p. 5]

Mobile Satellite Service (MSS). The military use of satellite based commercial communications service providing digital voice, data, paging or fax services to users equipped with small (typically handheld) terminals. For the purpose of the MUS, this definition refers to Military use of PCS.

[Ref. 16: p. 5]

Mobile User. A highly mobile and or disadvantaged user that requires a small terminal and or antenna (includes hand held terminals and terminals for platforms such as trucks, submarines, small ships, boats, and aircraft). [Ref. 16: p. 5]

Nadir. An earth pointing orientation or in the direction of the earth.

Odyssey. A medium earth orbit constellation consisting of 12 active satellites with spares launched as required, which will operate at 10,355 km (circular orbit), providing worldwide coverage at all latitudes. The system will consist of 3 orbital planes with an inclination of 50°. Proposed by TRW, the system is planned for IOC in the 4th quarter of 2001, with FOC planned for the 4th quarter of 2002. ODYSSEY will use CDMA for modulation, and will support 9,500 simultaneous handheld users per satellite, as well as fixed and transportable users. Space segment cost is projected to be 3.2 Billion, estimated handset cost is \$500-\$700, and projected operating cost is less than \$1.00/minute. [Ref. 16: p. 6]

Personal Communications System (PCS). Satellite based commercial communications service providing digital voice, data, paging or fax services to users equipped with small (typically handheld) terminals. [Ref. 16: p. 6]

Polar Coverage. Coverage that extends to the extreme northern and southern polar regions (90° N to 90° S). [Ref. 16: p. 6]

Secular Torque. A torque that is continuous thus causing a build up of Angular Momentum to occur.

Slew. A reorientation of the spacecraft about the roll, pitch or yaw axes.

A - Area.

β - The angle in the orbital plane between the point with minimum distance (sub solar point) to the sun and the satellite.

$\vec{\beta}$ - The Geomagnetic Field.

C_d - Coefficient of drag.

$\underline{d_r}$ - Vectors from the center of mass to each external piece's center of pressure.

$\underline{M_s}$ - Moment due to solar radiation pressure.

$\underline{\rho_s}$ - Photons that are specularly reflected from a surface.

$\underline{\rho_d}$ - Photons that are diffusely reflected from a surface.

$\underline{\rho_a}$ - Photons absorbed by a surface.

$\underline{\rho}$ - Atmospheric density.

$\underline{\delta}$ - The angle between the orbital plane and the direction of the sun.

$\underline{\delta_1}$ - Critical value of δ where an alternative control scheme must take place.

$\underline{\vec{F}_a}$ - Radiation force due to absorbed photons.

$\underline{\vec{F}_d}$ - Force due to solar radiation pressure.

$\underline{\vec{F}_s}$ - Radiation force due to specularly reflected photons.

\underline{i} - Satellite orbit inclination.

$\underline{I_{cp}}$ - Vector distance from center of mass to center of pressure.

$\underline{\eta}$ - Solar Array angle of rotation.

$\underline{\hat{u}_v}$ - Unit vector in velocity direction.

$\underline{\hat{s}}$ - Solar radiation unit vector.

$\underline{\Omega}$ - Right Ascension of the ascending node.

$\underline{T^{(a)}}$ - Spacecraft torque due to aerodynamic effects.

$\underline{T^{(g)}}$ - Spacecraft torque due to gravity effects.

$\underline{T^{(m)}}$ - Spacecraft torque due to the magnetic field effects.

T_x - Torque about the spacecraft's roll axis.

T_y - Torque about the spacecraft's pitch axis.

T_z - Torque about the spacecraft's yaw axis.

ν - Earth centered true anomaly.

\vec{X}_s - The satellite's roll axis.

\vec{Y}_s - The satellite's pitch axis.

$Z_s - axis$ - Yaw axis or axis parallel to spacecraft UHF antenna

ψ - Yaw rotation angle.

APPENDIX C

MATLAB CODE FOR YAW STEERING

```
% Danny Busch                                21 August 1997
% AA 4871
% This .m file plots the Yaw Rotation Angle and Solar
% Array Rotation angle as a function of time and as
% a function of the Sun Rotation Angle in order to
% maintain solar array tracking.

a=17378;
u=398600.5;
t=0:1:22798;
x=(u/(a^3))^(1/2);
B=(x)*t;

figure(1)
d=1*(pi/180);
Psi=(atan((-sin(B)/tan(d))))*(180/pi);
subplot(2,1,1);
plot((B*(180/pi)),Psi);

hold on
d=5*(pi/180);
Psi=(atan((-sin(B)/tan(d))))*(180/pi);
plot((B*(180/pi)),Psi);

d=15*(pi/180);
Psi=(atan((-sin(B)/tan(d))))*(180/pi);
plot((B*(180/pi)),Psi);

d=30*(pi/180);
Psi=(atan((-sin(B)/tan(d))))*(180/pi);
plot((B*(180/pi)),Psi);

d=45*(pi/180);
Psi=(atan((-sin(B)/tan(d))))*(180/pi);
plot((B*(180/pi)),Psi);

d=60*(pi/180);
Psi=(atan((-sin(B)/tan(d))))*(180/pi);
plot((B*(180/pi)),Psi);

d=75*(pi/180);
```

```
Psi=(atan((-sin(B)/tan(d))))*(180/pi);
plot((B*(180/pi)),Psi);
```

```
d=90*(pi/180);
Psi=(atan((-sin(B)/tan(d))))*(180/pi);
plot((B*(180/pi)),Psi), grid;
xlabel('Sun Rotation Angle (degrees)');
ylabel('Yaw Command Angle (degrees)');
title('Nominal Yaw Trajectories');
axis([0,360,-100,100]);
```

```
gtext('d=1');
gtext('d=5');
gtext('d=15');
gtext('d=30');
gtext('d=45');
gtext('d=60');
gtext('d=75');
gtext('d=90');
hold off
```

```
subplot(2,1,2);
d=1*(pi/180);
Psi=(atan((-sin(B)/tan(d))));
n=atan(-(sin(Psi)/tan(B)));
plot((B*(180/pi)),(n*(180/pi)));
ylabel('Solar Array Rotation Angle in degrees');
xlabel('Sun Rotation Angle in Degrees');
title('Solar Array Trajectories');
hold on
```

```
d=5*(pi/180);
Psi=(atan((-sin(B)/tan(d))));
n=atan(-(sin(Psi)/tan(B)));
plot((B*(180/pi)),(n*(180/pi)));
```

```
d=15*(pi/180);
Psi=(atan((-sin(B)/tan(d))));
n=atan(-(sin(Psi)/tan(B)));
plot((B*(180/pi)),(n*(180/pi)));
```

```
d=30*(pi/180);
Psi=(atan((-sin(B)/tan(d))));
n=atan(-(sin(Psi)/tan(B)));
plot((B*(180/pi)),(n*(180/pi)));
```

```

d=45*(pi/180);
Psi=(atan((-sin(B)/tan(d))));
n=atan(-(sin(Psi)/tan(B)));
plot((B*(180/pi)),(n*(180/pi)));

d=60*(pi/180);
Psi=(atan((-sin(B)/tan(d))));
n=atan(-(sin(Psi)/tan(B)));
plot((B*(180/pi)),(n*(180/pi)));

d=75*(pi/180);
Psi=(atan((-sin(B)/tan(d))));
n=atan(-(sin(Psi)/tan(B)));
plot((B*(180/pi)),(n*(180/pi)));

d=90*(pi/180);
Psi=(atan((-sin(B)/tan(d))));
n=atan(-(sin(Psi)/tan(B)));
plot((B*(180/pi)),(n*(180/pi))), grid;
axis([0,360,-100,100]);

gtext('d=1');
gtext('d=5');
gtext('d=15');
gtext('d=30');
gtext('d=45');
gtext('d=60');
gtext('d=75');
gtext('d=90');

figure(2)
t=t*(1/60);

d=1*(pi/180);
Psi=(atan((-sin(B)/tan(d)))*(180/pi);
subplot(2,1,1);
plot(t,Psi);

hold on
d=5*(pi/180);
Psi=(atan((-sin(B)/tan(d)))*(180/pi);
plot(t,Psi);

d=15*(pi/180);
Psi=(atan((-sin(B)/tan(d)))*(180/pi);

```

% Convert time to minutes

```

plot(t,Psi);

d=30*(pi/180);
Psi=(atan((-sin(B)/tan(d))))*(180/pi);
plot(t,Psi);

d=45*(pi/180);
Psi=(atan((-sin(B)/tan(d))))*(180/pi);
plot(t,Psi);

d=60*(pi/180);
Psi=(atan((-sin(B)/tan(d))))*(180/pi);
plot(t,Psi);

d=75*(pi/180);
Psi=(atan((-sin(B)/tan(d))))*(180/pi);
plot(t,Psi);
axis([0,380,-100,100]);

d=90*(pi/180);
Psi=(atan((-sin(B)/tan(d))))*(180/pi);
plot((B*(180/pi)),Psi), grid
xlabel('Time in minutes');
ylabel('Yaw Command Angle (degrees)');
title('Nominal Yaw Trajectories');

%gtext('d=1');
%gtext('d=5');
%gtext('d=15');
%gtext('d=30');
%gtext('d=45');
%gtext('d=60');
%gtext('d=75');
%gtext('d=90');
hold off

subplot(2,1,2);
d=1*(pi/180);
Psi=(atan((-sin(B)/tan(d))));
n=atan(-(sin(Psi)/tan(B)));
plot(t,(n*(180/pi)));
ylabel('Solar Array Rotation Angle in degrees');
xlabel('Time in minutes');
title('Solar Array Trajectories');
hold on

```

```

d=5*(pi/180);
Psi=(atan((-sin(B)/tan(d))));
n=atan(-(sin(Psi)/tan(B)));
plot(t,(n*(180/pi))), grid;

```

```

d=15*(pi/180);
Psi=(atan((-sin(B)/tan(d))));
n=atan(-(sin(Psi)/tan(B)));
plot(t,(n*(180/pi)));

```

```

d=30*(pi/180);
Psi=(atan((-sin(B)/tan(d))));
n=atan(-(sin(Psi)/tan(B)));
plot(t,(n*(180/pi)));

```

```

d=45*(pi/180);
Psi=(atan((-sin(B)/tan(d))));
n=atan(-(sin(Psi)/tan(B)));
plot(t,(n*(180/pi)));

```

```

d=60*(pi/180);
Psi=(atan((-sin(B)/tan(d))));
n=atan(-(sin(Psi)/tan(B)));
plot(t,(n*(180/pi)));

```

```

d=75*(pi/180);
Psi=(atan((-sin(B)/tan(d))));
n=atan(-(sin(Psi)/tan(B)));
plot(t,(n*(180/pi)));

```

```

d=90*(pi/180);
Psi=(atan((-sin(B)/tan(d))));
n=atan(-(sin(Psi)/tan(B)));
plot(t,(n*(180/pi)));
axis([0,380,-100,100]);

```

```

%gtext('d=1');
%gtext('d=5');
%gtext('d=15');
%gtext('d=30');
%gtext('d=45');
%gtext('d=60');
%gtext('d=75');
%gtext('d=90');

```

```

figure(3)

subplot(2,1,1);
d=5*(pi/180);
Psi=(atan((-sin(B)/tan(d))))*(180/pi);
plot(t,Psi);

for i=1:length(Psi);
    Psi(i)=90;
end;

hold on
plot(t,Psi), grid;
xlabel('Time in minutes');
ylabel('Yaw Command Angle (degrees)');
title('Nominal Yaw Trajectories');
%gtext('d=5');
%gtext('Yaw Angle = Constant 90 degrees for d < 5');
axis([0,380,-140,140])

y=[120,-120,120,-120];
q=[t(1),t(10695),t(12045),t(22799)];

subplot(2,1,2);
plot(q,y)

hold on
d=5*(pi/180);
Psi=(atan((-sin(B)/tan(d)))));
n=atan(-(sin(Psi)/tan(B)));
plot(t,(n*(180/pi))), grid;
axis([0,380,-150,150]);
xlabel('Time in minutes');
ylabel('Solar Array Rotation Angle in degrees');
title('Solar Array Trajectory for d < 5 degrees');
%gtext('d=5');

```

APPENDIX D

MATLAB CODE TO COMPUTE DIRECTION COSINE MATRIX

```
% Danny K. Busch                                4 October 1997
% Thesis
%
% This is a supplemental .m file to compute the initial dcm
% from the orbit/nominal frame to the principal axis frame.
% I am making the assumption that the orbit/nominal frame
% is lined up body axes when this starts. So this is the initial
% dcm from both the body axes and orbit frame to the principal
% axes.

% From the spreadsheet we have the Inertia Matrix.

Iold=[13337 -28.97 0;-28.97 14083 17.72;0 17.72 14113];

[evvec,princ]=eig(Iold)

% Where princ is the matrix containing the principal moments
% of inertias, and Evvec is the transpose of the dcm to get there.

dcm=evvec'

% To prove this, multiply dcm*Iold*dcm' to get from the old
% (non-principal) system to the new (principal) system.

Inew=dcm*Iold*dcm'
```

% Danny K. Busch
% Thesis

4 October 1997

% Plot the body frame vs the Principal Inertia Axis

```
dcm=[0.9992,0.0388,0.0009;0.0354,-0.9026,0.4290;-0.0158,0.4287,0.9033]
x=[0,0,0;dcm(1,1),dcm(1,2),dcm(1,3)];
y=[0,0,0;dcm(2,1),dcm(2,2),dcm(2,3)];
z=[0,0,0;dcm(3,1),dcm(3,2),dcm(3,3)];

u=[0,0,0;1,0,0];
v=[0,0,0;0,1,0];
w=[0,0,0;0,0,1];

figure(1);
plot3(x(:,1),x(:,2),x(:,3),'r',y(:,1),y(:,2),y(:,3),'r',z(:,1),z(:,2),z(:,3),'r')
hold on
plot3(u(:,1),u(:,2),u(:,3),'b',v(:,1),v(:,2),v(:,3),'b',w(:,1),w(:,2),w(:,3),'b')
hold off
grid;
xlabel('X'),ylabel('Y'),zlabel('Z');
title('Body Frame vs Principal Inertial Frame');
```

APPENDIX E

SIMULATION OF THE TOTAL EXTERNAL DISTURBANCES

% Danny K. Busch

27 July 1997

% Thesis

% ADCS Design

%

% Gravity Gradient + Solar Pressure + Aerodynamic Pressure Torques

%

% Simulates the attitude motion of a s/c vs time.

% That is the orientation of the b frame wrt to the

% orbit/nominal frame. Without attitude control.

%

function xdot=total(x);

% Define constants

I1=45.01961;

I2=35.53275;

I3=59.65711;

Ky=(I3-I2)/I1;

Kr=(I3-I1)/I2;

Kp=(I2-I1)/I3;

% Semi-major axis of sun/earth system

asun=1.49598e8;

% Sun constant

us=1.327e11;

to=0;

Mos=pi;

% Argument of perigee

w=0.4363323;

% Longitude of the ascending node

omega=(pi/2);

% Inclination

inc=(pi/4);

% Eccentricity of Sun/Earth system

```

es=.016708;

% Eccentricity of Earth/Satellite system
ee=0;

ue=3.986012e5;

% Radius of the Earth
Re=6378;

% Generaic cause normalize later, vector from sun to earth
r=10;

% R=dist fm center of earth to center of mass of s/c

% User friendly conversions

w1=x(1);
w2=x(2);
w3=x(3);
a11=x(4);
a12=x(5);
a13=x(6);
a21=x(7);
a22=x(8);
a23=x(9);
a31=x(10);
a32=x(11);
a33=x(12);
r1=x(13);
r2=x(14);
r3=x(15);
rdot1=x(16);
rdot2=x(17);
rdot3=x(18);
time=x(19);

R=sqrt(r1^2+r2^2+r3^2);
v=sqrt(rdot1^2+rdot2^2+rdot3^2);
nudot=v/R;

%[eRs]h=r vector fm sun to earth expressed in heliocentric
%frame
%[eRs]I=r vector fm sun to earth expressed in earth

```

```

%centered inertial
%[eRs]o= r vector fm sun to earth expressed in the
%orbit frame
%[eRs]b= r vector fm sun to earth expressed in the
%body frame

% Find nu and d as a function of time

Mearth=0;
toearth=0;
%a = semimajor axis of satellite earth system
a=21000;
ne=(ue/a^3)^(1/2);
% ne mean orbital rate
%M-Mo=n(t-to) general equation mean anomaly

Me=ne*time;
%nu earth
nu=Me + 2*ee*sin(Me) + 1.25*((ee)^2)*sin(2*Me);
ns=sqrt(us/asun^3);
%Ms-Mos=ns(time-to); mean anomaly for earth sun system;
Ms=ns*time+pi;
%orbital parameter nu for sun earth system
d=Ms+2*es*sin(us)+1.25*(es^2)*sin(2*Ms);

%Now we have nu and d or nu for sun and earth

% R vector from sun to earth in earth centered inertial

eRsI=[-r*cos(d);-r*cos(.4084)*sin(d);-r*sin(.4084)*sin(d)];
% multiply by -1 so we R points from earth to sun according to Agrwal

% Define dcm from earth centered inertial to rotating orbital frame

J = [cos(nu) sin(nu) 0;-sin(nu) cos(nu) 0;0 0 1];
K = [cos(w) sin(w) 0;-sin(w) cos(w) 0;0 0 1];
L = [1 0 0;0 cos(inc) sin(inc);0 -sin(inc) cos(inc)];
Q = [cos(omega) sin(omega) 0;-sin(omega) cos(omega) 0;0 0 1];

oCi = J*K*L*Q;

% Now transform to the orbit frame

eRso = oCi*eRsI;

```

```

%define dcm from orbit to body frame

bCo = [a11 a21 a31;a12 a22 a32;a13 a23 a33];

% Now tranform R vector to orbit frame

eRsb = bCo*eRso;

% Now compute the unit vector from earth to sun
Shatb = eRsb/(norm(eRsb));
s= Shatb;

% Now we have S hat expressed in the b frame as a
% function of d and nu, which is a function of time

% Define n hat vectors in the body frame

n1 = [0; 1; 0];
n2 = [0.866; 0.5; 0];
n3 = [0.866; -0.5; 0];
n4 = [0; -1; 0];
n5 = [-0.866; -0.5; 0];
n6 = [-0.866; 0.5; 0];
n7 = [0; 1; 0];
n8 = [0; -1; 0];
n9 = [-1; 0; 0];
n10 = [0; 0; 1];
n11 = [0; 0; -1];
n12 = [0; 0; -1];
n13 = [0; 0; 1];

% Now define the dr vectors from center of mass to center
% of pressure

dr1 = [0.11; 0.5; 0];
dr2 = [0.543; .25; 0];
dr3 = [0.543; -.25; 0];
dr4 = [0.11; -0.5; 0];
dr5 = [-0.543; -0.25; 0];
dr6 = [-0.543; 0.25; 0];
dr7 = [-0.756; 0.5; 0];
dr8 = [-0.756; -0.5; 0];
dr9 = [-0.39; 0; 0];
dr10 = [-.756; 0; 0.5];
dr11 = [-.756; 0; -0.5];

```

```
dr12 = [0.11; 0; -0.5];  
dr13 = [0.11; 0; 0.5];
```

```
Fe = 1358;  
C = 2.9979E8;  
P = Fe/C;  
A = zeros(1,13);
```

```
% F = PA(nhat dot shat)(2*nhat)  
% Calculate the (nhat dot shat)
```

```
hat = zeros(1,13);  
    hat(1) = sum(n1.*s);  
    if hat(1)<0;  
        hat(1)=0;  
    else  
        hat(1)=hat(1);  
    end
```

```
    hat(2) = sum(n2.*s);  
    if hat(2)<0;  
        hat(2)=0;  
    else  
        hat(2)=hat(2);  
    end
```

```
    hat(3) = sum(n3.*s);  
    if hat(3)<0;  
        hat(3)=0;  
    else  
        hat(3)=hat(3);  
    end
```

```
    hat(4) = sum(n4.*s);  
    if hat(4)<0;  
        hat(4)=0;  
    else  
        hat(4)=hat(4);  
    end
```

```
    hat(5) = sum(n5.*s);  
    if hat(5)<0;  
        hat(5)=0;  
    else  
        hat(5)=hat(5);
```

end

hat(6) = sum(n6.*s);

if hat(6)<0;

 hat(6)=0;

else

 hat(6)=hat(6);

end

hat(7) = sum(n7.*s);

if hat(7)<0;

 hat(7)=0;

else

 hat(7)=hat(7);

end

hat(8) = sum(n8.*s);

if hat(8)<0;

 hat(8)=0;

else

 hat(8)=hat(8);

end

hat(9) = sum(n9.*s);

if hat(9)<0;

 hat(9)=0;

else

 hat(9)=hat(9);

end

hat(10) = sum(n10.*s);

if hat(10)<0;

 hat(10)=0;

else

 hat(10)=hat(10);

end

hat(11) = sum(n11.*s);

if hat(11)<0;

 hat(11)=0;

else

 hat(11)=hat(11);

end

hat(12) = sum(n12.*s);

```

    if hat(12)<0;
        hat(12)=0;
    else
        hat(12)=hat(12);
    end
    hat(13) = sum(n13.*s);
    if hat(13)<0;
        hat(13)=0;
    else
        hat(13)=hat(13);
    end

% hat = nhat(i) dot shat(i)
% hat = [-o---oo--o--o]

% Define the area matrix

A = [.5 .5 .5 .5 .5 .5 .331 .331 1.77 .331 .331 .724 .724];

ps = .4;
pd = .4;

% From Agrwal's Book p. 134
% Ms = PA(n dot s)*r X [(1-ps)*s + 2(ps + 1/3pd)n]

Ms = zeros(3,13);

% Assign intermediate variables

G = zeros(3,13);
G(:,1) = P*A(1)*hat(1)*dr1;
G(:,2) = P*A(2)*hat(2)*dr2;
G(:,3) = P*A(3)*hat(3)*dr3;
G(:,4) = P*A(4)*hat(4)*dr4;
G(:,5) = P*A(5)*hat(5)*dr5;
G(:,6) = P*A(6)*hat(6)*dr6;
G(:,7) = P*A(7)*hat(7)*dr7;
G(:,8) = P*A(8)*hat(8)*dr8;
G(:,9) = P*A(9)*hat(9)*dr9;
G(:,10) = P*A(10)*hat(10)*dr10;
G(:,11) = P*A(11)*hat(11)*dr11;
G(:,12) = P*A(12)*hat(12)*dr12;
G(:,13) = P*A(13)*hat(13)*dr13;

T = zeros(3,13);

```

```

T(:,1) = ((1-ps)*s) + ((2*(ps + 0.333*pd))*n1);
T(:,2) = ((1-ps)*s) + ((2*(ps + 0.333*pd))*n2);
T(:,3) = ((1-ps)*s) + ((2*(ps + 0.333*pd))*n3);
T(:,4) = ((1-ps)*s) + ((2*(ps + 0.333*pd))*n4);
T(:,5) = ((1-ps)*s) + ((2*(ps + 0.333*pd))*n5);
T(:,6) = ((1-ps)*s) + ((2*(ps + 0.333*pd))*n6);
T(:,7) = ((1-ps)*s) + ((2*(ps + 0.333*pd))*n7);
T(:,8) = ((1-ps)*s) + ((2*(ps + 0.333*pd))*n8);
T(:,9) = ((1-ps)*s) + ((2*(ps + 0.333*pd))*n9);
T(:,10) = ((1-ps)*s) + ((2*(ps + 0.333*pd))*n10);
T(:,11) = ((1-ps)*s) + ((2*(ps + 0.333*pd))*n11);
T(:,12) = ((1-ps)*s) + ((2*(ps + 0.333*pd))*n12);
T(:,13) = ((1-ps)*s) + ((2*(ps + 0.333*pd))*n13);

```

```

Z = cross(G,T);

```

% We now have a 3 by 13 matrix containing torques in b1 direction for
 % thirteen areas in the first row, etc...

% Solar pressure moments in b direction

```

Msp1 = sum(Z(1,:));

```

```

Msp2 = sum(Z(2,:));

```

```

Msp3 = sum(Z(3,:));

```

% $(1/2)*p*Cd*A*v*v*(\hat{u} \times I_{cp})$

% Define p as a function of R

```

if R < 6578;

```

```

    p=4e-10;

```

```

elseif R < 6678;

```

```

    p=5e-11;

```

```

elseif R < 6778;

```

```

    p=1.5e-11;

```

```

elseif R < 6878;

```

```

    p=5e-12;

```

```

elseif R < 6978

```

```

    p=2e-12

```

```

else

```

```

    p=8e-13;

```

```

end

```

% Define Cd as a constant given on P.90 of handout.

```

Cd=3.2;

```

```
% Define Area constants in the b1, b2 and b3 directions. This is the total
% cross sectional area in the b1 hat direction,...b2 hat direction and b3
% hat direction.
```

```
Ab1=1.77;
Ab2=.884;
Ab3=1.61;
```

```
Abody=[Ab1 Ab2 Ab3]';
```

```
% Now build the velocity vector for the I frame
```

```
RDOTi=[rdot1 rdot2 rdot3]';
```

```
% Now convert velocity from I frame to B frame
```

```
RDOTb=bCo*oCi*RDOTi;
```

```
% Now find the unit vector of RDOTb, uvhat.
```

```
uvhatb=RDOTb./norm(RDOTb);
```

```
% Now compute area perpendicular to uvhat.
```

```
AT=abs(Abody.*uvhatb);
```

```
% Compute total area
```

```
ATOTAL=sum(AT);
```

```
% Now compute (uvhatb X Icp)
```

```
Icp=zeros(3,13);
Icp=[dr1 dr2 dr3 dr4 dr5 dr6 dr7 dr8 dr9 dr10 dr11 dr12 dr13];
Maero=(1/2)*p*Cd*ATOTAL*v*v*(cross(uvhatb,Icp));
Maerototal=[sum(Maero(1,:)) sum(Maero(2,:)) sum(Maero(3,:))]';
```

```
Msp1=sum(Z(1,:));
```

```
Msp2=sum(Z(2,:));
```

```
Msp3=sum(Z(3,:));
```

```
M1gg=((3*ue)/R^3)*(I3-I2)*a12*a13;
```

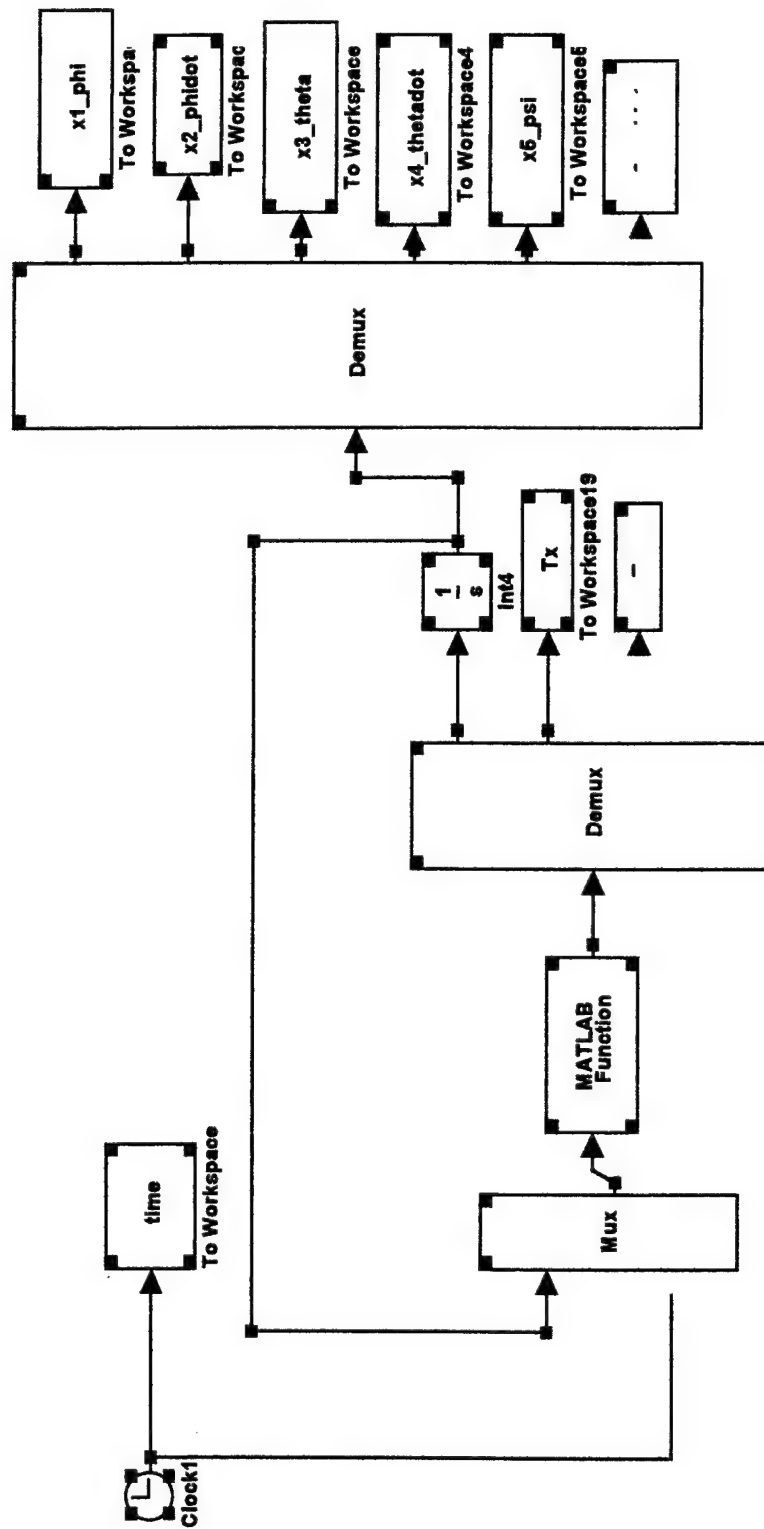
```
M2gg=((3*ue)/R^3)*(I1-I3)*a13*a11;
```

```
M3gg=((3*ue)/R^3)*(I2-I1)*a11*a12;
```

```

xdot(1)= ((Msp1+Maerototal(1)+M1gg)/I1) - Ky*w2*w3;
xdot(2)= ((Msp2+Maerototal(2)+M2gg)/I2) - Kr*w3*w1;
xdot(3)= ((Msp3+Maerototal(3)+M3gg)/I3) - Kp*w1*w2;
xdot(4)=a12*(w3-a33*nudot)-a13*(w2-a32*nudot);
xdot(5)=a13*(w1-a31*nudot)-a11*(w3-a33*nudot);
xdot(6)=a11*(w2-a32*nudot)-a12*(w1-a31*nudot);
xdot(7)=a22*(w3-a33*nudot)-a23*(w2-a32*nudot);
xdot(8)=a23*(w1-a31*nudot)-a21*(w3-a33*nudot);
xdot(9)=a21*(w2-a32*nudot)-a22*(w1-a31*nudot);
xdot(10)=a32*(w3-a33*nudot)-a33*(w2-a32*nudot);
xdot(11)=a33*(w1-a31*nudot)-a31*(w3-a33*nudot);
xdot(12)=a31*(w2-a32*nudot)-a32*(w1-a31*nudot);
xdot(13)=x(16);
xdot(14)=x(17);
xdot(15)=x(18);
xdot(16)=((-ue)/R^3)*r1;
xdot(17)=((-ue)/R^3)*r2;
xdot(18)=((-ue)/R^3)*r3;
xdot(19)=Msp1+Maerototal(1)+M1gg;
xdot(20)=Msp2+Maerototal(2)+M2gg;
xdot(21)=Msp3+Maerototal(3)+M3gg;

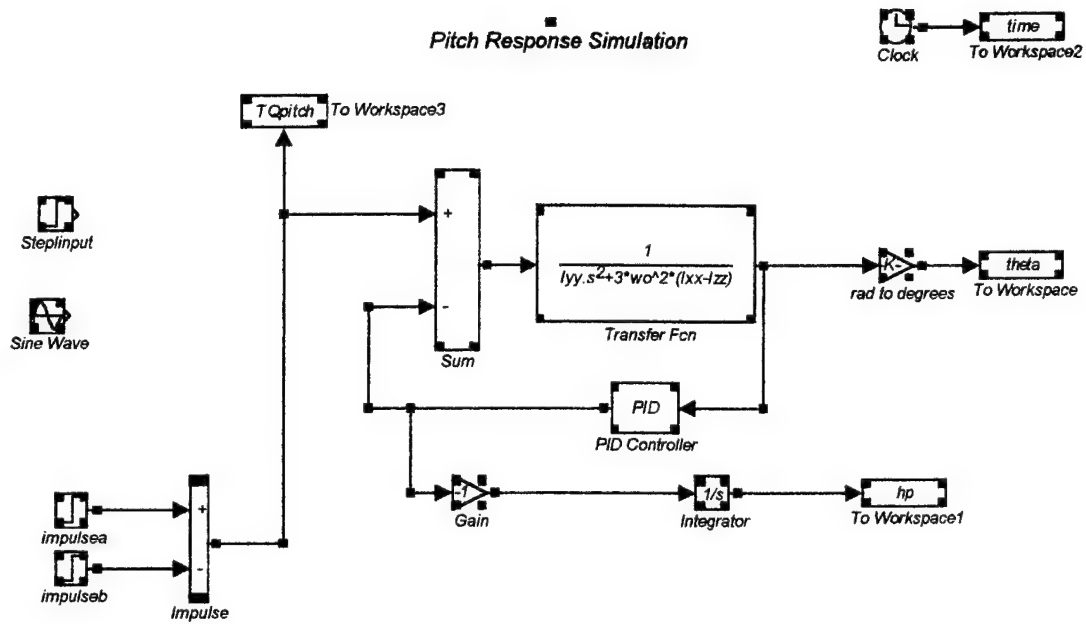
```



This Page Intentionally Left Blank

APPENDIX F

SMALL ANGLE SIMULATION



% Danny K. Busch

4 October 1997

% Thesis

% This is the initial conditions used with the simulink.

wo=2.75578e-4;

Ixx=13337;

Iyy=14083;

Izz=14113;

Kp=.3;

Tp=433;

Ky=.1;

Ty=751;

Kr=.5;

Tr=2060;

% Danny Busch

4 October 1997

% Thesis

% This file plots torque, angle (theta), and reaction

% wheel momentum vs time.

figure(1)

subplot(3,1,1);

plot(time, TQpitch), grid;

title('Pitch Torque vs Time');

xlabel('Time (sec)');

ylabel('Torque (N-m)');

orient tall

subplot(3,1,2);

plot(time, theta), grid;

title('Pitch Angle vs Time');

xlabel('Time (sec)');

ylabel('Pitch Angular Response (deg)');

orient tall

subplot(3,1,3)

plot(time, hp), grid;

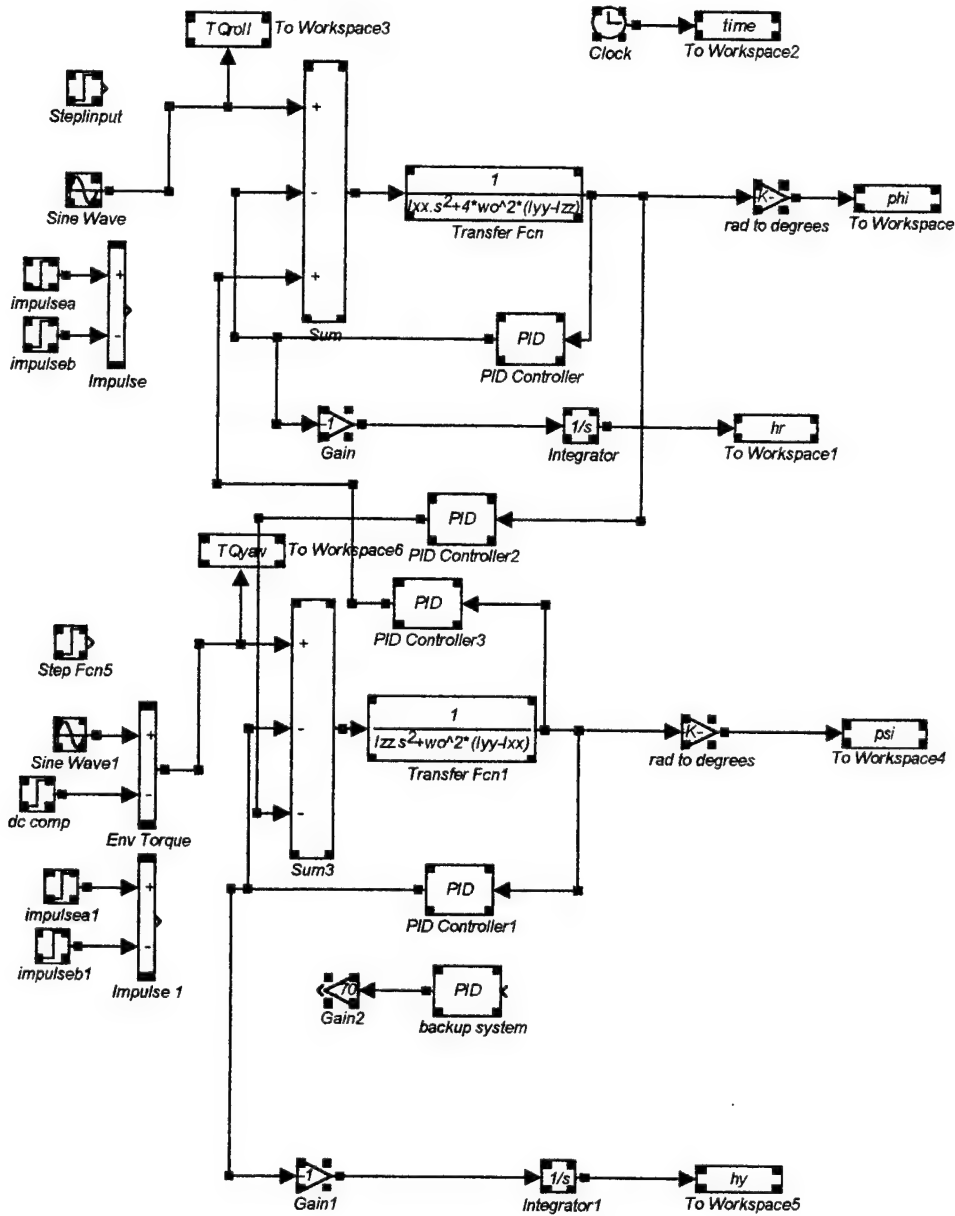
title('Pitch Wheel Angular Momentum vs Time');

xlabel('Time (sec)');

ylabel('Angular Momentum (N-m-s)');

orient tall

Roll Yaw Response Simulation



% Danny K. Busch

4 October 1997

% Thesis

% Plot .m file used for thesis to aid in plotting

% the results from Roll and Yaw

% Plots torque, angle and momentum vs time.

```
figure(1)
subplot(3,1,1);
plot(time,TQroll), grid;
title('Roll Torque vs Time');
xlabel('Time (sec)');
ylabel('Torque (N-m)');
orient tall
subplot(3,1,2);
plot(time,phi), grid;
title('Roll angle phi');
xlabel('Time (sec)');
ylabel('Roll Angular Response (deg)');
orient tall
subplot(3,1,3)
plot(time,hr), grid;
title('Angular Momentum vs Time');
xlabel('Time (sec)');
ylabel('Angular Momentum (N-m-s)');
orient tall
figure(2)
subplot(3,1,1);
plot(time,TQyaw), grid;
title('Yaw Torque vs Time');
xlabel('Time (sec)');
ylabel('Torque (N-m)');
orient tall
subplot(3,1,2);
plot(time,psi), grid;
title('Yaw angle psi');
xlabel('Time (sec)');
ylabel('Yaw Angular Response (deg)');
orient tall
subplot(3,1,3)
plot(time,hy), grid;
title('Angular Momentum vs Time');
xlabel('Time (sec)');
ylabel('Angular Momentum (N-m-s)');
orient tall
```

This Page Intentionally Left Blank

APPENDIX G

LARGE ANGLE SIMULATION

% Danny K. Busch

3 October 1997

% Thesis

%

% Using S Function to model the dynamics of the Spacecraft

% Define S-Function

function[sys, xo]=large(t,x,u,flag)

% VDPM EOM as an M-file

Ixx=13337;

Iyy=14083;

Izz=14113;

wo=2.75578e-4;

if abs(flag)==1,

% Return rates

sys(1)=x(2);

sys(2)=(-1/Ixx)*(x(4)*cos(x(1))*Izz*x(6)+x(6)*x(6)*cos(x(3))*sin(x(1))*Izz-
wo*cos(x(1))*cos(x(5))*Izz*x(6)-
wo*sin(x(1))*sin(x(3))*sin(x(5))*Izz*x(6)+x(4)*x(4)*sin(x(1))*Iyy-
x(6)*cos(x(3))*cos(x(1))*Iyy*x(4)-
wo*sin(x(1))*cos(x(5))*Iyy*x(4)+wo*cos(x(1))*sin(x(3))*sin(x(5))*Iyy*x(4)+u(4)+x(4)
*cos(x(1))*u(3)+x(6)*cos(x(3))*sin(x(1))*u(3)-wo*cos(x(1))*cos(x(5))*u(3)-
wo*sin(x(1))*sin(x(3))*sin(x(5))*u(3)+x(4)*sin(x(1))*u(2)-
x(6)*cos(x(3))*cos(x(1))*u(2)-
wo*sin(x(1))*cos(x(5))*u(2)+wo*cos(x(1))*sin(x(3))*sin(x(5))*u(2)-
3*wo*wo*sin(x(1))*cos(x(1))*cos(x(3))*cos(x(3))*Izz+3*wo*wo*sin(x(1))*cos(x(1))*c
os(x(3))*cos(x(3))*Iyy);

sys(3)=x(4);

sys(4)=(-1/Iyy)*(-
x(4)*sin(x(1))*Ixx*x(2)+x(6)*cos(x(3))*cos(x(1))*Ixx*x(2)+wo*sin(x(1))*cos(x(5))*Ixx
*x(2)-wo*cos(x(1))*sin(x(3))*sin(x(5))*Ixx*x(2)-
x(2)*Izz*x(6)+x(6)*x(6)*sin(x(3))*Izz+wo*cos(x(3))*sin(x(5))*Izz*x(6)-
x(4)*sin(x(1))*u(1)+x(6)*cos(x(3))*cos(x(1))*u(1)+wo*sin(x(1))*cos(x(5))*u(1)-
wo*cos(x(1))*sin(x(3))*sin(x(5))*u(1)-
x(2)*u(3)+x(6)*sin(x(3))*u(3)+wo*cos(x(3))*sin(x(5))*u(3)+u(5)-

```
3*wo*wo*sin(x(3))*cos(x(3))*cos(x(1))*Izz+3*wo*wo*sin(x(3))*cos(x(3))*cos(x(1))*I
xx);
```

```
sys(5)=x(6);
sys(6)=(-1/Izz)*(x(2)*Iyy*x(4)-x(6)*sin(x(3))*Iyy*x(4)-
wo*cos(x(3))*sin(x(5))*Iyy*x(4)-x(4)*cos(x(1))*Ixx*x(2)-
x(6)*cos(x(3))*sin(x(1))*Ixx*x(2)+wo*cos(x(1))*cos(x(5))*Ixx*x(2)+wo*sin(x(1))*sin(
x(3))*sin(x(5))*Ixx*x(2)+x(2)*u(2)-x(6)*sin(x(3))*u(2)-wo*cos(x(3))*sin(x(5))*u(2)-
x(4)*cos(x(1))*u(1)-
x(6)*cos(x(3))*sin(x(1))*u(1)+wo*cos(x(1))*cos(x(5))*u(1)+wo*sin(x(1))*sin(x(3))*sin(
x(5))*u(1)+u(6)-
3*wo*wo*sin(x(3))*cos(x(3))*sin(x(1))*Ixx+3*wo*wo*sin(x(3))*cos(x(3))*sin(x(1))*Iy
y);
```

```
elseif flag==0
```

```
    % Return initial conditions
```

```
    sys=[6;0;6;6;0;0];
```

```
    % [continuous states, discrete states, outputs, inputs, discontinuous roots,
    % direct feed through]
```

```
    xo=[0;0;0;0;0;0];
```

```
elseif flag==3
```

```
    % If flag = 3, return system outputs
```

```
    sys(1)=x(1);
    sys(2)=x(2);
    sys(3)=x(3);
    sys(4)=x(4);
    sys(5)=x(5);
    sys(6)=x(6);
```

```
else
```

```
    sys=[];
```

```
end;
```

% Danny K. Busch

4 October 1997

% Thesis

% This is the initial conditions used with the simulink.

wo=2.75578e-4;

Ixx=13337;

Iyy=14083;

Izz=14113;

Kr=1;

Kp=2.0;

Ky=.2;

%Kr=0.5;

Tr=2060;

%Kp=.3;

Tp=433;

%Ky=.1;

Ty=751;

% Danny Busch

13 October 1997

% Thesis

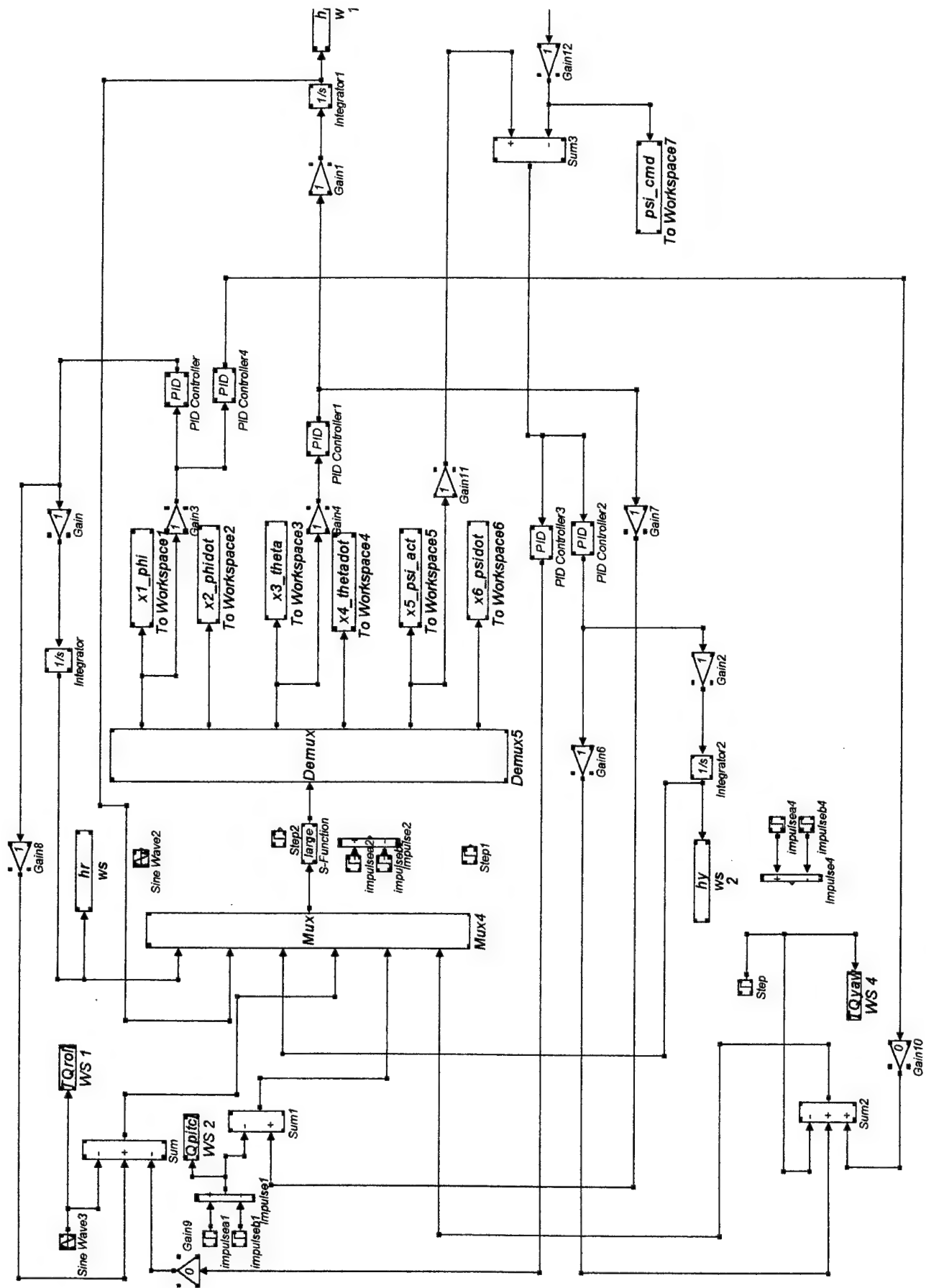
%

% .m file used to simulate the motion of the satellite

function act=psicmd(t)

act=(-1.000507)*atan(11.43005*sin((0.0002755937)*(t)));

end;



This Page Intentionally Left Blank

LIST OF REFERENCES

1. Headquarters, Air Force Space Command, *Military Satellite Communications Handbook*, Vol. 2, January 2, 1996.
2. Martin, Donald H., *Communications Satellites 1958-1995*, The Aerospace Corporation, El Segundo, California, May 1996.
3. U.S. Space Command, Department of Defense, *Advanced Satellite Communications Capstone Requirements Document*, Draft, UNCLASSIFIED, 10 June 1996.
4. Department of Defense Space Architect, *MILSATCOM Architecture Development FINAL REPORT*, Draft Version 1.0, 28 February 1997.
5. Boyd, Austin W., CDR, USN, *MILSATCOM Transition Planning Effort White Paper*, Draft, 18 March 1997.
6. Larson, Wiley J and Wertz, James R., *Space Mission Analysis and Design*, Microcosm, Inc and Kluwer Academic Publishers, 1992.
7. Thomas Baird and Wes Bush, *Odyssey System Overview*, TRW Space and Electronics Group, February 1996.
8. *ICO System Overview*, Surinder Hundal, Director of Public Relations for the ICO Global Communications, December 1996.
9. Hughes Space and Communications Company, *The ICO Global Mobile Satellite System in Support of Department of Defense C3I Requirements*.
10. B. Johnson, *The ICO Global Mobile Satellite System in Support of Department of Defense C3I Requirements*, Hughes Space and Communications Company, El Segundo, California.
11. Bruce Gerding, *Personal Communications vis Satellite: An Overview*, February 1996.
12. Brian Ackroyd, *MEOs versus LEOs...the race for mobility*.
13. W.J. Ciesluk, L.M. Gaffney, and S.J. Morin, *Military PCS at Medium Orbit -- An Alternative UHF SATCOM Concept*, The MITRE Corporation, 30 June 1996
14. *Application For Modification of License of TRW Incorporated in the Mobile Satellite Service above 1GHz*, TRW Space and Electronics Group, 29 September 1995.

15. Dana L. Haskell, *An Analysis of Commercial Low Earth Orbit and Medium Earth Orbit Mobile Satellite Systems and Their Potential For Military Use*, The Naval Postgraduate School, September, 1996.
16. Mobile Users Study Document, The U.S. Naval Space Command, May 1997.
17. CDR Austin Boyd and LT Mike Finnegan, *Joint MILSATCOM Mobile User Study (MUS) Prioritized Requirements*, The U.S. Naval Space Command.
18. CDR Austin Boyd, *History of the Joint MILSATCOM Transition Planning Effort*, The U.S. Naval Space Command, 29 April, 1997.
19. CDR Austin Boyd, *Mobile User's Study Slide Presentation*, U.S. Naval Space Command.
20. CDR Austin Boyd, *Mobile User's Study Definitions List*, U.S. Naval Space Command.
21. Lynn Boyer, John Flynn, Ty Gallander, Jim Jones, Eric Ruttenberg, Al Scott, Dan Starling, Kirk Treanor, Kevin Wilson and Kevin Ziomek, *Spectral Sensing Space System Spacecraft Design Project*, The Naval Postgraduate School, March, 1996.
22. Chobotov, *Spacecraft Attitude Dynamics and Control*, Kreiger, 1991.
23. Dr. Sandi Scrivener, *AA3818 - Attitude Dynamics and Control Class Notes*, November, 1996.
24. Sandi Scrivener, *AA2820 - Introduction to Spacecraft Structures Class Notes*, February, 1996.
25. Brij N. Agrawal, *Design of Geosynchronous Spacecraft*, Prentice-Hall, 1986.
26. Hughes Space and Communications Company, *Spacecraft Bus Subsystems*, February, 1988.
27. NAVSTAR Global Positioning System, *Intermediate Design Review*, 28 September, 1989.
28. Hughes Space and Communications Company, *UHF Follow-On Communications Satellite Program*, 29 November, 1989.
29. Honeywell Space Systems - Phoenix, *Data Control Systems*, April, 1997.
30. ITHACO Space Systems, *Magnetic Acquisition/Despin System*, July, 1997.
31. ITHACO Space Systems, *TORQRODS*, July, 1997.
32. ITHACO Space Systems Products Catalog, *Earth Sensor / Sun Sensor Assembly*, July, 1997.

33. ITHACO Space Systems, *Reaction and Momentum Wheel Assemblies*, July, 1997.
34. ITHACO Space Systems, *Heat Operated Grease Replenishment System*, July, 1997.
35. Bill Bialke, *Operational Lifetime Experience with Attitude Determination and Control Mechanisms*, 19th Annual American Astronautical Society Guidance and Control Conference, 7 February, 1996.
36. Hughes Danbury Optical Systems, *HD-1003 Star Trackers - Packed With Performance and Room to Grow*, July, 1997.
37. Marcel Engelsman, Agus Prawiranegra, and Leo Timmermans, *Project Pygmalion - A Feasibility Study for a LEO Telecommunication Satellite*, Delft University of Technology, September, 1991.
38. Carl Josefson, Jack Myers, Mike Cloutier, Steve Paluszek, Gerry Michael, Dan Hunter, Dan Sakoda, Wes Walters, Dennis Johnson, Terry Bauer, Charlie Racoosin, and Butch Lugtu, *High Latitude Communications Satellite*, The Naval Postgraduate School, December, 1989.
39. R.C. Olsen and D.D. Cleary, *Introduction to the Space Environment*, November, 1996.
40. *MUSCRAT-Spacecraft Design Project*, The Naval Postgraduate School, September, 1997.

This Page Intentionally Left Blank

INITIAL DISTRIBUTION LIST

1. Defense Technical Information Center..... 2
8725 John J. Kingman Rd., STE 0944
Ft. Belvoir, VA 22060-6218

2. Dudley Knox Library..... 2
Naval Postgraduate School
411 Dyer Rd.
Monterey, CA 93943-5101

3. Commander, Naval Space Command..... 1
Head, SATCOM Plans & Policy Branch (N-52)
5280 Fourth Street
Dahlgren, VA 22448-5170

4. Professor Brig Agrawal.....2
Code AA/Ag
Naval Postgraduate School
Monterey, CA 93943-5101

5. Department of Aeronautics and Astronautics..... 1
Code AA
Naval Postgraduate School
Monterey, CA 93943-5101

6. Office of the Chief of Naval Operations..... 1
OPNAV N633
Washington, D.C. 20350

7. Professor Gangbing Song..... 1
Code AA/Ag
Naval Postgraduate School
Monterey, CA 93943-5101

8. LT Danny K. Busch..... 5
10105 Mindy Ct.
Fredericksburg, VA 22408